NASA TECHNICAL NOTE

NASA TN D-7507

NASA TN D-7507

ENGINEERING PREDICTION OF TURBULENT SKIN FRICTION AND HEAT TRANSFER IN HIGH-SPEED FLOW

by Aubrey M. Cary, Jr., and Mitchel H. Bertram

Langley Research Center
Hampton, Va. 23665

NATIONAL AERONAUTICS AND SPACE ADMINISTRATION • WASHINGTON, D. C. • JULY 1974

1. Report No.	2. Government Accession No.	3. Recipient's Catalog No.
NASA TN D-7507		

4. Title and Subtitle	5. Report Date
ENGINEERING PREDICTION OF TURBULENT SKIN FRICTION AND HEAT TRANSFER IN HIGH-SPEED FLOW	July 1974
	6. Performing Organization Code

7. Author(s)	8. Performing Organization Report No.
Aubrey M. Cary, Jr., and Mitchel H. Bertram	L-9206
	10. Work Unit No.
9. Performing Organization Name and Address	501-06-08-01
NASA Langley Research Center Hampton, Va. 23665	11. Contract or Grant No.
	13. Type of Report and Period Covered
12. Sponsoring Agency Name and Address	Technical Note
National Aeronautics and Space Administration Washington, D.C. 20546	14. Sponsoring Agency Code

15. Supplementary Notes

16. Abstract

A large collection of experimental turbulent-skin-friction and heat-transfer data for flat plates and cones was used to determine the most accurate of six of the most popular engineering-prediction methods; the data represent a Mach number range from 4 to 13 and ratio of wall to total temperature ranging from 0.1 to 0.7. The Spalding and Chi method incorporating virtual-origin concepts was found to be the best prediction method for Mach numbers less than 10; the limited experimental data for Mach numbers greater than 10 were not well predicted by any of the engineering methods except the Coles method.

17. Key Words (Suggested by Author(s))	18. Distribution Statement
Turbulent boundary layer Turbulent prediction methods Skin friction Heat transfer High-speed flow	Unclassified – Unlimited STAR Category 12

19. Security Classif. (of this report)	20. Security Classif. (of this page)	21. No. of Pages	22. Price*
Unclassified	Unclassified	86	$4.00

*For sale by the National Technical Information Service, Springfield, Virginia 22151

ENGINEERING PREDICTION OF TURBULENT SKIN FRICTION AND HEAT TRANSFER IN HIGH-SPEED FLOW

By Aubrey M. Cary, Jr., and Mitchel H. Bertram
Langley Research Center

SUMMARY

A large collection of experimental turbulent-skin-friction and heat-transfer data for flat plates and cones was used to determine the most accurate of six of the most popular engineering-prediction methods; the data represent a Mach number range from 4 to 13 and ratio of wall to total temperature ranging from 0.1 to 0.7. The Spalding and Chi method incorporating virtual-origin concepts was found to be the best prediction method for Mach numbers less than 10; the limited experimental data for Mach numbers greater than 10 were not well predicted by any of the engineering methods except the Coles method.

INTRODUCTION

Engineering predictions of turbulent boundary-layer skin friction and heat transfer in high-speed flow are needed for the development of flight vehicles since the structural and thermodynamic design, as well as the aircraft performance, depends upon knowledge of surface heating and drag. Available engineering prediction methods are empirical in nature, and their reliability can only be as good as the experimental data used to formulate the methods. Through the years various correlations of turbulent-skin-friction and heating data for two-dimensional and conical flows have met with mixed success. Earlier correlations extended into the supersonic range but were based primarily on data for adiabatic or near-adiabatic wall conditions. In recent years, the increased capability of hypersonic wind tunnels has provided experimental turbulent-skin-friction and heating data through a wide range of Mach number, wall cooling, and Reynolds number. Thus, with these newer data it is now possible to evaluate more definitively the available prediction methods. Finite-difference solutions to the turbulent-boundary-layer equations will eventually eliminate the necessity for engineering prediction methods; however, significant advances must be made in turbulence modeling before these numerical procedures can accurately predict skin friction and heating in nonadiabatic, hypersonic flows.

Some evaluations of turbulent prediction methods (refs. 1 to 9) suffer from comparisons with insufficient experimental data and, in many cases, lack of generality and consis-

tency in applying the prediction methods. In addition, parameters in any of the engineering prediction methods (such as virtual-origin location, Reynolds analogy factor, and recovery factor) provide a sizable range of possible predictions for specific experimental data. A good engineering prediction method should be simple to apply in a consistent manner and should predict correctly the effects of Mach number, Reynolds number, and the ratio of wall to adiabatic-wall temperature.

In the present investigation, a large body of skin-friction and heat-transfer data (two-dimensional and conical) obtained in high-speed wind-tunnel flows are used to evaluate which of the more promising engineering prediction methods most accurately and consistently correlates the data. The questions of the existence of a unique relationship between momentum-thickness Reynolds number and skin friction in turbulent-boundary-layer flow and the choice of virtual origin are discussed in light of the experimental results. Since many popular methods successfully predict adiabatic, supersonic skin friction and heating (refs. 5 and 8), only experimental data with significantly low ratios of wall to total temperature (Mach numbers from 4 to 13) have been included. Two-dimensional, zero-pressure-gradient flows with negligible wall-temperature gradient are emphasized, and an extension to conical flow is illustrated.

SYMBOLS

C_f skin-friction coefficient based on local flow conditions

$F_c, F_{R_x}, F_{R_\theta}$ functions defined by equations (1) to (3)

H total enthalpy, $h + \frac{u^2}{2}$

h static enthalpy

M Mach number

N number of data points

N_{Pr} Prandtl number

N_{St} Stanton number, $\frac{\dot{q}}{\rho_e u_e (H_{aw} - H_w)}$

n exponent defined by equation (A5)

$\dot{q}$ wall heat-transfer rate

R local unit Reynolds number, $\frac{\rho_e u_e}{\mu_e}$

R_x local Reynolds number based on distance from leading edge or cone tip

$R_{x,a}$ local Reynolds number based on distance to "best" virtual origin

$R_{x,c}$ local Reynolds number based on distance from virtual origin on cone

$R_{x,i}$ local Reynolds number based on distance to minimum heating near beginning of transition

$R_{x,o}$ local Reynolds number based on distance to virtual origin

$R_{x,p}$ local Reynolds number based on distance to peak heating near end of transition

$R_{x,T}$ local Reynolds number based on distance from virtual origin, $R_x - R_{x,o}$

R_Γ energy-thickness Reynolds number (eq. (38)), $\frac{\rho_e u_e \Gamma}{\mu_e}$

R_θ momentum-thickness Reynolds number based on local flow conditions

$R_{\theta,a}$ momentum-thickness Reynolds number at best virtual origin (eq. (44))

$R_{\theta,i}$ momentum-thickness Reynolds number at location of minimum heating near beginning of transition

$R_{\theta,o}$ momentum-thickness Reynolds number at virtual origin

$R_{\theta,p}$ momentum-thickness Reynolds number at peak heating near end of transition

$R_{\theta,T}$ Reynolds number based on incremental growth of momentum thickness in turbulent flow, $R_\theta - R_{\theta,o}$

r recovery factor

S Reynolds analogy factor, $\frac{2N_{St}}{C_f}$

T temperature

u velocity

x distance along flat plate or cone measured from leading edge or cone apex

Y local cone radius

y distance normal to surface

Γ energy thickness, $\frac{\int_0^x \dot{q}(x) Y^{\epsilon}\, dx}{\rho_e u_e \left(H_w - H_e\right) Y^{\epsilon}}$

γ ratio of specific heats

δ boundary-layer thickness

θ momentum thickness, $\int_0^{\delta} \frac{\rho u}{\rho_e u_e}\left(1 - \frac{u}{u_e}\right)\left(\frac{Y - y}{Y}\right) dy$ for cone, $\int_0^{\delta} \frac{\rho u}{\rho_e u_e}\left(1 - \frac{u}{u_e}\right) dy$ for flat plate

μ dynamic viscosity

ρ density

ϕ cone half-angle

ψ angle of attack

Subscripts:

aw adiabatic wall

c cone

e based on local flow conditions

exp experimental

fp flat plate

Ht heat transfer

N_{St} derived from Stanton number data

Sf skin friction

s reference condition defined in equation (30)

T turbulent

t total or stagnation conditions

th theoretical

w wall conditions

∞ free-stream conditions

Superscripts:

* based on reference temperature conditions

ϵ index, $\epsilon = 0$ for flat plate and $\epsilon = 1$ for cone

A bar over a symbol indicates incompressible flow.

PREDICTION METHODS

The general approach used here to compare flat-plate experimental data with analytical prediction methods is to transform the data to the incompressible plane (according to each prediction scheme) and then compare the transformed data with classical incompressible predictions. By using this approach, experimental data covering a wide range of Mach number and ratio of wall to total temperature can be collectively compared with

a single incompressible prediction. The assumed relationships between the compressible and incompressible variables for references 3 and 9 to 12 can be expressed as:

$$\overline{C}_f = F_c C_f \tag{1}$$

$$\overline{R}_{\bar{\theta}} = F_{R_\theta} R_\theta \tag{2}$$

$$\overline{R}_{\bar{x}} = \int_0^{R_x} \frac{F_{R_\theta}}{F_c} dR_x = F_{R_x} R_x \tag{3}$$

and

$$F_{R_x} = \frac{F_{R_\theta}}{F_c} \tag{4}$$

The parameters F_{R_θ}, F_{R_x}, and F_c are functions of Mach number, ratio of wall to total temperature, and recovery factor only. In reference 13 where F_c and F_{R_θ} are also dependent on x, one must perform an integration to determine $\overline{R}_{\bar{x}}$.

A description of each of the two-dimensional prediction methods will be given below. These particular engineering methods were chosen because of their success in predicting some experimental data (as reported in the literature) and/or because they are the most frequently used engineering predictors in practice.

Eckert (ref. 10)

$$F_c = \frac{T^*}{T_e} \tag{5}$$

$$F_{R_\theta} = \frac{\mu_e}{\mu^*} \tag{6}$$

$$F_{R_x} = \frac{\mu_e T_e}{\mu^* T^*} \tag{7}$$

where

$$\frac{T^*}{T_e} = 0.5\left(\frac{T_w}{T_e} + 1\right) + 0.22\left(\frac{T_{aw}}{T_e} - 1\right) \tag{8}$$

White and Christoph (ref. 9)

$$F_c = \left(F^2 \frac{T_w}{T_e}\right)^{-1} \tag{9}$$

$$F_{R_\theta} = \frac{\frac{\rho_w \mu_e}{\rho_e \mu_w}}{F \frac{T_w}{T_e}} \tag{10}$$

$$F_{R_x} = F\left(\frac{\rho_w \mu_e}{\rho_e \mu_w}\right) \tag{11}$$

where

$$F = \frac{\frac{T_w}{T_e} + 0.22\left(\frac{T_{aw}}{T_e} - 1\right)}{\frac{T_w}{T_e} + 0.3\left(\frac{T_{aw} - T_w}{T_e}\right)} \tag{12}$$

and

$$\frac{T_{aw}}{T_e} = 1 + \left(\frac{\gamma - 1}{2}\right) r M_e^2 \tag{13}$$

Moore (ref. 11)

$$F_c = \left\{ \frac{\left[\sin^{-1}\left(1 - \frac{T_e}{T_w}\right)^{1/2} \right]^2}{1 - \frac{T_e}{T_w}} \frac{T_e}{T_w} Z \right\}^{-1} \tag{14}$$

$$F_{R_\theta} = \frac{0.11557 \exp\left\{0.4\left[11.5 + 6.6\left(1 - \frac{T_w}{T_{aw}}\right)\right]\right\}}{\left[11.5 + 6.6\left(1 - \frac{T_w}{T_{aw}}\right)\right]\frac{\mu_w}{\mu_e}} \tag{15}$$

$$F_{R_x} = \frac{F_{R_\theta}}{F_c} \tag{16}$$

where

$$Z = 0.9212 \exp\left[0.0706\left(1 - \frac{T_e}{T_w}\right)\right] \tag{17}$$

Van Driest II (ref. 12)

$$F_c = \frac{\frac{T_{aw}}{T_e} - 1}{\left(\sin^{-1}\alpha + \sin^{-1}\beta\right)^2} \tag{18}$$

$$F_{R_\theta} = \frac{\mu_e}{\mu_w} \tag{19}$$

$$F_{R_x} = \frac{F_{R_\theta}}{F_c} \tag{20}$$

where

$$\alpha = \frac{\frac{T_{aw}}{T_e} + \frac{T_w}{T_e} - 2}{\left[\left(\frac{T_{aw}}{T_e} + \frac{T_w}{T_e}\right)^2 - 4\frac{T_w}{T_e}\right]^{1/2}} \tag{21}$$

and

$$\beta = \frac{\frac{T_{aw}}{T_e} - \frac{T_w}{T_e}}{\left[\left(\frac{T_{aw}}{T_e} + \frac{T_w}{T_e}\right)^2 - 4\frac{T_w}{T_e}\right]^{1/2}} \tag{22}$$

Note that equations (18), (21), and (22) are modified as in reference 6 to account for non-unity Prandtl number.

Spalding and Chi (ref. 3)

$$F_c = \frac{\frac{T_{aw}}{T_e} - 1}{\left(\sin^{-1}\alpha + \sin^{-1}\beta\right)^2} \tag{23}$$

$$F_{R_\theta} = \left(\frac{T_{aw}}{T_e}\right)^{0.772} \left(\frac{T_w}{T_e}\right)^{-1.474} \tag{24}$$

$$F_{R_x} = \frac{F_{R_\theta}}{F_c} \tag{25}$$

where

$$\alpha = \frac{\frac{T_{aw}}{T_e} + \frac{T_w}{T_e} - 2}{\left[\left(\frac{T_{aw}}{T_e} + \frac{T_w}{T_e}\right)^2 - 4\frac{T_w}{T_e}\right]^{1/2}} \tag{26}$$

$$\beta = \frac{\frac{T_{aw}}{T_e} - \frac{T_w}{T_e}}{\left[\left(\frac{T_{aw}}{T_e} + \frac{T_w}{T_e}\right)^2 - 4\frac{T_w}{T_e}\right]^{1/2}} \tag{27}$$

Coles (ref. 13)

$$F_c = \left(\frac{T_w}{T_e}\right)\left(\frac{\mu_s}{\mu_w}\right) \tag{28}$$

$$F_{R_\theta} = \frac{\mu_e}{\mu_s} \tag{29}$$

where

$$\frac{T_s}{T_w} = 1 - 17.2\left(1 - \frac{T_{t,e}}{T_w}\right)\left(\frac{\overline{C}_f}{2}\right)^{1/2} - 305\left(\frac{T_{t,e} - T_e}{T_w}\right)\left(\frac{\overline{C}_f}{2}\right) \tag{30}$$

Since $F_c = \frac{\bar{C}_f}{C_f} = \left(\frac{T_w}{T_e}\right)\left(\frac{\mu_s}{\mu_w}\right)$ from equation (28) and since μ_s is a function only of T_s, then equations (28) and (30) can be solved by iteration for the two unknowns $\bar{C}_f$ and T_s $\left(C_f \text{ is known from experiment}\right)$.

For all the prediction methods the gas was assumed to be ideal and the viscosity was calculated by the Keyes formula (ref. 14). Therefore, for air

$$\mu = \frac{1.49 \times 10^{-6}\, T^{1/2}}{1 + \frac{122.22}{T} \times 10^{-5/T}} \tag{31}$$

and for helium

$$\mu = 5.026 \times 10^{-7}\, T^{0.647} \tag{32}$$

where T is in K and μ is in N-s/m^2.

Incompressible Prediction

The incompressible equations of Spalding and Chi (ref. 3) were chosen for evaluation of all skin-friction methods (the Spalding and Chi equations are explicit). As shown in reference 8, the incompressible predictions of Kármán-Schoenherr (ref. 15) and Sivells and Payne (ref. 16) show good agreement with the Spalding and Chi results over a wide Reynolds number range $\left(10^2 \leqq \bar{R}_{\bar{\theta}} \leqq 10^5\right)$. The Spalding and Chi incompressible relations are

$$\bar{R}_{\bar{x}} = \frac{1}{12}(u^+)^4 + (K^3E)^{-1}\left\{\left[6 - 4(Ku^+) + (Ku^+)^2\right]\exp(Ku^+) - 6 - 2(Ku^+) - \frac{1}{12}(Ku^+)^4 - \frac{1}{20}(Ku^+)^5 - \frac{1}{60}(Ku^+)^6 - \frac{1}{252}(Ku^+)^7\right\} \tag{33}$$

$$\bar{R}_{\bar{\theta}} = \frac{1}{6}(u^+)^2 + \left[\left(1 - \frac{2}{Ku^+}\right)\exp(Ku^+) + \frac{2}{Ku^+} + 1.0 - \frac{1}{6}(Ku^+)^2 - \frac{1}{12}(Ku^+)^3 - \frac{1}{40}(Ku^+)^4 - \frac{1}{180}(Ku^+)^5\right](KE)^{-1} \tag{34}$$

where

$$K = 0.4$$

$$E = 12$$

and

$$u^+ = \left(\frac{2}{\bar{C}_f}\right)^{1/2}$$

Reynolds Analogy Factor

Since all of the methods described herein are skin-friction prediction methods, it is necessary to define a Reynolds analogy relating skin friction to heat transfer for comparing experimental heat-transfer data with predictions. For Mach numbers less than approximately 5 and near-adiabatic wall conditions, it appears from references 17 and 18 that

$$S = 2\frac{N_{St}}{C_f} = 1.16 \tag{35}$$

adequately represents the available experimental wind-tunnel data. However, for turbulent flow with significant wall cooling and for Mach numbers greater than 5 at any ratio of wall to total temperature the Reynolds analogy factor is ill defined. An analysis of available experimental data for Mach number greater than 5 (ref. 18) found that Kármán's expression for Reynolds analogy best represented the general level of the data; however, more recent data from references 19 and 20 indicate that for local Mach numbers greater than 6 and T_w/T_t less than approximately 0.3 the Reynolds analogy factor scatters around a value of 1.0 (nearly 10 percent less than Kármán's prediction for these conditions). Thus, two definitions for the Reynolds analogy factor were used herein; the first is Kármán's value expressed as

$$S = \left\{1 + 5\left(\frac{F_c C_f}{2}\right)^{1/2}\left[\left(N_{Pr} - 1\right) + \ln\left(\frac{5N_{Pr} + 1}{6}\right)\right]\right\}^{-1} \tag{36}$$

with $N_{Pr} = 0.725$, and the second is

$$S = 1.0 \tag{37}$$

which corresponds to equation (36) with $N_{Pr} = 1.0$.

Momentum Thickness

Unfortunately, corresponding measurements of momentum thickness are not available for most of the experimental skin-friction and heat-transfer data. Therefore, for the data used in the present analysis, the momentum thickness was obtained by integrating heat-transfer distributions over the plate or cone to obtain an energy thickness and relating this energy thickness to momentum thickness through a Reynolds analogy factor (this procedure is completely outlined in ref. 5). From integration of the energy-integral equation and by assuming uniform wall temperature, the energy-thickness Reynolds number is expressed as

$$R_\Gamma = \frac{\int_0^x \dot{q} Y^\epsilon \, dx}{\mu_e \left(H_w - H_e\right) Y^\epsilon} \tag{38}$$

where $\epsilon = 0$ for a flat plate and $\epsilon = 1$ for a cone. Obviously, the experimental heat-transfer distribution $\dot{q}$ must be known from the laminar region of the boundary layer through the transition region and into the turbulent region of interest in order to define R_Γ. For laminar flow ahead of the first measuring station, R_Γ was calculated by assuming $\dot{q} \approx x^{-1/2}$. By assuming a uniform Reynolds analogy factor and recovery factor, momentum-thickness Reynolds number is calculated by

$$R_\theta = \frac{R_\Gamma}{S\left(\frac{H_w - H_{aw}}{H_w - H_e}\right)} \tag{39}$$

where

$$\frac{H_{aw}}{H_e} = \frac{1 + r\left(\frac{\gamma - 1}{2}\right) M_e^2}{1 + \left(\frac{\gamma - 1}{2}\right) M_e^2} \tag{40}$$

The recovery factor r was assumed to vary linearly in the transition region from a value of 0.845 near the beginning of transition (minimum heating) to a value of 0.89 near the end of transition (maximum heating). Although the transitional distribution of recovery factor is more like a Gaussian distribution rather than linear, this assumption introduces insignificant error in the R_θ calculations. Obviously, the accuracy of predicting R_θ will depend on a knowledge of the Reynolds analogy factor S which, as discussed earlier, is not well defined by available data.

One set of experimental data exists which allows a comparison between values of R_θ from measured boundary-layer profiles and values obtained from integrating heat-transfer distributions (eqs. (38) and (39)). The profiles and resulting R_θ values were obtained from reference 21, and the corresponding heat-transfer distributions (unpublished) were obtained from T. E. Polek of NASA Ames Research Center. The experiments were for local Mach numbers from 6.3 to 7.8 and ratios of wall to total temperature from 0.26 to 0.45. The comparisons are made for three values of S in figure 1 where R_θ from heat transfer (Polek) is plotted against R_θ from profiles (ref. 21) with the line of perfect agreement shown in each case. These data indicate that the best agreement between the two approaches for determining R_θ is obtained when Kármán's Reynolds analogy is used and the worst agreement is for $S = 1.0$. This result was unexpected since skin friction measured simultaneously with this heat-transfer data indicated that the Reynolds analogy factor was nearer to 1.0 than to Kármán's values (ref. 19); however, the assumptions necessary to convert heating distributions to momentum thickness could account for a portion of this disagreement. At any rate, it is obvious from figure 1 that integration of heat-transfer distributions can provide an adequate representation of the momentum-thickness Reynolds number. For the purpose of this investigation the R_θ values from heat-transfer distributions are considered sufficiently accurate since a small error in R_θ will cause an even smaller error in skin-friction or heating predictions (error in C_f or N_{St} would only be approximately 1/4 the error in R_θ).

Virtual-Origin Concepts

Each of the prediction methods discussed herein assumes that the flow is fully turbulent and that the origin of turbulent flow is at $x = 0$. In low-speed flow, where transition Reynolds numbers are generally low, transition can occur very near the leading edge, and the assumption of turbulent flow from $x = 0$ may be plausible. However, boundary-layer transition in high-speed flow does not, in general, occur very near the leading edge and in fact may occur far downstream for high Mach numbers. The turbulent boundary layer which results from a laminar boundary layer having undergone transition far downstream of the leading edge will obviously have a hypothetical origin $(x_T = \theta_T = 0)$ not corresponding to $x = 0$; this origin has commonly been called the virtual origin. If this virtual origin is defined correctly, predictions of C_f or N_{St} based on either a length or

momentum-thickness Reynolds number measured from the virtual origin should be consistent and equally valid.

Perhaps the most common means of obtaining a virtual origin for turbulent flow is to assume that the skin-friction coefficient (heat-transfer coefficient) is a unique function of the momentum-thickness Reynolds number; then backward extrapolation from a value of R_θ in the turbulent region to zero yields the virtual-origin location. In several investigations (e.g., refs. 6 and 8) the use of this approach is defended by the assertion that an arbitrary definition of the origin of turbulent flow does not have to be made; however, by assuming that C_f varies uniquely with R_θ an equally arbitrary definition of the virtual origin is specified. The integral momentum equation shows that skin friction varies uniquely with the slope of R_θ with R_x; this, however, does not imply that C_f is a unique function of R_θ itself. In references 22, 23, and 24, Coles discusses the question of uniqueness and concludes that for turbulent flow the test of uniqueness will depend upon experiment and not analytical considerations.

In the present investigation, virtual origins are chosen by using both the assumption that C_f is unique in R_θ and that it is not. When it is assumed that C_f is not a unique function of R_θ, then R_θ in turbulent flow can be defined as

$$R_\theta = R_{\theta,o} + R_{\theta,T} \tag{41}$$

where $R_{\theta,o}$ is the value of R_θ at the virtual-origin location and $R_{\theta,T}$ is the turbulent contribution downstream of the virtual origin (see illustration in fig. 2). Obviously $R_{\theta,o}$ will be composed of the laminar or laminar and transitional-momentum deficit and will probably depend on all the variables that affect transition Reynolds numbers (ref. 25). In a similar manner R_x is defined as

$$R_x = R_{x,o} + R_{x,T} \tag{42}$$

Both $R_{\theta,o}$ and $R_{x,o}$ are defined at the virtual origin where $R_{\theta,T}$ and $R_{x,T}$ equal zero (see fig. 2 for a graphical description of these Reynolds numbers). Also, both $R_{\theta,o}$ and $R_{x,o}$ are independent of x for a given flow case (i.e., they depend on the virtual-origin location which is at a constant x-value). When equations (41) and (42) are differentiated the conventional integral momentum equation is preserved as

$$\frac{dR_\theta}{dR_x} = \frac{dR_{\theta,T}}{dR_{x,T}} = \frac{C_f}{2} \tag{43}$$

Numerous investigations have assumed equation (42) to be valid (e.g., refs. 26 and 27) in analyzing experimental turbulent skin friction and heating with $R_{x,o}$ evaluated at the location of peak heating or shear near the end of transition. For the present investigation the location of $R_{x,o}$ $\left(\text{and thus } R_{\theta,o}\right)$ is not specified a priori, but large quantities of experimental data are utilized for an empirical definition of the best and most consistent location for the virtual origin.

EXPERIMENTAL DATA

As stated earlier, turbulent predictions for two-dimensional subsonic and low-supersonic adiabatic flows are well in hand for both engineering methods (ref. 5) and finite-difference methods (ref. 28). For this investigation a comprehensive literature survey was made for data in the region where turbulent-boundary-layer predictions are more questionable ($M > 4$ and flows with significant heat transfer). The available skin-friction and heat-transfer data for two-dimensional turbulent boundary layers (flat-plate-type flows with nominally zero pressure and wall-temperature gradients) were compiled. Flight data were not included since most of these data do not meet the flat-plate-type flow criteria and, furthermore, a major portion of these data are classified. A limited amount of heating data obtained in wind tunnels on sharp tip cones at zero angle of attack were included, however, to test the extension of the prediction methods to conical-type flows.

Only skin-friction data directly measured with gages and heating data obtained by transient techniques (considered most accurate) are included in this analysis. In order to define the momentum-thickness distribution the entire heating distribution (from laminar, through transitional, and into the turbulent flow) must be known; therefore, only skin-friction or heat-transfer data for which the heating distribution through transition was specified were included in this analysis. The range of conditions covered by the available experimental data is shown below:

Type flow	Type data	References	M_e range	T_w/T_t range	No. of data points
Two-dimensional	C_f	5, 20, 21, 29, 30	6.4 to 12.9	0.14 to 0.47	270 (85 for $M > 10$)
	N_{St}	5, 20, 29 to 34	4.0 to 12.9	.14 to .70	1523 (232 for $M > 10$)
Conical $5^o \leqq \theta_c \leqq 15^o$	N_{St}	26, 35, 36	4.2 to 8.8	0.10 to 0.64	296

In addition to data referred to above, several sets of unpublished data were utilized as listed below:

Type flow	Experimenter	Location	Type data	M_e range	T_w/T_t range
Two-dimensional	E. L. Morrisette	NASA Langley	N_{St}	6.0	0.60
	T. E. Polek	NASA Ames	N_{St}	6.2 to 7.8	0.26 to 0.45
	D. V. Maddalon	NASA Langley	N_{St} (helium)	6.7	0.45 to 0.67
Cone	G. C. Mateer	NASA Ames	N_{St}	4.9 to 6.6	0.10 to 0.54

The number of data points given includes the above unpublished data. Real gas effects were negligible for all experimental data included in this analysis; therefore, temperature and enthalpy ratios are equivalent.

Flow conditions and pertinent transition data for two-dimensional-flow cases are presented in table I for the skin-friction data and in table II for the heat-transfer data. The various parameters are given for each individual skin-friction or heating distribution (each individual data run). The R_x and R_θ values are given for both the beginning and end of transition. Each data run is assigned an identity number and a symbol as shown in the tables; thus, tables I and II can be used to identify symbols used on subsequent figures 3 to 23. Listings of the skin-friction coefficients are given in table III and heat-transfer coefficients in table IV for all the two-dimensional data used in this investigation. Also included with the data listings are the Reynolds number based on x and on θ. For these listings a Reynolds analogy factor of 1.16 was used to determine R_θ (see eq. (39)); however, R_θ may be converted for any other Reynolds analogy factor simply by multiplying R_θ by the ratio of 1.16 to the new Reynolds analogy factor. All of the data listed are in the "turbulent region" of the boundary layer downstream of transition. The first data point listed for each run is the first experimental point located at a Reynolds number based on the distance from peak heating near the end of transition greater than 1/3 the Reynolds number based on the distance to peak heating $\left(\text{i.e., } \left(R_x - R_{x,p}\right)\Big/R_{x,p} > 1/3\right)$; this minimum value of Reynolds number for turbulent flow was chosen based on the results of reference 26. Each data listing has an identity number which corresponds to the identity numbers given in tables I and II. The flow conditions and data listings for the conical heat-transfer data are given in tables V and VI, respectively.

COMPARISONS OF PREDICTIONS WITH EXPERIMENTAL DATA

Comparisons of experimental data with predictions will be made in the incompressible plane allowing simultaneous comparisons of all data with a given prediction method.

The experimental data were transformed to their corresponding incompressible values by using computer calculations, and comparison figures were obtained from Calcomp data plotters. The general format for presentation shows transformed heat-transfer data against transformed Reynolds number with the incompressible prediction, transformed skin-friction data against transformed Reynolds number with the incompressible prediction, and error plots indicating variation of the difference between experiment and prediction (hereafter called "error") as a function of both the ratio of wall to total temperature and local Mach number. Each symbol on the error plots represents a numerical average of differences between data and prediction for one data run (the data included under one identity number in tables III, IV, and VI). The error spread for any data run is indicated by the dashed bar through each symbol. With the data presented in this form, the criteria used herein to judge which is the best prediction method are:

(1) The level of the transformed data relative to the level of incompressible prediction

(2) The slope with Reynolds number of the transformed data relative to the slope of incompressible prediction

(3) The consistency between comparisons of heating and skin friction (agreement of data and prediction should be same for both)

(4) The distribution of errors (i.e., difference between data and prediction) with either ratio of wall to total temperature or local Mach number (there should be no obvious trend in errors with either parameter)

In addition to these criteria, the additional requirement that the transformed data and the incompressible prediction agree at high Reynolds number regardless of the choice of virtual-origin location is obviously necessary.

Two-Dimensional Predictions $\left(M_e \leq 10\right)$

Comparisons of transformed data with predictions are shown in figures 3 to 8 for each of the six prediction methods assuming that C_f is a unique function of R_θ and $S = 1.0$ (these assumptions are recommended in refs. 5, 6, 8, and 21). Only data for M_e less than 10 is first considered; the higher Mach number data will be included later. From these figures we can select more promising calculation methods for further consideration.

Van Driest II.- The Van Driest II method (ref. 12) as shown in figure 3 was found in references 5, 6, 8, and 21 to be the best turbulent prediction method for a collection of experimental data. However, for this larger collection of data covering a wider range of conditions, both the transformed heat transfer and skin friction show disagreement with the trend of the incompressible curves; the data are underpredicted at low $F_{R_\theta} R_\theta$ and

overpredicted at high $F_{R_\theta} R_\theta$. Since the transformed data do not asymptotically approach the incompressible values at high $F_{R_\theta} R_\theta$, the choice of a sensibly different virtual origin will not remedy this disagreement. Another disturbing feature of this method is that the disagreement between data and prediction appears to be a function of the ratio of wall to total temperature as shown at the bottom of figure 3. This temperature dependency will not be modified by choosing other values of the virtual origin or Reynolds analogy factor. The disagreement does not appear to be a function of M_e. While the Van Driest II method predicts the data reasonably well for a range of Reynolds number $\left(10^3 \leqq F_{R_\theta} R_\theta \leqq 5 \times 10^3\right)$ and ratio of wall to total temperature $\left(0.25 \leqq T_w/T_t \leqq 0.5\right)$, the overall agreement is considered unsatisfactory.

Spalding and Chi.- The data transformed according to the Spalding and Chi method (ref. 3) are shown in figure 4. The slope of the transformed data does not agree with the slope of the incompressible curve; however, the data do appear to be approaching the incompressible results at high values of $F_{R_\theta} R_\theta$. Since the slope of the transformed data can be modified $\left(\text{at least for moderate } F_{R_\theta} R_\theta\right)$ by defining a different virtual origin, it is thus possible to bring the slope of the transformed data into better agreement with the incompressible slope (this will be attempted after all the prediction methods have been compared). There is no significant trend of the relative errors for the Spalding and Chi method with either T_w/T_t or M_e (see bottom of fig. 4).

Coles.- The Coles method (ref. 13) shown in figure 5 was found in references 5, 6, 8, and 21 to provide good predictions of experimental data for $T_w/T_t > 0.3$. When applied to the large mass of data here, the Coles method apparently does not achieve the same slope of the transformed data as the incompressible curve for either heat transfer or skin friction; also, the transformed data are not asymptotically approaching the incompressible results at high Reynolds number. Thus, as for the Van Driest method, a different choice of virtual origin will not bring the transformed data into agreement with the incompressible results. At the bottom of figure 5, it is apparent that the prediction errors are even more strongly dependent on T_w/T_t than was found for the Van Driest method and are not apparently dependent on local Mach number; this again indicates a functional deficiency in the formulation of the method. Therefore, it appears that the Coles method will not, in general, provide adequate predictions regardless of the virtual origin or Reynolds analogy factor chosen.

Eckert.- The Eckert method (ref. 10) shown in figure 6 has historically been popular for predicting turbulent heating and skin friction because of the simplicity of a reference

enthalpy approach. The data transformed according to the Eckert method as shown in figure 6 do not match the trend with Reynolds number of the incompressible curve but do appear to be approaching the incompressible level at high Reynolds numbers. Thus, the proper choice of virtual origin could conceivably bring the transformed data into better agreement with the incompressible slope. However, the prediction errors shown at the bottom of figure 6 indicate that the Eckert method also does not properly account for the functional dependence of turbulent skin friction and heating on temperature. Thus, the Eckert method will not, in general, provide reliable estimates.

Moore.- The Moore method (ref. 11) was found in reference 6 to give good predictions of skin friction at high Reynolds numbers but to underpredict the data at lower Reynolds numbers and was found in reference 9 to be the best of six prediction methods. The data transformed according to the Moore method are shown in figure 7 for the present collection of data. The slope of a fairing of the transformed data would be significantly different from the incompressible results with the disagreement between data and prediction increasing with increasing Reynolds number. This, along with the strong temperature dependency of the error function (see bottom of fig. 7), shows that the Moore method is unacceptable; thus, it is not further considered in this investigation.

White and Christoph.- The method of White and Christoph was described in reference 9 where it was found that for their collection of data with heat transfer the rms error of the method was about the same as for the Van Driest II, Moore, and Spalding and Chi methods. The present data transformed according to the White and Christoph method are shown in figure 8 along with the prediction errors. Adverse conclusions for the White and Christoph method similar to those for the Moore method are obvious from figure 8. The wide disparity between transformed data and the incompressible results at high Reynolds number and the strong dependence of the error function on temperature (bottom of fig. 8) preclude any further consideration herein of the White and Christoph method.

Improvement of Predictions

None of the prediction methods applied as shown in figure 3 to 8 satisfies the criteria for a "good" engineering prediction method as discussed earlier. The Spalding and Chi method is promising since prediction errors were apparently random (not a discernable function of either T_w/T_t or M_e) and the transformed data are approaching the incompressible prediction at high Reynolds numbers (see fig. 4). Agreement between the transformed data and the incompressible prediction at low $F_{R_\theta} R_\theta$ can be improved by a judicious choice of a virtual origin and of S when the turbulent boundary layer is assumed to be nonunique. Various virtual-origin locations (or $R_{\theta,o}$ values, see discussion on Virtual-Origin Concepts) were selected for the Spalding and Chi method, and the resulting transformed data were compared with the incompressible results until optimum agreement

was obtained. The best virtual origin resulting from these comparisons was the location where

$$R_{\theta,o} = \frac{R_{\theta,i} + R_{\theta,p}}{2} = R_{\theta,a} \tag{44}$$

At this location $R_{\theta,T}$ was assumed to be zero and downstream of the virtual origin, therefore

$$R_{\theta,T} = R_{\theta} - R_{\theta,a} \tag{45}$$

Results obtained by using this virtual origin and Kármán's Reynolds analogy factor with the Spalding and Chi method are shown in figure 9(a) for the momentum-thickness Reynolds number correlation. The transformed heat-transfer and skin-friction data now, in general, agree with the slope and level of the incompressible prediction over the entire Reynolds number range. Prediction errors are not strongly dependent on T_w/T_t or M_e (see bottom of fig. 9(a)). Disagreement between transformed data and the prediction generally falls within a band of ±20 percent with a mean error near zero.

If this choice of virtual origin is realistic, then equally good results should be obtained when the data are correlated on the corresponding R_x basis. In order to be consistent, the length Reynolds number should be based on the same virtual origin as was used for the R_{θ} correlation; this Reynolds number is defined as

$$R_{x,T} = R_x - R_{x,a} \tag{46}$$

where $R_{x,a}$ corresponds to the x-location where $R_{\theta,o}$ occurs for each case. Thus when $R_x = R_{x,a}$, then $R_{\theta} = R_{\theta,a}$ and $R_{x,T} = R_{\theta,T} = 0$. The results of this transformation are shown in figure 9(b) again using Kármán's Reynolds analogy. The slope and level of a fairing of the transformed data again agree well with the incompressible results, and the prediction errors are of equivalent magnitude as for the correlation of $F_c C_f$ against $F_{R_\theta}\left(R_{\theta} - R_{\theta,a}\right)$. Therefore, this definition of the virtual origin appears to provide a consistent and accurate prediction of turbulent heating and skin friction when used with the Spalding and Chi method.

Since the momentum-thickness distribution is not usually known a priori, the definition of the virtual origin as the location where $R_{\theta} = R_{\theta,a}$ does not facilitate engineering calculations. To define better the virtual origin corresponding to the $R_{\theta,a}$ location, the

values of $R_{x,a}$ corresponding to $R_{\theta,a} = \frac{R_{\theta,i} + R_{\theta,p}}{2}$ are shown in figure 10 as the ratio of $R_{x,a}/R_{x,p}$ against $R_{\theta,a}/R_{\theta,p}$ for the present data. Approximately 98 percent of the data fall in the range $0.8 \leqq R_{x,a}/R_{x,p} \leqq 0.87$ with a mean value of $R_{x,a}/R_{x,p} = 0.825$; thus, the best virtual origin is located slightly upstream of the end of transition as hypothesized in reference 37. The values of $R_{\theta,a}/R_{\theta,p}$ show a wider variation than $R_{x,a}/R_{x,p}$ and fall between $0.67 \leqq R_{\theta,a}/R_{\theta,p} \leqq 0.78$ with a mean value of approximately 0.722. By using the definition of $R_{\theta,a}$, it can be shown that if $R_{\theta,a}/R_{\theta,p} = 0.722$ then $R_{\theta,p}/R_{\theta,i} \approx 2.25$; this is analogous to the result $R_{x,p}/R_{x,i} \approx 2$ found in many experimental investigations of high-speed flow (e.g., ref. 20), and approximately true for the present data. The transition data from table II are shown in figure 11 as $R_{\theta,p}$ against $R_{\theta,i}$ and show that the ratio $R_{\theta,p}/R_{\theta,i}$ is equal to 2.25 ± 15 percent for the present data. While these results are only approximate, their consistency, along with the fact that a small error in R_θ does not appreciably affect predicted skin friction or heating, justifies their use to determine $R_{x,a}$ or $R_{\theta,a}$. The outlined approach for determining the virtual origin assumes a knowledge of the location of boundary-layer transition; however, the location of transition is a necessary input to any analysis of high-speed heating or drag.

If, as in figure 12, the location of the virtual origin is assumed to be the same as the location of peak heating near the end of transition $\left(R_{x,o} = R_{x,p}\right)$ as suggested in references 26 and 27, the resulting comparison of the data transformed by the Spalding and Chi method with the incompressible prediction is nearly the same as for the best virtual origin (compare figs. 9(b) and 12). This result is expected since the best virtual origin was located only slightly upstream of peak heating at transition.

No attempt was made to determine a best virtual origin for prediction methods other than the Spalding and Chi method because none of the other methods satisfies all the criteria for a good engineering prediction method. However, for comparison purposes the methods previously shown to be more promising (Van Driest II, Eckert, and Coles) are shown in figures 13 to 15 using Kármán's Reynolds analogy factor and in figures 16 to 18 using the Reynolds analogy factor equal unity; the virtual origin is the best origin determined from the Spalding and Chi method in both cases. An appraisal of figures 13 to 18 shows that the use of virtual-origin concepts does not improve the high Reynolds number asymptotic behavior of the transformed data for any of these methods, and the temperature dependence of the prediction error is not affected. Note, however, that the Eckert method with Kármán's analogy and the Coles and Van Driest methods with $S = 1.0$ predict the data within approximately ±20 percent, but the error depends on the ratio of wall to total temperature.

One way by which the temperature dependence of the prediction error for heat transfer can be changed is to use a Reynolds analogy factor which is a function of temperature. In an attempt to improve the heating predictions of the Van Driest II method as applied in references 5, 6, 8, and 21 (see fig. 3 of this report), two different definitions of a temperature dependent Reynolds analogy factor were assumed, the first being Kármán's and the second being an empirical variation based upon experimental evidence (refs. 18, 19, and 20). Kármán's Reynolds analogy factor varies nonlinearly from approximately 1.08 at $T_w/T_t \approx 0.1$ to 1.17 at $T_w/T_t \approx 1.0$, while the empirical factor varies linearly from 1.0 at $T_w/T_t = 0.1$ to 1.16 at $T_w/T_t = 1.0$. The resulting comparisons of transformed data and the incompressible prediction are shown in figure 19 where Kármán's factors are used and in figure 20 where the empirical factors are used. Including the temperature variation of Kármán or the empirical Reynolds analogy tends to reduce the error dependence on temperature but the overall prediction accuracy is not significantly better than when $S = 1.0$ (compare figs. 19 and 20 with fig. 3). In addition, the overall trend with Reynolds number of the transformed data relative to the incompressible prediction is not improved.

A summary of the errors between prediction and experiment for various methods is presented in table VII which includes both a mean error defined by

$$\text{Mean error } (\%) = \frac{\sum^{N} \left(\Delta C_f\right)}{N} \times 100 \tag{47}$$

$$\text{Mean error } (\%) = \frac{\sum^{N} \left(\Delta N_{St}\right)}{N} \times 100 \tag{48}$$

and a root-mean-square error defined by

$$\text{rms error } (\%) = \left[\frac{\sum^{N} \left(\Delta C_f\right)^2}{N}\right]^{1/2} \times 100 \tag{49}$$

or

$$\text{rms error } (\%) = \left[\frac{\sum^{N} \left(\Delta N_{St}\right)^2}{N}\right]^{1/2} \times 100 \tag{50}$$

where

$$\Delta C_f = \frac{C_{f,exp} - C_{f,th}}{C_{f,th}} \qquad \Delta N_{St} = \frac{N_{St,exp} - N_{St,th}}{N_{St,th}}$$

In these equations, N is the number of data points. Table VII shows that the Spalding and Chi method using the best virtual-origin location is the most accurate of the prediction techniques investigated for Mach numbers less than 10. Thus, this analysis of six engineering prediction methods for turbulent skin friction and heating in two-dimensional boundary layers for Mach numbers less than 10 has shown that the Spalding and Chi method utilizing virtual-origin concepts best meets the specified criteria for a good prediction method. All the other methods have defects which limit their use to a more specific range of flow variables.

Two-Dimensional Predictions $(M_e > 10)$

One set of experimental data (ref. 20) is available where two-dimensional turbulent skin friction and heat transfer were obtained for local Mach numbers greater than 10 and with high local unit Reynolds numbers. The high Mach number results were not included in the previous discussion because they were not consistent with the data for $M_e \leqq 10$. These high Mach number data along with the lower Mach number results were transformed according to the Spalding and Chi method using the best virtual origin and the Van Driest II and Coles methods assuming C_f is a unique function of R_θ and are shown in figures 21, 22, and 23, respectively. The data for $M_e < 10$ are shown by the shaded regions on the error plots. The transformed data for $M_e > 10$ (ref. 20) do not appear to follow the trends of the data for $M_e < 10$ (see error plots at the bottom of figs. 21, 22, and 23). The prediction errors for these high Mach number data deviate markedly from the errors for $M_e < 10$ with the deviation becoming larger with increasing M_e; however, the Coles method is obviously superior to the other methods for predicting these high Mach number data. While this unexpected trend may be an effect of Mach number, it is possible that the data at high Mach numbers (particularly for $M_e = 11$ to 13) are more characteristic of low Reynolds number turbulent flows (ref. 38) which are not equivalent to "equilibrium" turbulent flows. The mean and rms errors for all the data $(4 < M_e < 13)$ are presented in the lower portion of table VII for the prediction methods as shown in figures 21, 22, and 23. Obviously much more data for local Mach numbers greater than 10 and over a large Reynolds number range are needed before a definitive conclusion as to the best engineering predictions method for $M_e > 10$ can be made.

Cone Predictions

The two-dimensional turbulent prediction methods can be extended to predict conical turbulent flows for sharp tipped cones at $\psi = 0^{o}$. A suitable cone-to-flat-plate transformation must be defined such that the conical data can be transformed to two-dimensional data and subsequently transformed to incompressible form according to each prediction method. For comparison purposes a representative sample of high-speed cone heat-transfer data was transformed according to the best two-dimensional prediction method found for two-dimensional flow (Spalding and Chi). The logic and equations for this procedure are presented in appendix A. These transformed turbulent heat-transfer data are compared in figure 24(a) and 24(b) with the incompressible prediction on both an R_{θ} and an R_{x} basis. The virtual origin was taken at the same location as for the best two-dimensional prediction. In figure 24 the transformed data agree in both level and trend with the incompressible prediction with a slight deviation at the lower Reynolds numbers. The prediction errors (bottom of fig. 24) fall between ±20 percent, as was true for the two-dimensional results, and the mean and rms errors are approximately the same as those for the two-dimensional results (see top of fig. 24). The prediction errors are not significantly affected by either ratio of wall to total temperature or local Mach number (see the bottom of fig. 24). It is therefore apparent that with a reasonable choice of a cone-to-flat-plate transformation, the Spalding and Chi method can provide a good prediction of cone heat transfer as well as for two-dimensional cases.

An outline of the recommended procedure for calculating both two-dimensional and conical turbulent boundary-layer skin friction and heat transfer is presented in appendix B. These recommendations are derived from the results of this investigation, and it is believed that this procedure will provide the most accurate and consistent engineering prediction method for high-speed turbulent flows available $\left(\text{at least for } M_{e} \leq 10\right)$.

CONCLUDING REMARKS

A large collection of experimental high-speed wind-tunnel data for two-dimensional turbulent boundary layers was used to determine which of the available engineering methods most accurately predicts turbulent skin friction and heat transfer. A limited amount of data for sharp cones was included to test the extension of the prediction methods to axisymmetric flows. The experimental data cover a range of Mach number from 4 to 13 and a range of ratio of wall to total temperature from 0.1 to 0.7. The six prediction methods chosen for comparison with the data are the most frequently used engineering methods for high-speed flow in the literature.

The use of virtual-origin concepts was shown to be reasonable and necessary for consistent predictions of skin friction and heating, and the prediction effort was not appreciably increased. The Spalding and Chi method using Kármán's Reynolds analogy was

shown to give the best predictions based either on a length or momentum-thickness Reynolds number when the proper virtual origin was specified. The prediction errors for the Spalding and Chi method were independent of Mach number ($M \leq 10$) and ratio of wall to total temperature and were lower than those for the other methods; other popular prediction methods were shown to produce errors which were larger and/or depended on the ratio of wall to total temperature. Turbulent heat transfer for conical flows was equally well predicted by the Spalding and Chi method when an appropriate cone-to-flat-plate-transformation was used. The small amount of available experimental data for Mach numbers greater than 10 were not well predicted by any of the engineering methods except the Coles method. Recommended calculation procedures for two-dimensional and conical turbulent flow are outlined in detail.

Langley Research Center,
National Aeronautics and Space Administration,
Hampton, Va., March 7, 1974.

APPENDIX A

TURBULENT PREDICTIONS FOR CONICAL FLOW BY THE SPALDING AND CHI METHOD

Experimental values of the heat-transfer coefficient and Reynolds numbers for the cone are transformed to the corresponding compressible flat-plate values and then transformed to incompressible form by using the conventional transformation functions for the Spalding and Chi method as described earlier in the text. The cone-to-flat-plate transformation is accomplished by defining the ratios of flat-plate-to-cone heat transfer, skin friction, and momentum thickness for the given compressible cone Reynolds number according to the method outlined below.

Flat-plate values of C_f, N_{St}, and R_θ for a given R_x are calculated from the flat-plate Spalding and Chi method as previously described. Cone values of C_f, N_{St}, and R_θ are calculated by using a modification of Van Driest's cone solution (ref. 39). Van Driest's results show that skin-friction coefficients on a cone and flat plate ($\psi = 0^o$) will be identical if

$$R_{x,c} = 2R_{x,fp} \tag{A1}$$

and the flow is entirely turbulent. If transition occurs along the cone, equation (B4) of reference 26 provides the following relationship between the cone and flat-plate Reynolds numbers at the same value of skin friction:

$$\frac{R_{x,c}}{R_{x,fp}} = \frac{2n - 1}{n - 1}\left[\left(1 + \frac{R_{x,o}}{R_{x,c}}\right) - \frac{R_{x,o}}{R_{x,c}}\left(\frac{\frac{R_{x,o}}{R_{x,c}}}{1 + \frac{R_{x,o}}{R_{x,c}}}\right)^{\frac{n}{n-1}}\right]^{-1} \tag{A2}$$

where $R_{x,o}$ is the Reynolds number based on the distance from the cone tip to the virtual origin of turbulent flow and $R_{x,c}$ is based on the distance from the virtual origin. Equations (A1) and (A2) should provide the same result when $R_{x,o} = 0$ (all turbulent flow), but this is only strictly true when $n = \infty$. For this case equation (A2) becomes

$$\frac{R_{x,c}}{R_{x,fp}} = 2\left(1 + \frac{\dfrac{R_{x,o}}{R_{x,c}}}{1 + \dfrac{R_{x,o}}{R_{x,c}}}\right)^{-1} \tag{A3}$$

Thus, in practice $R_{x,c}$ and $R_{x,o}$ are known; from equation (A3) $R_{x,fp}$ is obtained, and from the Spalding and Chi method $C_{f,fp}$ is calculated $\left(M_e \text{ and } T_w/T_e \text{ are also known}\right)$. This value of $C_{f,fp}$ is now taken as $C_{f,c}$.

An alternative to using equation (A3) is to use equation (B4) of reference 26 along with the correct definition of n $\left(\text{the exponent in the equation } C_f \propto R^{-1/n}\right)$. Equation (B4) of reference 26 may be written as

$$\frac{C_{f,c}}{C_{f,fp}} = \left(\frac{2n - 1}{n - 1}\right)^{1/n}\left[1 + \frac{R_{x,o}}{R_{x,c}} - \frac{R_{x,o}}{R_{x,c}}\left(\frac{\dfrac{R_{x,o}}{R_{x,c}}}{1 + \dfrac{R_{x,o}}{R_{x,c}}}\right)^{\frac{n}{n-1}}\right]^{-1/n} \tag{A4}$$

when the cone and flat-plate Reynolds numbers are taken to be the same. The exponent n may be obtained by comparing the skin-friction power law with the Spalding and Chi incompressible skin-friction relation as a function of $F_{R_x}R_{x,c} = F_{R_x}R_{x,fp}$. This relationship for n can be expressed as

$$n = 0.429 + 0.404 \ln\left(F_{R_x}R_{x,c}\right) \tag{A5}$$

within 1 percent for $10^5 \leqq F_{R_x}R_{x,c} \leqq 10^9$. Thus, by knowing $R_{x,c}$, M_e, and T_w/T_e the value of n can be calculated from equation (A5); then, along with $R_{x,o}$, the ratio $C_{f,c}/C_{f,fp}$ is obtained from equation (A4). The values of $C_{f,fp}$ for the given Reynolds number $\left(R_{x,fp} = R_{x,c} \text{ in this case}\right)$ are calculated from the Spalding and Chi method, and the product of $C_{f,c}/C_{f,fp}$ and $C_{f,fp}$ gives $C_{f,c}$.

For comparison of these two methods of calculating cone skin friction, a plot of $C_{f,c}/C_{f,fp}$ against $F_{R_x}R_x$ is presented in figure 25 for $n = \infty$, $n = n\left(F_{R_x}R_x\right)$, and

$n = 4$ as used in reference 26. Flow conditions for figure 25 were chosen to be typical of data presented herein as $M_e = 6.63$, $T_w/T_t = 0.28$, and a cone semiapex angle of 5^o. Predictions are shown for $R_{x,o} = 0$ and 8.6×10^6. Curves for $n = \infty$ and $n = n\left(F_{R_x} R_x\right)$ agree within about 3 percent over the entire Reynolds number range for either virtual origin; the $n = 4$ results are substantially different from the other curves, particularly at the higher Reynolds numbers. The $n = 4$ transformation is obviously incorrect because of the large disagreement with Van Driest's cone solution. Since the $n = \infty$ and $n = n\left(F_{R_x} R_x\right)$ transformations are essentially equivalent and agree with Van Driest's solution for $R_{x,o} = 0$, the more simple $n = \infty$ transformation (eq. (A3)) was used herein to calculate the ratio of cone-to-flat-plate skin friction as a function of cone Reynolds number. Equation (A3) also yields exactly Van Driest's cone transformation in the limit of $R_{x,o}$ approaching zero.

The cone Stanton number was calculated for a given Reynolds number by using Kármán's Reynolds analogy as

$$2\frac{N_{St,c}}{C_{f,c}} = S_c = \left\{1 + 5\sqrt{\frac{F_c C_{f,c}}{2}}\left[\left(N_{Pr} - 1\right) + \ln\left(\frac{5N_{Pr} + 1}{6}\right)\right]\right\}^{-1} \tag{A6}$$

where $N_{Pr} = 0.725$. Thus, $N_{St,c}$ was obtained from equation (A6) and the flat-plate Stanton number $N_{St,fp}$ from the Spalding and Chi method at the same Reynolds number to give the ratio of $N_{St,c}$ to $N_{St,fp}$ as a function of cone Reynolds number. The cone momentum-thickness Reynolds number was obtained from integration of the momentum equation for conical flow. This equation is

$$R_{\theta,c} = \frac{1}{2\left(R_{x,o} + R_{x,c}\right)} \int_0^{R_{x,c}} \left(R_{x,o} + R_{x,c}\right) C_{f,c}\, dR_{x,c} \tag{A7}$$

where $R_{x,c}$ is measured from the virtual-origin location. Note that the total cone R_θ is the sum of $R_{\theta,c}$ from equation (A7) and the value of R_θ at the virtual origin. Thus from the value of $R_{\theta,c}$ in equation (A7) and the corresponding flat-plate value of R_θ from Spalding and Chi the ratio $R_{\theta,c}/R_{\theta,fp}$ is obtained as a function of Reynolds number.

The experimental input data is $N_{St,c}$, $C_{f,e}$, $R_{x,c}$, $R_{\theta,c}$, $R_{x,o}$, and $R_{\theta,o}$. These cone data are transformed to corresponding flat-plate values by the following relations:

$$R_{x,fp} = R_{x,c} \tag{A8}$$

$$R_{\theta,fp} = R_{\theta,c}\left(\frac{R_{\theta,fp}}{R_{\theta,c}}\right) \tag{A9}$$

$$N_{St,fp} = N_{St,c}\left(\frac{N_{St,fp}}{N_{St,c}}\right) \tag{A10}$$

$$C_{f,fp} = C_{f,c}\left(\frac{C_{f,fp}}{C_{f,c}}\right) \tag{A11}$$

Once the cone data are converted to flat-plate quantities by using equations (A8) to (A11), the compressible to incompressible transformation is accomplished as previously described for flat-plate data.

APPENDIX B

RECOMMENDED CALCULATION PROCEDURE $\left(M_e \leq 10\right)$

Two-Dimensional Flow

It is assumed that the following quantities are known for a two-dimensional perfect-gas boundary-layer flow:

(1) Local Mach number M_e

(2) Ratio of wall to total temperature T_w/T_t

(3) Local unit Reynolds number R

(4) Recovery factor r

(5) Prandtl number N_{Pr}

(6) Transition location

The values of recovery factor and Prandtl number used for all the present calculations were:

$r = 0.845$ for laminar flow

$r = 0.89$ for turbulent flow

$N_{Pr} = 0.725$

The procedure for calculating local C_f or N_{St} based on R_x is as follows:

(1) Calculate F_c, F_{R_θ}, and F_{R_x} from equations (23) to (27)

(2) Specify R_x locations at which calculations are to be made. Let
$R_{x,T} = R_x - R_{x,a} = R_x - 0.825R_{x,p}$

(3) Form the product $F_{R_x}R_{x,T}$ and obtain corresponding F_cC_f from equation (33)

(4) If N_{St} is desired, obtain the Reynolds analogy factor S from equation (36) and F_cN_{St} from

$$F_cN_{St} = \frac{S}{2}\left(F_cC_f\right) \tag{B1}$$

(5) Obtain C_f or N_{St} from

$$C_f = \frac{1}{F_c}\left(F_c C_f\right) \tag{B2}$$

$$N_{St} = \frac{1}{F_c}\left(F_c N_{St}\right) \tag{B3}$$

The resulting values of C_f or N_{St} then occur at the specified $R_x = R_{x,T} + R_{x,a}$ locations; these skin-friction and heating predictions are generally useful for $R_{x,T} > \frac{1}{3} R_{x,p}$ as deduced from experimental evidence (ref. 26).

If a prediction based on R_θ is desired, the following steps are necessary:

(1) Calculate the momentum-thickness Reynolds number at the x-location of the beginning of transition $R_{\theta,i}$ by using a laminar prediction technique (e.g., ref. 40)

(2) Determine $R_{\theta,p}$ from the empirical equation

$$R_{\theta,p} = 2.25 R_{\theta,i} \tag{B4}$$

(3) Determine $R_{\theta,a} = \frac{1}{2}\left(R_{\theta,i} + R_{\theta,p}\right)$

(4) Specify the R_θ locations at which calculations are to be made

(5) Let $R_{\theta,T} = R_\theta - R_{\theta,a}$

(6) Form the product $F_{R_\theta} R_{\theta,T}$ and obtain the corresponding $F_c C_f$ from equation (34)

(7) If N_{St} is desired, obtain S from equation (36) and $F_c N_{St} = \frac{S}{2}\left(F_c C_f\right)$

(8) Obtain C_f or N_{St} from $C_f = \frac{1}{F_c}\left(F_c C_f\right)$ or $N_{St} = \frac{1}{F_c}\left(F_c N_{St}\right)$

These values of C_f or N_{St} then occur at the specified values of $R_\theta = R_{\theta,T} + R_{\theta,a}$. An interesting correlation resulting from this investigation is shown in figure 26 where the momentum-thickness distribution through the transition region is related to the x-distance through transition in an apparently universal manner. Only a few representative data runs are shown which cover the range of flow conditions for the present data; the

rest of the data correlate equally well. Figure 26 along with an estimated value of $R_{\theta,i}$ and the correlation $R_{\theta,p} = 2.25R_{\theta,i}$ can be used to calculate the momentum-thickness distribution through the transition region.

For all the recommended calculations a knowledge of the x-location of the beginning and end of boundary-layer transition has been assumed. This is no more restrictive for the present recommended method than for any other since for high-speed flight, prior knowledge of this transition information is necessary in order to make any reliable estimate of the surface heating. The more simple prediction technique using Reynolds numbers based on x is recommended to be used with the Spalding and Chi method for calculations at $M_e \leqq 10$.

Conical Flow

Skin friction and heating on a sharp-tipped cone with the cone axis aligned with the flow are calculated in the same manner as for two-dimensional flow except that the Reynolds number is redefined. The calculation procedure is as follows:

(1) Calculate the local flow conditions for the cone

(2) Calculate F_c and F_{R_x} from equations (23) to (27)

(3) Specify values of R_x (based on local flow conditions) for which calculations are to be made

(4) Determine $R_{x,c} = R_x - 0.825R_{x,p,c}$

(5) Determine $R_{x,fp}$ from

$$R_{x,fp} = \frac{1}{2} R_{x,c} \left(1 + \frac{\dfrac{R_{x,p,c}}{R_{x,c}}}{1 + \dfrac{R_{x,p,c}}{R_{x,c}}} \right) \tag{B5}$$

(6) Form the product $F_{R_x} R_{x,fp}$

(7) Obtain $F_c C_{f,c}$ from equation (33) for the $F_{R_x} R_{x,fp}$ values in step (5)

(8) Calculate $C_{f,c}$ from

$$C_{f,c} = \frac{1}{F_c} \left(F_c C_{f,c} \right) \tag{B6}$$

(9) If $N_{St,c}$ is desired, determine S_c from equation (A6)

(10) Calculate $N_{St,c}$ from

$$N_{St,c} = \frac{1}{2}\left(S_c\right)\left(C_{f,c}\right) \tag{B7}$$

These values of $C_{f,c}$ and $N_{St,c}$ then occur at the corresponding values of R_x in step (3).

REFERENCES

1. Nestler, D. E.; and Goetz, R.: Survey of Theoretical and Experimental Determinations of Skin Friction in Compressible Boundary Layers: Part II. The Turbulent Boundary Layer on a Flat Plate. Tech. Inform. Ser. No. R58SD270 (Contract AF 04(645)-24), Missile Ord. Syst. Dep., Gen. Elec. Co., Jan. 29, 1959.

2. Peterson, John B., Jr.: A Comparison of Experimental and Theoretical Results for the Compressible Turbulent-Boundary-Layer Skin Friction With Zero Pressure Gradient. NASA TN D-1795, 1963.

3. Spalding, D. B.; and Chi, S. W.: The Drag of a Compressible Turbulent Boundary Layer on a Smooth Flat Plate With and Without Heat Transfer. J. Fluid Mech., vol. 18, pt. 1, Jan. 1964, pp. 117-143.

4. Hornung, H. G.: A Survey of Compressible Flow Boundary Layers – Theory and Experiment. Rep. ACA 67, Dep. Supply, Australian Aeronaut. Res. Comm., Feb. 1966.

5. Hopkins, Edward J.; Rubesin, Morris W.; Inouye, Mamoru; Keener, Earl R.; Mateer, George C.; and Polek, Thomas E.: Summary and Correlation of Skin-Friction and Heat-Transfer Data for a Hypersonic Turbulent Boundary Layer on Simple Shapes. NASA TN D-5089, 1969.

6. Hopkins, Edward J.; Keener, Earl R.; and Louie, Pearl T.: Direct Measurements of Turbulent Skin Friction on a Nonadiabatic Flat Plate at Mach Number of 6.5 and Comparisons With Eight Theories. NASA TN D-5675, 1970.

7. Pearce, Blaine: A Comparison of Four Simple Calculation Methods for the Compressible Turbulent Boundary Layer on a Flat Plate. Rep. No. TOR-0066(5758-02)-3, Syst. Eng. Oper., Aerosp. Corp., Mar. 16, 1970. (Available from DDC as AD 708 147.)

8. Hopkins, Edward J.; and Inouye, Mamoru: An Evaluation of Theories for Predicting Turbulent Skin Friction and Heat Transfer on Flat Plates at Supersonic and Hypersonic Mach Numbers. AIAA J., vol. 9, no. 6, June 1971, pp. 993-1003.

9. White, F. M.; and Christoph, G. H.: A Simple New Analysis of Compressible Turbulent Two-Dimensional Skin Friction Under Arbitrary Conditions. AFFDL-TR-70-133, U.S. Air Force, Feb. 1971.

10. Eckert, E. R. G.: Engineering Relations of Friction and Heat Transfer to Surfaces in High Velocity Flow. J. Aeronaut. Sci., vol. 22, no. 8, Aug. 1955, pp. 585-587.

11. Moore, Dave R.: Velocity Similarity in the Compressible Turbulent Boundary Layer With Heat Transfer. Ph. D. Dissertation, Univ. of Texas, 1962.

12. Van Driest, E. R.: The Problem of Aerodynamic Heating. Aeronaut. Eng. Rev., vol. 15, no. 10, Oct. 1956, pp. 26-41.

13. Coles, D. E.: The Turbulent Boundary Layer in a Compressible Fluid. R-403-PR (Contract No. AF 49(638)-700), RAND Corp., Sept. 1962. (Available from DDC as AD 285 651.)

14. Keyes, F. G.: A Summary of Viscosity and Heat-Conduction Data for He, A, H_2, O_2, N_2, CO, CO_2, H_2O, and Air. Trans. ASME, vol. 73, no. 5, July 1951, pp. 589-596.

15. Schoenherr, Karl E.: Resistance of Flat Surfaces Moving Through a Fluid. Trans. Soc. Naval Architects & Marine Eng., vol. 40, 1932, pp. 279-313.

16. Sivells, James C.; and Payne, Robert G.: A Method of Calculating Turbulent-Boundary-Layer Growth at Hypersonic Mach Numbers. AEDC-TR-59-3, DDC Doc. No. AD 208 774, U.S. Air Force, Mar. 1959.

17. Chi, S. W.; and Spalding, D. B.: Influence of Temperature Ratio on Heat Transfer to a Flat Plate Through a Turbulent Boundary Layer in Air. Proceedings of the Third International Heat Transfer Conference, Vol. II, Amer. Inst. Chem. Eng., c.1966, pp. 41-49.

18. Cary, Aubrey M., Jr.: Summary of Available Information on Reynolds Analogy for Zero-Pressure-Gradient, Compressible, Turbulent-Boundary-Layer Flow. NASA TN D-5560, 1970.

19. Keener, Earl R.; and Polek, Thomas E.: Measurements of Reynolds Analogy for a Hypersonic Turbulent Boundary Layer on a Nonadiabatic Flat Plate. AIAA J., vol. 10, no. 6, June 1972, pp. 845-846.

20. Holden, Michael S.: An Experimental Investigation of Turbulent Boundary Layers at High Mach Number and Reynolds Numbers. NASA CR-112147, 1972.

21. Hopkins, Edward J.; Keener, Earl R.; Polek, Thomas E.; and Dwyer, Harry A.: Hypersonic Turbulent Skin-Friction and Boundary-Layer Profiles on Nonadiabatic Flat Plates. AIAA J., vol. 10, no. 1, Jan. 1972, pp. 40-48.

22. Coles, Donald: Measurements in the Boundary Layer on a Smooth Flat Plate in Supersonic Flow. I – The Problem of the Turbulent Boundary Layer. Rep. No. 20-69 (Contract No. DA-04-495-Ord 18), Jet Propulsion Lab., California Inst. Technol., June 1, 1953.

23. Coles, Donald: Measurements in the Boundary Layer on a Smooth Flat Plate in Supersonic Flow. III – Measurements in a Flat-Plate Boundary Layer at the Jet Propulsion Laboratory. Rep. No. 20-71 (Contract No. DA-04-495-Ord 18), Jet Propulsion Lab., California Inst. Technol., June 1, 1953.

24. Coles, Donald: Measurements of Turbulent Friction on a Smooth Flat Plate in Supersonic Flow. J. Aeronaut. Sci., vol. 21, no. 7, July 1954, pp. 433-448.

25. Markovin, Mark V.: Critical Evaluation of Transition From Laminar to Turbulent Shear Layers With Emphasis on Hypersonically Traveling Bodies. AFFDL-TR-68-149, U.S. Air Force, Mar. 1969. (Available from DDC as AD 686 178.)

26. Bertram, Mitchel H.; and Neal, Luther, Jr.: Recent Experiments in Hypersonic Turbulent Boundary Layers. Presented to the AGARD Specialists Meeting on Recent Developments in Boundary-Layer Research (Naples, Italy), May 1965. (Available as NASA TM X-56335.)

27. Bertram, Mitchel H.; Cary, Aubrey M., Jr.; and Whitehead, Allen H., Jr.: Experiments With Hypersonic Turbulent Boundary Layers on Flat Plates and Delta Wings. Hypersonic Boundary Layers and Flow Fields, AGARD CP No. 30, May 1968.

28. Harris, Julius E.: Numerical Solution of the Equations for Compressible Laminar, Transitional, and Turbulent Boundary Layers and Comparisons With Experimental Data. NASA TR R-368, 1971.

29. Heronimus, G. A.: Hypersonic Shock Tunnel Experiments on the W7 Flat Plate Model – Expansion Side, Turbulent Flow and Leading Edge Transpiration Data. CAL Rep. No. AA-1952-Y-2 (Contract No. AF 33(615)-1847), Cornell Aeronaut. Lab., Inc., Feb. 1966.

30. Wallace, J. E.: Hypersonic Turbulent Boundary-Layer Studies at Cold Wall Conditions. Proceedings of the 1967 Heat Transfer and Fluid Mechanics Institute, Paul A. Libby, Daniel B. Olfe, and Charles W. Van Atta, eds., Stanford Univ. Press, c.1967, pp. 427-451.

31. Cary, Aubrey M., Jr.: Turbulent-Boundary-Layer Heat-Transfer and Transition Measurements With Surface Cooling at Mach 6. NASA TN D-5863, 1970.

32. Cary, Aubrey M., Jr.; and Morrisette, E. Leon: Effect of Two-Dimensional Multiple Sine-Wave Protrusions on the Pressure and Heat-Transfer Distributions for a Flat Plate at Mach 6. NASA TN D-4437, 1968.

33. Weinstein, Leonard M.: Effects of Two-Dimensional Sinusoidal Waves on Heat Transfer and Pressure Over a Plate at Mach 8.0. NASA TN D-5937, 1970.

34. Coleman, G. T.: Tabulated Heat Transfer Rate Data for a Hypersonic Turbulent Boundary Layer Over a Flat Plate. I. C. Aero Rep. 72-06, Dep. Aeronaut, Imp. Coll. Sci. & Technol., Mar. 1972.

35. Julius, Jerome D.: Measurements of Pressure and Local Heat Transfer on a 20^{o} Cone at Angles of Attack up to 20^{o} for a Mach Number of 4.95. NASA TN D-179, 1959.

36. Jones, Jim J.: Experimental Investigation of the Heat-Transfer Rate to a Series of 20^{o} Cones of Various Surface Finishes at a Mach Number of 4.95. NASA MEMO 6-10-59L, 1959.

37. Henderson, Arthur, Jr.: Hypersonic Viscous Flows. Modern Developments in Gas Dynamics, W. H. T. Loh, ed., Plenum Press, 1969, pp. 83-129.

38. Bushnell, Dennis M.; and Morris, Dana J.: Shear-Stress, Eddy-Viscosity, and Mixing-Length Distributions in Hypersonic Turbulent Boundary Layers. NASA TM X-2310, 1971.

39. Van Driest, E. R.: Turbulent Boundary Layer on a Cone in a Supersonic Flow at Zero Angle of Attack. J. Aeronaut. Sci., vol. 19, no. 1, Jan. 1952, pp. 55-57.

40. Monaghan, R. J.: An Approximate Solution of the Compressible Laminar Boundary Layer on a Flat Plate. R. & M. No. 2760, Brit. A.R.C., 1953.

TABLE I.- CONDITIONS FOR SKIN-FRICTION DATA – FLAT PLATE

Symbol	Identity number	Reference	M_∞	Me	ψ, deg	r	T_W, K	$H_W/H_{t,\infty}$	R, cm^{-1}, $\times 10^{-5}$	$R_{x,i}$ $\times 10^{-6}$	$R_{x,p}$ $\times 10^{-6}$	$R_{\theta,i}$ $\times 10^{-3}$	$R_{\theta,p}$ $\times 10^{-3}$
○	1	21	≈7.40	6.27	6.20	0.89	317	0.29	0.69	2.46	4.92	0.91	2.07
	2			6.33			313	.29	1.16	2.50	5.28	.88	2.07
	3			6.41			303	.29	.68	2.07	4.65	.84	2.20
	4			6.42			328	.29	1.31	2.80	5.66	1.28	2.87
	5			6.39			317	.28	1.64	1.96	4.17	.89	1.88
	6			6.83	3.10		303	.28	.95	2.65	6.03	.86	2.25
	7			6.72			317	.28	.90	2.64	5.46	.86	2.04
	8			6.87			302	.27	1.16	2.66	5.62	.91	1.94
	9			6.43	6.20		307	.43	1.37	2.43	5.04	1.02	2.43
	10			6.42			307	.43	2.19	2.68	5.58	1.00	2.25
	11			6.45			303	.42	2.69	3.00	6.20	.92	2.47
	12			6.41			311	.45	3.73	2.08	5.21	.90	2.44
	13			6.91	3.10		306	.44	1.24	2.52	4.91	.88	2.06
	14			6.91			308	.44	1.98	3.27	6.54	.95	2.18
	15			6.91			304	.43	2.52	4.10	7.68	1.00	2.40
	16			6.91			307	.43	3.08	3.76	7.83	.96	2.46
□	17		7.31	7.31	0		316	.29	1.28	4.24	8.81	1.02	2.44
	18		7.42	7.42			300	.26	1.18	3.60	7.20	1.14	2.60
	19		7.32	7.32			318	.29	1.44	4.39	9.51	1.01	2.87
	20		7.45	7.45			305	.44	1.02	2.60	5.58	.98	2.39
	21		7.43	7.43			303	.43	1.60	3.25	6.50	.90	2.17
	22		7.46	7.46			297	.41	1.99	4.04	7.88	.89	2.17
	23		7.42	7.42			304	.42	2.77	5.64	9.86	1.12	2.04
	24		≈7.40	7.80	-2.10		306	.44	2.41	4.89	9.53	1.06	2.42
	25		7.36	7.36	0		306	.27	.95	2.91	5.86	.88	1.97
◇	26	5	≈7.40	6.76	3.00		310	.38	.49	1.99	3.97	.89	2.00
	27			6.76			312	.41	.92	2.82	5.64	.89	2.00
	28			6.76			318	.46	1.33	3.39	6.78	.89	2.00
	29		7.37	7.37	0		318	.29	1.49	4.53	9.06	1.28	2.90
◁	30	29 and 30	8.80	8.80			296	.22	8.07	9.20	16.90	1.89	3.89
▷	31		7.00	7.00				.26	8.47	3.23	7.00	1.27	3.00
	32		7.58	7.58				.14	5.14	2.61	6.50	.97	2.76
	33		6.41	6.41				.14	8.67	4.40	11.00	1.24	2.70
◁	34		8.80	8.80				.19	5.98	6.07	11.50	1.58	4.14
▷ ▷	35		7.20	7.20				.20	6.48	3.30	8.00	1.09	2.97
▷	36	20	7.37	7.37	0		293	.16	4.71	7.18	14.34	1.57	3.76
	37		7.44	7.44			298	.19	5.11	8.10	18.14	1.72	4.68
◇	38		7.97	7.97			292	.30	5.25	11.20	22.14	1.80	4.49
	39		7.74	7.74			293	.15	5.40	8.22	19.18	1.67	4.79
	40		7.98	7.98			292	.20	5.66	8.63	20.13	1.75	4.65
	41		8.32	8.32			294	.28	19.17	9.74	48.70	1.90	13.12
	42		7.71	7.71			296	.29	15.58	11.88	31.70	2.07	7.18
◇	43		10.18	10.18			298	.16	1.51	4.61	9.23	1.21	2.62
	44		10.95	10.95			294	.15	1.47	4.11	7.86	1.25	2.59
	45		11.29	11.29			297	.18	3.43	6.09	12.18	1.47	3.17
	46		11.06	11.06			295	.20	1.62	3.70	8.22	1.16	2.68
	47		10.72	10.72			297	.18	4.47	7.26	14.75	1.55	3.43
	48		10.57	10.57			296	.19	3.46	6.30	12.30	1.60	2.98
▷	49		12.89	12.89			293	.14	1.69	6.44	15.00	1.45	4.07

TABLE II.- CONDITIONS FOR HEAT TRANSFER DATA – FLAT PLATE

Symbol	Identity number	Reference	M_∞	M_e	ψ, deg	r	T_w, K	$H_w/H_{t,\infty}$	R, cm^{-1}, $\times 10^{-5}$	$R_{x,i}$ $\times 10^{-6}$	$R_{x,p}$ $\times 10^{-6}$	$R_{\theta,i}$ $\times 10^{-3}$	$R_{\theta,p}$ $\times 10^{-3}$
○	101	31	6.00	6.00	0	0.89	320	0.60	2.59	2.30	5.00	0.95	2.17
	102						320	.60	1.43	1.53	3.27	.76	1.68
	103						280	.53	2.50	2.07	4.73	.90	1.76
	104						266	.49	2.40	1.95	4.15	.88	1.87
	105						226	.43	2.51	2.23	4.63	.95	2.07
	106						172	.33	2.53	2.41	5.30	.99	2.45
	107						189	.36	2.51	2.07	4.77	.92	2.18
	108						214	.41	1.33	1.44	3.39	.76	1.70
	109						339	.70	2.83	1.98	3.96	.86	1.69
	110						107	.20	2.68	3.07	6.00	1.12	2.41
	111						107	.20	1.39	2.30	4.60	1.05	2.11
	112	Unpublished[a]					320	.60	2.76	2.80	6.00	1.03	2.48
	113	Unpublished[a]					320	.60	1.66	2.11	4.46	.87	1.98
□	114	31		4.85	8.5		312	.60	3.72	1.89	3.78	.85	1.74
	115						278	.53	3.69	1.99	3.99	.88	1.84
	116						262	.51	3.77	2.20	5.26	.93	2.54
	117						239	.45	3.53	1.95	3.90	.88	1.82
	118						210	.39	3.54	2.16	4.49	.94	2.15
	119						161	.31	3.70	1.88	3.76	.88	1.80
	120						136	.26	3.59	2.28	5.02	.97	2.41
	121						123	.24	3.72	1.75	3.45	.86	1.75
◇	122	5	≈7.40	6.76	3.1		308	.28	.98	3.00	6.30	.98	2.30
	123						318	.29	1.27	2.80	7.26	1.13	2.66
	124						317	.29	1.61	3.00	8.30	.86	2.63
	125	Unpublished[b]		6.45	6.2		303	.42	2.68	3.00	6.28	.92	2.47
	126			6.91	3.1		304	.43	2.52	4.10	7.68	1.00	2.40
	127			6.41	6.2		303	.28	.68	2.07	4.65	.84	2.20
	128			6.39	6.2		317	.28	1.64	1.96	4.17	.89	1.88
	129			6.87	3.1		302	.27	1.16	2.66	5.62	.91	1.94
	130			6.91	3.1		307	.43	3.08	3.76	7.83	.96	2.46
	131			6.41	6.2		311	.45	3.73	2.08	5.21	.90	2.44
	132			6.43	6.2		307	.43	.97	2.43	5.04	1.02	2.43
	133			6.91	3.1		306	.44	1.24	2.52	4.91	.88	2.06
	134			6.42	6.2		307	.43	2.19	2.68	5.58	1.00	2.25
	135			6.91	3.1		308	.44	1.98	3.27	6.54	.95	2.18
	136			6.72	3.1		317	.28	.90	2.64	5.46	.86	2.04
	137			6.33	3.1		313	.29	1.12	2.55	4.82	1.02	2.15
	138			6.83	3.1		303	.28	.95	2.65	6.03	.86	2.25
	139			6.33	6.2		313	.29	1.12	2.50	5.28	.88	2.07
	140			6.27	6.2		317	.29	.68	2.46	4.92	.91	2.07
△	141	5	7.37	7.37	0		314	.29	1.04	4.50	9.00	1.35	3.00
	142						322	.29	1.27	4.80	9.00	1.23	2.71
	143						322	.29	1.43	4.20	9.00	1.10	2.87
	144	Unpublished[b]	7.46	7.46			297	.41	1.99	4.04	7.88	.89	2.17
	145		7.42	7.42			300	.26	1.18	3.60	7.20	1.14	2.60
	146		7.36	7.36			306	.27	.97	2.91	5.86	.88	1.97
	147		7.40	7.80	-2.1		306	.27	2.40	4.89	9.53	1.06	2.42
	148		7.42	7.42	0		304	.42	2.78	5.64	9.86	1.12	2.04
	149		7.31	7.31			316	.29	1.28	4.24	8.81	1.02	2.44
	150		7.32	7.32			318	.29	1.44	4.39	9.51	1.01	2.87
	151		7.45	7.45			305	.44	1.03	2.60	5.58	.98	2.39
	152		7.43	7.43			303	.43	1.60	3.25	6.50	.90	2.17

See footnote at end of table, p. 41.

TABLE II.- CONDITIONS FOR HEAT TRANSFER DATA – FLAT PLATE – Concluded

Symbol	Identity number	Reference	M_∞	M_e	ψ, deg	r	T_w, K	$H_w/H_{t,\infty}$	R, cm^{-1}, $\times 10^{-5}$	$R_{x,i}$ $\times 10^{-6}$	$R_{x,p}$ $\times 10^{-6}$	$R_{\theta,i}$ $\times 10^{-3}$	$R_{\theta,p}$ $\times 10^{-3}$
△	153	29 and 30	8.80	8.80	0	0.89	296	0.22	8.07	9.20	16.90	1.89	3.89
	154		8.80	8.80				.19	5.98	6.07	11.50	1.58	4.14
△	155		7.00	7.00				.22	8.47	3.23	7.00	1.27	3.00
	156		7.58	7.58				.14	5.14	2.61	6.50	.97	2.76
	157		6.41	6.41				.14	8.67	4.40	11.00	1.24	2.70
	158		7.20	7.20				.20	6.48	3.30	8.00	1.09	2.97
	159		7.12	7.12				.11	1.61	1.93	4.22	.87	2.39
∩[c]	160	Unpublished[d]	21.70	6.76	10.0	.895	299	.67	1.99	3.03	6.82	.80	1.88
	161		20.80	6.76	10.0	.895	299	.67	1.33	2.19	5.39	.64	1.48
	162		21.70	6.76	10.0	.895	139	.45	3.11	4.75	10.68	1.12	2.79
◇	163	32	6.00	5.32	5.0	.89	329	.63	3.38	1.72	4.94	.80	2.19
	164			5.32	5.0		333	.64	2.14	1.90	4.35	.85	2.19
	165			4.65	10.0		333	.64	3.87	1.96	3.93	.86	1.98
	166			4.65	10.0		336	.65	2.45	1.86	4.04	.84	1.89
	167			4.00	15.0		321	.61	3.79	2.89	5.78	1.06	2.60
	168			4.00	15.0		333	.64	2.43	1.39	3.24	.73	1.85
◇	169	33	8.00	6.86	5.0		317	.38	4.45	1.02	6.56	.62	2.45
	170			6.86	5.0		317	.38	4.45	1.78	7.46	.82	2.42
	171			5.76	10.0		329	.42	5.22	2.83	7.02	.99	1.74
	172			5.76	10.0		309	.40	2.00	3.39	4.62	1.08	2.28
	173			5.76	10.0		329	.42	5.22	.94	5.30	.60	2.41
	174			5.76	10.0		309	.40	2.00	1.88	3.25	.85	2.08
	175			4.75	15.0		310	.39	1.85	2.38	2.63	.90	1.87
	176			4.75	15.0		310	.39	1.85	3.58	4.14	1.10	2.14
⌓	177	34	9.22	9.22	0		295	.25	4.43	6.76	14.40	1.09	2.93
	178	34	9.08	9.08	0		295	.26	2.14	4.36	8.16	1.27	2.51
	179	34	8.96	8.96	0		295	.26	1.19	2.72	5.44	1.00	1.92
	180	34	9.22	5.09	15.0		295	.25	6.22	1.58	3.95	.84	2.19
	181	34	8.96	7.00	7.0		295	.27	1.83	2.09	4.18	.71	1.59
	182	34	9.22	7.15	7.0		295	.25	6.85	3.48	7.31	1.12	2.61
⊕	183	20	7.37	7.37	0		294	.16	4.71	7.18	14.34	1.57	3.76
	184		7.44	7.44			298	.19	5.11	8.10	18.14	1.72	4.68
	185		7.97	7.97			292	.30	5.25	11.20	22.14	1.80	4.49
	186		7.74	7.74			293	.15	5.40	8.22	19.18	1.67	4.79
	187		7.98	7.98			292	.20	5.66	8.63	20.13	1.75	4.65
	188		8.32	8.32			294	.28	19.17	9.74	48.70	1.90	13.12
	189		7.71	7.71			296	.29	15.58	11.88	31.70	2.07	7.18
⊞	190		10.18	10.18			298	.16	1.51	4.61	9.23	1.21	2.62
	191		10.95	10.95			294	.15	1.47	4.11	7.86	1.25	2.59
	192		11.29	11.29			297	.18	3.43	6.09	12.18	1.47	3.17
	193		11.06	11.06			295	.20	1.62	3.70	8.22	1.16	2.68
	194		10.72	10.72			297	.18	4.47	7.26	14.75	1.55	3.43
	195		10.57	10.57			296	.19	3.46	6.30	12.30	1.60	2.98
⊕	196		12.89	12.89			293	.14	1.69	6.44	15.00	1.45	4.07

[a]Source, E. L. Morrisette, NASA.

[b]Source, T. E. Polek, NASA.

[c]Helium data.

[d]Source, D. V. Maddalon, NASA.

TABLE III.- LOCAL SKIN-FRICTION DATA - FLAT PLATE

C_f	R_x	R_θ
Identity No. 1		
1.42E-03	6.90E+06	3.47E+03
No. 2		
1.23E-03	1.12E+07	5.37E+03
No. 3		
1.56E-03	6.79E+06	3.23E+03
No. 4		
1.10E-03	1.31E+07	7.08E+03
No. 5		
1.04E-03	1.64E+07	8.98E+03
No. 6		
1.24E-03	9.50E+06	4.18E+03
No. 7		
1.18E-03	9.04E+06	4.41E+03
No. 8		
1.09E-03	1.16E+07	5.79E+03
No. 9		
1.08E-03	1.37E+07	7.02E+03
No. 10		
9.30E-04	2.19E+07	1.07E+04
No. 11		
8.90E-04	2.69E+07	1.36E+04
No. 12		
8.30E-04	3.73E+07	1.74E+04
No. 13		
1.03E-03	1.24E+07	6.24E+03
No. 14		
9.00E-04	1.58E+07	9.22E+03
No. 15		
8.30E-04	2.52E+07	1.14E+04
No. 16		
8.00E-04	3.08E+07	1.38E+04
No. 17		
1.09E-03	1.28E+07	5.20E+03
No. 18		
1.11E-03	1.18E+07	5.42E+03
No. 19		
1.08E-03	1.44E+07	5.98E+03
No. 20		
1.04E-03	1.02E+07	4.91E+03
No. 21		
8.90E-04	1.60E+07	7.56E+03
No. 22		
8.50E-04	1.99E+07	9.09E+03
No. 23		
7.90E-04	2.77E+07	1.12E+04
No. 24		
7.60E-04	2.40E+07	1.12E+04
No. 25		
1.17E-03	9.54E+06	4.56E+03
No. 26		
1.52E-03	4.84E+06	2.50E+03
No. 27		
1.23E-03	9.17E+06	2.50E+03
No. 28		
1.06E-03	1.32E+07	2.50E+03
No. 29		
1.08E-03	1.47E+07	6.00E+03
No. 30		
8.06E-04	2.37E+07	6.08E+03
6.05E-04	2.62E+07	6.96E+03
7.02E-04	2.88E+07	7.78E+03
6.50E-04	3.13E+07	8.46E+03
6.00E-04	3.39E+07	9.22E+03
6.22E-04	3.75E+07	1.03E+04
6.92E-04	4.10E+07	1.12E+04
5.50E-04	4.46E+07	1.22E+04
5.93E-04	4.82E+07	1.32E+04
No. 31		
1.11E-03	9.46E+06	4.07E+03
1.03E-03	1.22E+07	5.76E+03
9.58E-04	1.48E+07	7.37E+03
9.26E-04	2.29E+07	1.07E+04
7.46E-04	2.56E+07	1.32E+04
8.06E-04	2.83E+07	1.43E+04
7.80E-04	3.10E+07	1.56E+04
6.85E-04	3.37E+07	1.68E+04
7.67E-04	3.75E+07	1.86E+04
8.55E-04	4.13E+07	2.03E+04
7.04E-04	4.51E+07	2.19E+04
No. 32		
1.76E-03	9.00E+06	4.58E+03
1.09E-03	1.06E+07	5.62E+03
1.08E-03	1.22E+07	6.63E+03
1.00E-03	1.39E+07	7.67E+03
8.72E-04	1.55E+07	8.60E+03
9.60E-04	1.71E+07	9.47E+03
8.89E-04	1.88E+07	1.04E+04
8.18E-04	2.04E+07	1.12E+04
9.04E-04	2.27E+07	1.24E+04
9.55E-04	2.49E+07	1.35E+04
7.83E-04	2.72E+07	1.47E+04
9.41E-04	2.95E+07	1.57E+04
No. 33		
1.16E-03	1.51E+07	6.49E+03
1.04E-03	1.79E+07	8.22E+03
1.01E-03	2.06E+07	9.78E+03
9.83E-04	2.34E+07	1.13E+04
9.03E-04	2.62E+07	1.28E+04
8.91E-04	2.89E+07	1.42E+04
8.69E-04	3.15E+07	1.55E+04
8.08E-04	3.44E+07	1.70E+04
8.83E-04	3.82E+07	1.90E+04
1.05E-03	4.21E+07	2.08E+04
8.72E-04	4.60E+07	2.26E+04
9.14E-04	4.98E+07	2.42E+04
No. 34		
8.61E-04	1.42E+07	5.50E+03
6.13E-04	1.61E+07	6.40E+03
6.92E-04	1.80E+07	7.26E+03
8.51E-04	1.99E+07	8.03E+03
6.39E-04	2.18E+07	8.82E+03
5.81E-04	2.37E+07	9.57E+03
6.52E-04	2.64E+07	1.06E+04
5.95E-04	2.90E+07	1.15E+04
5.70E-04	3.17E+07	1.24E+04
6.10E-04	3.43E+07	1.34E+04
No. 35		
1.01E-03	1.34E+07	6.47E+03
9.76E-04	1.54E+07	7.61E+03
6.96E-04	1.75E+07	8.67E+03
8.21E-04	1.96E+07	9.84E+03
1.04E-03	2.16E+07	1.09E+04
8.05E-04	2.37E+07	1.19E+04
6.93E-04	2.57E+07	1.29E+04
7.41E-04	2.86E+07	1.42E+04
7.57E-04	3.15E+07	1.55E+04
7.45E-04	3.44E+07	1.68E+04
8.17E-04	3.72E+07	1.82E+04

The symbol E and the following plus or minus sign and two digits represent the exponent of 10 by which to multiply the number to place the decimal correctly.

For identity nos. 1-29 R_θ was obtained from pitot-temperature profiles.

For identity nos. 30-35 R_θ was obtained from integration of heat transfer measured simultaneously with C_f and with S = 1.16.

TABLE III.-- LOCAL SKIN-FRICTION DATA - FLAT PLATE-Concluded

C_f	R_x	R_θ
Identity No. 36		
8.56E-04	2.34E+07	7.55E+03
8.18E-04	2.84E+07	9.42E+03
8.07E-04	2.90E+07	9.62E+03
8.44E-04	2.96E+07	9.90E+03
8.59E-04	3.02E+07	1.01E+04
8.80E-04	3.18E+07	1.07E+04
8.19E-04	3.29E+07	1.11E+04
8.56E-04	3.40E+07	1.15E+04
7.60E-04	3.51E+07	1.18E+04
9.03E-04	3.63E+07	1.22E+04
8.19E-04	3.74E+07	1.26E+04
7.89E-04	3.86E+07	1.32E+04
7.84E-04	4.09E+07	1.38E+04
No. 37		
8.86E-04	2.53E+07	7.42E+03
8.09E-04	3.08E+07	9.35E+03
7.12E-04	3.14E+07	9.60E+03
5.96E-04	3.21E+07	9.80E+03
8.39E-04	3.28E+07	1.01E+04
8.53E-04	3.44E+07	1.07E+04
7.59E-04	3.56E+07	1.10E+04
8.33E-04	3.69E+07	1.14E+04
7.31E-04	3.81E+07	1.17E+04
7.85E-04	3.93E+07	1.22E+04
8.19E-04	4.06E+07	1.26E+04
7.28E-04	4.18E+07	1.30E+04
7.42E-04	4.43E+07	1.38E+04
No. 38		
8.51E-04	2.60E+07	6.35E+03
8.09E-04	3.16E+07	8.60E+03
8.33E-04	3.23E+07	8.90E+03
6.52E-04	3.30E+07	9.20E+03
8.09E-04	3.37E+07	9.55E+03
7.45E-04	3.54E+07	1.02E+04
7.31E-04	3.66E+07	1.07E+04
7.38E-04	3.79E+07	1.12E+04
7.88E-04	3.92E+07	1.17E+04
7.52E-04	4.04E+07	1.22E+04
1.04E-03	4.17E+07	1.27E+04
7.32E-04	4.30E+07	1.32E+04
7.45E-04	4.56E+07	1.42E+04

C_f	R_x	R_θ
No. 39		
6.93E-04	2.68E+07	7.75E+03
7.73E-04	3.25E+07	9.85E+03
8.80E-04	3.32E+07	1.02E+04
7.50E-04	3.39E+07	1.04E+04
7.11E-04	3.46E+07	1.07E+04
7.21E-04	3.64E+07	1.14E+04
6.75E-04	3.76E+07	1.17E+04
7.33E-04	3.89E+07	1.22E+04
8.93E-04	4.03E+07	1.27E+04
6.56E-04	4.15E+07	1.32E+04
6.70E-04	4.29E+07	1.36E+04
6.80E-04	4.42E+07	1.40E+04
6.69E-04	4.68E+07	1.50E+04
No. 40		
7.97E-04	2.81E+07	7.90E+03
7.67E-04	3.41E+07	1.02E+04
7.84E-04	3.48E+07	1.04E+04
7.55E-04	3.56E+07	1.07E+04
7.97E-04	3.63E+07	1.11E+04
8.06E-04	3.82E+07	1.17E+04
7.53E-04	3.95E+07	1.22E+04
7.91E-04	4.09E+07	1.27E+04
7.30E-04	4.23E+07	1.32E+04
7.66E-04	4.36E+07	1.36E+04
7.44E-04	4.50E+07	1.42E+04
7.95E-04	4.64E+07	1.47E+04
7.25E-04	4.92E+07	1.57E+04
No. 41		
6.63E-04	9.51E+07	3.05E+04
5.61E-04	1.15E+08	3.70E+04
3.40E-04	1.18E+08	3.78E+04
4.95E-04	1.20E+08	3.86E+04
5.14E-04	1.23E+08	3.97E+04
6.97E-04	1.29E+08	4.12E+04
6.38E-04	1.34E+08	4.26E+04
6.72E-04	1.38E+08	4.40E+04
6.05E-04	1.43E+08	4.52E+04
6.75E-04	1.48E+08	4.64E+04
6.18E-04	1.52E+08	4.78E+04
5.45E-04	1.57E+08	4.93E+04
6.33E-04	1.66E+08	5.19E+04

C_f	R_x	R_θ
No. 42		
7.28E-04	7.73E+07	2.14E+04
7.09E-04	9.39E+07	2.63E+04
7.20E-04	9.58E+07	2.68E+04
8.13E-04	9.80E+07	2.75E+04
6.40E-04	1.00E+08	2.84E+04
8.51E-04	1.05E+08	2.93E+04
6.85E-04	1.09E+08	3.08E+04
9.05E-04	1.13E+08	3.20E+04
6.33E-04	1.16E+08	3.32E+04
7.44E-04	1.20E+08	3.42E+04
7.37E-04	1.24E+08	3.55E+04
7.82E-04	1.28E+08	3.67E+04
6.18E-04	1.35E+08	3.90E+04
No. 43		
8.39E-04	1.25E+07	3.92E+03
7.98E-04	1.41E+07	3.48E+03
8.47E-04	1.43E+07	4.56E+03
9.00E-04	1.45E+07	4.64E+03
8.09E-04	1.47E+07	4.70E+03
8.31E-04	1.52E+07	4.85E+03
7.55E-04	1.56E+07	4.95E+03
8.11E-04	1.59E+07	5.07E+03
7.93E-04	1.63E+07	5.20E+03
7.78E-04	1.67E+07	5.30E+03
7.08E-04	1.70E+07	5.44E+03
7.31E-04	1.74E+07	5.55E+03
7.72E-04	1.81E+07	5.80E+03
No. 44		
8.66E-04	1.22E+07	4.73E+03
8.27E-04	1.37E+07	5.35E+03
8.29E-04	1.39E+07	5.45E+03
8.18E-04	1.41E+07	5.50E+03
8.71E-04	1.43E+07	5.60E+03
8.23E-04	1.48E+07	5.75E+03
7.72E-04	1.51E+07	5.90E+03
6.97E-04	1.55E+07	6.02E+03
7.82E-04	1.58E+07	6.18E+03
6.94E-04	1.62E+07	6.30E+03
6.85E-04	1.66E+07	6.45E+03
6.76E-04	1.69E+07	6.58E+03
7.81E-04	1.76E+07	6.82E+03

C_f	R_x	R_θ
No. 45		
6.72E-04	2.83E+07	8.35E+03
5.38E-04	3.19E+07	9.35E+03
5.19E-04	3.24E+07	9.50E+03
6.02E-04	3.28E+07	9.60E+03
5.53E-04	3.33E+07	9.78E+03
6.39E-04	3.44E+07	1.01E+04
5.90E-04	3.60E+07	1.04E+04
5.67E-04	3.69E+07	1.06E+04
5.49E-04	3.77E+07	1.09E+04
6.33E-04	3.85E+07	1.11E+04
5.59E-04	3.93E+07	1.14E+04
5.54E-04	4.11E+07	1.17E+04
No. 46		
9.20E-04	1.34E+07	4.94E+03
8.50E-04	1.51E+07	5.60E+03
8.51E-04	1.53E+07	5.65E+03
9.41E-04	1.55E+07	5.77E+03
8.56E-04	1.57E+07	5.82E+03
9.43E-04	1.63E+07	6.02E+03
8.04E-04	1.66E+07	6.17E+03
7.90E-04	1.70E+07	6.28E+03
7.72E-04	1.74E+07	6.45E+03
8.07E-04	1.78E+07	6.55E+03
6.97E-04	1.82E+07	6.71E+03
8.63E-04	1.86E+07	6.83E+03
7.78E-04	1.94E+07	7.10E+03
No. 47		
6.63E-04	3.69E+07	1.04E+04
5.46E-04	4.17E+07	1.18E+04
5.22E-04	4.22E+07	1.17E+04
6.46E-04	4.28E+07	1.19E+04
5.50E-04	4.34E+07	1.20E+04
6.38E-04	4.49E+07	1.23E+04
5.80E-04	4.70E+07	1.28E+04
5.34E-04	4.81E+07	1.32E+04
5.39E-04	4.92E+07	1.33E+04
5.43E-04	5.36E+07	1.44E+04

C_f	R_x	R_θ
No. 48		
6.63E-04	2.86E+07	8.30E+03
5.77E-04	3.23E+07	9.20E+03
6.20E-04	3.27E+07	9.30E+03
5.25E-04	3.32E+07	9.42E+03
6.30E-04	3.36E+07	9.55E+03
6.13E-04	3.48E+07	9.80E+03
5.87E-04	3.56E+07	1.00E+04
5.98E-04	3.64E+07	1.02E+04
5.61E-04	3.73E+07	1.04E+04
5.73E-04	3.81E+07	1.06E+04
6.52E-04	3.89E+07	1.07E+04
5.58E-04	3.97E+07	1.10E+04
5.68E-04	4.15E+07	1.14E+04
No. 49		
8.17E-04	2.02E+07	6.12E+03

R_θ was obtained from integration of heat transfer measured simultaneously with C_f and with S = 1.16.

The symbol E and the following plus or minus sign and two digits represent the exponent of 10 by which to multiply the number to place the decimal correctly.

TABLE IV.- HEAT-TRANSFER DATA - FLAT PLATE

N_{St}	R_x	R_θ
Identity No. 101		
6.93E-04	7.13E+06	3.58E+03
6.53E-04	7.43E+06	3.75E+03
6.40E-04	7.60E+06	3.86E+03
6.45E-04	7.82E+06	3.97E+03
6.25E-04	8.21E+06	4.19E+03
6.25E-04	9.17E+06	4.69E+03
5.85E-04	9.62E+06	4.90E+03
5.60E-04	1.00E+07	5.09E+03
5.60E-04	1.01E+07	5.17E+03
5.65E-04	1.07E+07	5.43E+03
5.35E-04	1.11E+07	5.73E+03
5.35E-04	1.16E+07	5.84E+03
5.25E-04	1.19E+07	5.97E+03
5.54E-04	1.27E+07	6.32E+03
5.34E-04	1.33E+07	6.62E+03
No. 102		
8.10E-04	4.03E+06	2.31E+03
8.00E-04	4.14E+06	2.39E+03
7.80E-04	4.30E+06	2.49E+03
7.40E-04	4.96E+06	2.92E+03
6.90E-04	5.26E+06	3.10E+03
6.75E-04	5.35E+06	3.16E+03
6.87E-04	5.50E+06	3.24E+03
6.70E-04	5.64E+06	3.32E+03
6.70E-04	6.04E+06	3.58E+03
6.15E-04	6.27E+06	3.70E+03
6.02E-04	6.57E+06	3.88E+03
No. 103		
6.78E-04	5.81E+06	2.84E+03
6.66E-04	6.04E+06	2.98E+03
6.47E-04	6.76E+06	3.38E+03
5.97E-04	7.00E+06	3.52E+03
6.05E-04	7.24E+06	3.63E+03
5.88E-04	7.48E+06	3.77E+03
5.68E-04	7.72E+06	3.88E+03
6.14E-04	7.95E+06	4.01E+03
5.76E-04	8.67E+06	4.37E+03
5.89E-04	8.90E+06	4.50E+03
5.41E-04	9.14E+06	4.59E+03
5.34E-04	9.38E+06	4.70E+03
5.45E-04	9.62E+06	4.84E+03
5.27E-04	9.86E+06	4.95E+03
5.34E-04	1.06E+07	5.28E+03
5.01E-04	1.08E+07	5.39E+03
4.86E-04	1.10E+07	5.50E+03
5.00E-04	1.13E+07	5.61E+03
4.78E-04	1.15E+07	5.72E+03
4.65E-04	1.18E+07	5.83E+03
4.77E-04	1.23E+07	6.08E+03
5.00E-04	1.26E+07	6.18E+03

N_{St}	R_x	R_θ
No. 104		
7.92E-04	5.34E+06	2.74E+03
7.51E-04	5.57E+06	2.89E+03
7.21E-04	5.80E+06	3.04E+03
7.13E-04	6.48E+06	3.46E+03
6.67E-04	6.71E+06	3.59E+03
6.82E-04	6.94E+06	3.73E+03
6.75E-04	7.17E+06	3.86E+03
6.55E-04	7.62E+06	4.14E+03
6.46E-04	8.32E+06	4.50E+03
6.30E-04	8.54E+06	4.63E+03
6.16E-04	8.77E+06	4.76E+03
6.02E-04	9.00E+06	4.88E+03
6.14E-04	9.23E+06	5.00E+03
5.89E-04	9.46E+06	5.13E+03
5.94E-04	1.01E+07	5.47E+03
5.58E-04	1.04E+07	5.58E+03
5.57E-04	1.06E+07	5.69E+03
5.64E-04	1.08E+07	5.80E+03
5.46E-04	1.10E+07	5.90E+03
5.42E-04	1.13E+07	6.01E+03
5.40E-04	1.18E+07	6.33E+03
No. 105		
7.57E-04	5.82E+06	2.86E+03
6.86E-04	6.06E+06	3.00E+03
7.13E-04	6.78E+06	3.43E+03
6.77E-04	7.02E+06	3.60E+03
6.26E-04	7.26E+06	3.72E+03
6.59E-04	7.50E+06	3.87E+03
6.25E-04	7.98E+06	4.11E+03
6.13E-04	8.69E+06	4.50E+03
6.40E-04	8.93E+06	4.62E+03
5.98E-04	9.17E+06	4.73E+03
5.63E-04	9.41E+06	4.89E+03
5.64E-04	9.65E+06	5.00E+03
5.17E-04	9.89E+06	5.13E+03
5.63E-04	1.06E+07	5.48E+03
5.35E-04	1.08E+07	5.61E+03
5.43E-04	1.11E+07	5.70E+03
5.25E-04	1.13E+07	5.81E+03
5.02E-04	1.16E+07	5.92E+03
5.07E-04	1.28E+07	6.51E+03

N_{St}	R_x	R_θ
No. 106		
7.73E-04	6.82E+06	3.63E+03
7.01E-04	7.30E+06	3.92E+03
6.92E-04	7.54E+06	4.08E+03
6.89E-04	8.02E+06	4.40E+03
6.62E-04	8.74E+06	4.81E+03
6.53E-04	8.99E+06	4.96E+03
6.17E-04	9.23E+06	5.11E+03
6.06E-04	9.47E+06	5.24E+03
6.24E-04	9.71E+06	5.37E+03
5.74E-04	9.95E+06	5.50E+03
5.66E-04	1.07E+07	5.89E+03
5.53E-04	1.11E+07	6.11E+03
5.78E-04	1.14E+07	6.26E+03
No. 107		
8.25E-04	5.82E+06	3.00E+03
7.79E-04	6.05E+06	3.16E+03
7.34E-04	6.77E+06	3.62E+03
6.84E-04	7.01E+06	3.81E+03
6.67E-04	7.24E+06	3.94E+03
6.59E-04	7.48E+06	4.09E+03
6.19E-04	7.72E+06	4.22E+03
6.67E-04	7.96E+06	4.36E+03
6.26E-04	8.68E+06	4.79E+03
6.34E-04	8.92E+06	4.91E+03
5.77E-04	9.16E+06	5.02E+03
5.68E-04	9.40E+06	5.12E+03
5.81E-04	9.64E+06	5.28E+03
5.54E-04	9.88E+06	5.39E+03
5.47E-04	1.06E+07	5.71E+03
5.36E-04	1.08E+07	5.85E+03
5.26E-04	1.11E+07	5.96E+03
5.17E-04	1.13E+07	6.10E+03
5.02E-04	1.15E+07	6.20E+03
5.03E-04	1.18E+07	6.28E+03
5.06E-04	1.23E+07	6.53E+03
No. 108		
7.82E-04	4.24E+06	2.30E+03
7.23E-04	4.67E+06	2.55E+03
7.92E-04	4.75E+06	2.63E+03
6.86E-04	4.87E+06	2.70E+03
7.05E-04	5.00E+06	2.78E+03
7.27E-04	5.13E+06	2.85E+03
6.53E-04	5.26E+06	2.93E+03
6.63E-04	5.64E+06	3.14E+03
6.49E-04	5.76E+06	3.22E+03
6.47E-04	5.89E+06	3.31E+03
6.56E-04	6.02E+06	3.38E+03
6.16E-04	6.14E+06	3.43E+03
6.03E-04	6.27E+06	3.50E+03
6.15E-04	6.57E+06	3.65E+03

N_{St}	R_x	R_θ
No. 109		
6.82E-04	5.49E+06	2.75E+03
6.53E-04	6.03E+06	3.10E+03
6.59E-04	6.30E+06	3.25E+03
6.47E-04	6.57E+06	3.48E+03
5.85E-04	6.84E+06	3.57E+03
5.63E-04	7.92E+06	4.15E+03
5.86E-04	8.19E+06	4.29E+03
5.59E-04	8.46E+06	4.43E+03
5.74E-04	9.00E+06	4.69E+03
5.61E-04	9.81E+06	5.11E+03
5.49E-04	1.01E+07	5.19E+03
5.27E-04	1.03E+07	5.35E+03
5.04E-04	1.06E+07	5.48E+03
5.37E-04	1.09E+07	5.59E+03
4.85E-04	1.12E+07	5.67E+03
5.13E-04	1.20E+07	6.07E+03
4.78E-04	1.22E+07	6.18E+03
4.88E-04	1.25E+07	6.35E+03
4.60E-04	1.28E+07	6.42E+03
4.36E-04	1.30E+07	6.53E+03
4.55E-04	1.33E+07	6.63E+03
5.06E-04	1.39E+07	6.90E+03
No. 110		
7.50E-04	7.44E+06	3.36E+03
7.00E-04	7.72E+06	3.50E+03
6.85E-04	7.81E+06	3.56E+03
7.10E-04	7.97E+06	3.63E+03
7.00E-04	8.24E+06	3.81E+03
6.90E-04	8.36E+06	3.88E+03
6.80E-04	8.52E+06	3.96E+03
6.82E-04	8.85E+06	4.16E+03
6.85E-04	9.55E+06	4.54E+03
6.55E-04	9.61E+06	4.57E+03
6.90E-04	9.78E+06	4.68E+03
6.60E-04	9.91E+06	4.76E+03
6.70E-04	1.01E+07	4.86E+03
6.60E-04	1.03E+07	4.99E+03
6.45E-04	1.07E+07	5.18E+03
6.30E-04	1.15E+07	5.56E+03
6.10E-04	1.19E+07	5.81E+03
5.90E-04	1.29E+07	6.21E+03
No. 111		
7.60E-04	5.84E+06	3.02E+03
7.50E-04	6.15E+06	3.21E+03
7.50E-04	6.27E+06	3.28E+03
7.50E-04	6.41E+06	3.38E+03
7.15E-04	6.53E+06	3.44E+03
6.70E-04	7.30E+06	3.86E+03

N_{St}	R_x	R_θ
No. 112		
7.40E-04	7.49E+06	3.56E+03
7.55E-04	7.78E+06	3.73E+03
7.00E-04	8.44E+06	4.15E+03
6.50E-04	8.60E+06	4.23E+03
6.45E-04	8.76E+06	4.32E+03
6.50E-04	8.88E+06	4.40E+03
6.43E-04	9.06E+06	4.50E+03
6.43E-04	9.38E+06	4.68E+03
6.40E-04	9.58E+06	4.78E+03
6.30E-04	1.01E+07	5.05E+03
5.92E-04	1.04E+07	5.15E+03
5.75E-04	1.09E+07	5.38E+03
5.75E-04	1.12E+07	5.50E+03
5.50E-04	1.16E+07	5.66E+03
No. 113		
7.80E-04	5.49E+06	2.75E+03
7.70E-04	5.73E+06	2.91E+03
7.55E-04	5.92E+06	3.02E+03
7.50E-04	6.24E+06	3.22E+03
7.10E-04	6.39E+06	3.30E+03
6.80E-04	6.60E+06	3.42E+03
6.70E-04	6.65E+06	3.46E+03
6.70E-04	6.75E+06	3.51E+03
6.60E-04	6.97E+06	3.63E+03

R_θ determined assuming S = 1.16

The symbol E and the following plus or minus sign and two digits represent the exponent of 10 by which to multiply the number to place the decimal correctly.

TABLE IV. - HEAT-TRANSFER DATA - FLAT PLATE - Continued

N_{St}	R_x	R_θ
Identity No. 114		
8.33E-04	5.20E+06	2.77E+03
8.04E-04	5.55E+06	3.01E+03
7.92E-04	5.90E+06	3.25E+03
7.16E-04	6.26E+06	3.47E+03
7.04E-04	7.20E+06	4.07E+03
6.91E-04	7.91E+06	4.49E+03
7.11E-04	8.27E+06	4.71E+03
6.78E-04	8.62E+06	4.91E+03
6.51E-04	8.98E+06	5.10E+03
6.47E-04	1.00E+07	5.71E+03
6.25E-04	1.04E+07	5.90E+03
6.21E-04	1.07E+07	6.09E+03
6.33E-04	1.11E+07	6.23E+03
5.96E-04	1.14E+07	6.44E+03
6.27E-04	1.18E+07	6.64E+03
6.14E-04	1.29E+07	7.20E+03
6.30E-04	1.32E+07	7.38E+03
5.88E-04	1.36E+07	7.57E+03
5.96E-04	1.39E+07	7.76E+03
5.86E-04	1.43E+07	7.94E+03
5.78E-04	1.46E+07	8.08E+03
5.76E-04	1.57E+07	8.60E+03
5.67E-04	1.61E+07	8.77E+03
5.63E-04	1.64E+07	8.95E+03
5.67E-04	1.68E+07	9.12E+03
5.60E-04	1.83E+07	9.81E+03
No. 115		
6.90E-04	7.16E+06	4.00E+03
6.67E-04	7.86E+06	4.92E+03
6.86E-04	8.21E+06	4.64E+03
6.56E-04	8.56E+06	4.81E+03
6.28E-04	8.91E+06	5.02E+03
6.27E-04	9.97E+06	5.59E+03
6.01E-04	1.03E+07	5.80E+03
6.05E-04	1.07E+07	5.98E+03
6.08E-04	1.10E+07	6.18E+03
5.76E-04	1.14E+07	6.35E+03
6.08E-04	1.17E+07	6.52E+03
5.91E-04	1.28E+07	7.07E+03
6.01E-04	1.31E+07	7.22E+03
5.64E-04	1.35E+07	7.39E+03
5.74E-04	1.38E+07	7.58E+03
5.66E-04	1.42E+07	7.78E+03
5.50E-04	1.45E+07	7.95E+03
5.60E-04	1.56E+07	8.42E+03
5.44E-04	1.59E+07	8.57E+03
5.42E-04	1.63E+07	8.80E+03
5.66E-04	1.66E+07	8.94E+03
5.51E-04	1.70E+07	9.05E+03
5.53E-04	1.73E+07	9.24E+03

N_{St}	R_x	R_θ
No. 116		
7.68E-04	7.30E+06	3.96E+03
7.28E-04	8.01E+06	4.43E+03
7.50E-04	8.38E+06	4.60E+03
7.28E-04	8.74E+06	4.85E+03
6.90E-04	9.09E+06	5.07E+03
6.94E-04	1.02E+07	5.67E+03
6.56E-04	1.05E+07	5.90E+03
6.62E-04	1.09E+07	6.10E+03
6.73E-04	1.13E+07	6.29E+03
6.36E-04	1.16E+07	6.47E+03
6.57E-04	1.20E+07	6.68E+03
6.36E-04	1.30E+07	7.23E+03
6.54E-04	1.34E+07	7.41E+03
6.16E-04	1.38E+07	7.62E+03
6.10E-04	1.41E+07	7.82E+03
6.06E-04	1.45E+07	7.97E+03
5.87E-04	1.48E+07	8.17E+03
5.96E-04	1.59E+07	8.72E+03
5.68E-04	1.63E+07	8.88E+03
5.66E-04	1.66E+07	9.08E+03
5.77E-04	1.70E+07	9.24E+03
5.50E-04	1.73E+07	9.40E+03
5.48E-04	1.77E+07	9.58E+03
No. 117		
8.20E-04	4.93E+06	2.57E+03
7.88E-04	5.27E+06	2.80E+03
7.70E-04	5.60E+06	3.02E+03
6.92E-04	6.84E+06	3.83E+03
6.92E-04	7.51E+06	4.21E+03
7.10E-04	7.85E+06	4.42E+03
6.90E-04	8.18E+06	4.60E+03
6.58E-04	8.52E+06	4.79E+03
6.64E-04	9.53E+06	5.32E+03
6.30E-04	9.87E+06	5.53E+03
6.35E-04	1.02E+07	5.70E+03
6.42E-04	1.05E+07	5.88E+03
6.10E-04	1.09E+07	6.08E+03
6.44E-04	1.12E+07	6.23E+03
6.28E-04	1.22E+07	6.75E+03
6.33E-04	1.26E+07	6.95E+03
5.96E-04	1.29E+07	7.08E+03
5.88E-04	1.32E+07	7.25E+03
5.98E-04	1.36E+07	7.41E+03
5.78E-04	1.39E+07	7.58E+03
5.59E-04	1.49E+07	8.02E+03
5.60E-04	1.52E+07	8.27E+03
5.62E-04	1.56E+07	8.42E+03
5.62E-04	1.59E+07	8.58E+03
5.52E-04	1.63E+07	8.72E+03
5.46E-04	1.66E+07	8.92E+03
5.70E-04	1.74E+07	9.25E+03

N_{St}	R_x	R_θ
No. 118		
7.35E-04	6.86E+06	3.81E+03
7.05E-04	7.53E+06	4.21E+03
7.23E-04	7.87E+06	4.43E+03
7.06E-04	8.20E+06	4.64E+03
6.70E-04	8.54E+06	4.83E+03
6.80E-04	9.56E+06	5.40E+03
6.49E-04	9.89E+06	5.59E+03
6.56E-04	1.02E+07	5.80E+03
6.66E-04	1.06E+07	5.97E+03
6.68E-04	1.12E+07	6.32E+03
6.46E-04	1.22E+07	6.85E+03
6.59E-04	1.26E+07	7.04E+03
6.23E-04	1.29E+07	7.21E+03
6.17E-04	1.33E+07	7.39E+03
6.18E-04	1.36E+07	7.55E+03
5.96E-04	1.39E+07	7.73E+03
5.96E-04	1.49E+07	8.20E+03
5.80E-04	1.53E+07	8.39E+03
5.75E-04	1.56E+07	8.55E+03
5.85E-04	1.59E+07	8.70E+03
5.72E-04	1.63E+07	8.92E+03
5.68E-04	1.66E+07	9.02E+03
5.84E-04	1.74E+07	9.42E+03
No. 119		
8.20E-04	5.17E+06	2.82E+03
8.00E-04	5.52E+06	3.04E+03
7.74E-04	5.98E+06	3.35E+03
7.08E-04	7.17E+06	4.08E+03
6.57E-04	8.22E+06	4.72E+03
6.26E-04	8.58E+06	4.90E+03
6.29E-04	8.93E+06	5.10E+03
6.44E-04	9.99E+06	5.69E+03
6.18E-04	1.03E+07	5.87E+03
6.22E-04	1.07E+07	6.07E+03
6.24E-04	1.10E+07	6.25E+03
5.97E-04	1.14E+07	6.42E+03
6.25E-04	1.17E+07	6.62E+03
6.03E-04	1.28E+07	7.18E+03
6.07E-04	1.32E+07	7.37E+03
5.97E-04	1.35E+07	7.55E+03
5.94E-04	1.39E+07	7.69E+03
5.92E-04	1.42E+07	7.83E+03
5.78E-04	1.46E+07	8.04E+03
5.80E-04	1.56E+07	8.58E+03
5.69E-04	1.60E+07	8.72E+03
5.65E-04	1.63E+07	8.90E+03
5.70E-04	1.67E+07	9.07E+03
5.52E-04	1.70E+07	9.26E+03
5.46E-04	1.74E+07	9.42E+03

N_{St}	R_x	R_θ
No. 120		
7.84E-04	6.96E+06	3.78E+03
7.42E-04	7.64E+06	4.26E+03
7.66E-04	7.98E+06	4.45E+03
7.37E-04	8.32E+06	4.67E+03
6.97E-04	8.66E+06	4.89E+03
7.18E-04	9.70E+06	5.51E+03
6.88E-04	1.00E+07	5.70E+03
7.01E-04	1.04E+07	5.92E+03
7.05E-04	1.07E+07	6.14E+03
7.24E-04	1.14E+07	6.55E+03
7.18E-04	1.24E+07	7.07E+03
7.29E-04	1.28E+07	7.35E+03
6.86E-04	1.31E+07	7.50E+03
6.93E-04	1.34E+07	7.67E+03
6.90E-04	1.38E+07	7.90E+03
6.60E-04	1.41E+07	8.09E+03
6.73E-04	1.51E+07	8.59E+03
6.61E-04	1.55E+07	8.78E+03
6.61E-04	1.58E+07	8.97E+03
6.74E-04	1.62E+07	9.13E+03
6.56E-04	1.65E+07	9.38E+03
6.42E-04	1.69E+07	9.55E+03
6.69E-04	1.77E+07	1.00E+04
6.73E-04	1.80E+07	1.03E+04
No. 121		
7.86E-04	5.55E+06	3.33E+03
7.86E-04	5.91E+06	3.58E+03
7.31E-04	7.21E+06	4.41E+03
7.09E-04	7.92E+06	4.85E+03
7.32E-04	8.27E+06	5.06E+03
7.16E-04	8.62E+06	5.29E+03
6.75E-04	8.98E+06	5.47E+03
6.86E-04	1.00E+07	6.04E+03
6.53E-04	1.04E+07	6.28E+03
6.58E-04	1.07E+07	6.47E+03
6.73E-04	1.11E+07	6.64E+03
6.40E-04	1.15E+07	6.81E+03
6.72E-04	1.18E+07	7.05E+03
6.57E-04	1.29E+07	7.58E+03
6.65E-04	1.32E+07	7.79E+03
6.28E-04	1.36E+07	7.97E+03
6.30E-04	1.39E+07	8.18E+03
6.31E-04	1.43E+07	8.38E+03
6.22E-04	1.46E+07	8.53E+03
6.31E-04	1.57E+07	9.01E+03
6.16E-04	1.61E+07	9.27E+03
6.13E-04	1.64E+07	9.47E+03
6.14E-04	1.68E+07	9.59E+03
5.85E-04	1.71E+07	9.72E+03
5.68E-04	1.75E+07	9.88E+03
6.00E-04	1.83E+07	1.04E+04
6.09E-04	1.87E+07	1.06E+04

N_{St}	R_x	R_θ
No. 122		
6.48E-04	7.99E+06	3.33E+03
6.25E-04	8.30E+06	3.50E+03
6.32E-04	8.61E+06	3.67E+03
6.09E-04	8.92E+06	3.84E+03
6.17E-04	9.23E+06	4.01E+03
5.85E-04	9.54E+06	4.17E+03
5.45E-04	1.02E+07	4.47E+03
5.43E-04	1.02E+07	4.51E+03
5.66E-04	1.05E+07	4.66E+03
No. 123		
5.73E-04	9.19E+06	4.07E+03
5.44E-04	9.60E+06	4.28E+03
5.74E-04	1.00E+07	4.49E+03
5.70E-04	1.04E+07	4.70E+03
5.43E-04	1.08E+07	4.90E+03
5.53E-04	1.12E+07	5.11E+03
5.38E-04	1.16E+07	5.32E+03
5.43E-04	1.20E+07	5.53E+03
5.38E-04	1.24E+07	5.74E+03
4.99E-04	1.32E+07	6.15E+03
5.01E-04	1.33E+07	6.19E+03
5.20E-04	1.37E+07	6.40E+03
No. 124		
5.95E-04	1.01E+07	3.96E+03
5.82E-04	1.06E+07	4.25E+03
5.54E-04	1.11E+07	4.52E+03
5.22E-04	1.16E+07	4.79E+03
5.01E-04	1.21E+07	5.03E+03
5.22E-04	1.27E+07	5.28E+03
5.33E-04	1.32E+07	5.53E+03
5.07E-04	1.37E+07	5.77E+03
5.13E-04	1.42E+07	6.01E+03
4.91E-04	1.47E+07	6.25E+03
5.02E-04	1.52E+07	6.49E+03
4.91E-04	1.57E+07	6.71E+03
4.78E-04	1.67E+07	7.19E+03
4.74E-04	1.68E+07	7.24E+03
4.94E-04	1.74E+07	7.47E+03

R_θ determined assuming S = 1.16

The symbol E and the following plus or minus sign and two digits represent the exponent 10 by which to multiply the number to place the decimal correctly.

TABLE IV. - HEAT-TRANSFER DATA - FLAT PLATE- Continued

N_{St}	R_x	R_θ
Identity No. 125		
7.32E-04	7.45E+06	3.35E+03
7.07E-04	8.35E+06	3.84E+03
6.44E-04	9.17E+06	4.42E+03
6.39E-04	9.99E+06	4.84E+03
6.52E-04	1.08E+07	5.42E+03
6.39E-04	1.16E+07	5.84E+03
6.02E-04	1.25E+07	6.40E+03
5.80E-04	1.43E+07	7.30E+03
5.61E-04	1.52E+07	7.70E+03
5.59E-04	1.62E+07	8.20E+03
5.43E-04	1.68E+07	8.50E+03
5.33E-04	1.77E+07	8.90E+03
5.12E-04	1.86E+07	9.30E+03
4.87E-04	1.95E+07	9.70E+03
4.73E-04	2.03E+07	1.00E+04
4.83E-04	2.12E+07	1.03E+04
4.93E-04	2.21E+07	1.08E+04
4.67E-04	2.29E+07	1.12E+04
4.73E-04	2.38E+07	1.15E+04
4.61E-04	2.46E+07	1.18E+04
4.77E-04	2.54E+07	1.22E+04
4.59E-04	2.63E+07	1.26E+04
4.40E-04	2.88E+07	1.35E+04
No. 126		
6.49E-04	9.37E+06	3.40E+03
6.41E-04	1.01E+07	3.95E+03
6.08E-04	1.09E+07	4.37E+03
5.71E-04	1.17E+07	4.85E+03
5.40E-04	1.34E+07	5.57E+03
5.24E-04	1.43E+07	6.00E+03
5.22E-04	1.52E+07	6.35E+03
5.11E-04	1.57E+07	6.60E+03
4.98E-04	1.66E+07	6.90E+03
4.83E-04	1.74E+07	7.30E+03
4.52E-04	1.83E+07	7.65E+03
4.41E-04	1.90E+07	7.90E+03
4.52E-04	1.99E+07	8.20E+03
4.67E-04	2.07E+07	8.60E+03
4.49E-04	2.15E+07	8.90E+03
4.52E-04	2.23E+07	9.15E+03
4.39E-04	2.30E+07	9.50E+03
4.47E-04	2.38E+07	9.70E+03
4.34E-04	2.47E+07	1.02E+04
4.13E-04	2.70E+07	1.09E+04

N_{St}	R_x	R_θ
No. 127		
7.94E-04	5.79E+06	3.02E+03
7.97E-04	6.00E+06	3.15E+03
7.52E-04	6.21E+06	3.28E+03
7.52E-04	6.42E+06	3.42E+03
7.21E-04	6.64E+06	3.53E+03
6.69E-04	7.28E+06	3.97E+03
No. 128		
7.92E-04	6.11E+06	3.37E+03
8.16E-04	6.61E+06	3.75E+03
7.64E-04	7.11E+06	4.07E+03
7.26E-04	7.66E+06	4.47E+03
6.88E-04	8.76E+06	5.13E+03
6.46E-04	9.31E+06	5.45E+03
6.41E-04	9.91E+06	5.80E+03
6.32E-04	1.03E+07	5.97E+03
6.13E-04	1.08E+07	6.30E+03
5.99E-04	1.14E+07	6.50E+03
5.53E-04	1.19E+07	6.70E+03
5.51E-04	1.24E+07	7.10E+03
5.50E-04	1.30E+07	7.35E+03
5.75E-04	1.35E+07	7.70E+03
5.51E-04	1.40E+07	7.90E+03
5.51E-04	1.45E+07	8.10E+03
5.36E-04	1.55E+07	8.60E+03
5.43E-04	1.61E+07	8.90E+03
5.31E-04	1.66E+07	9.10E+03
4.98E-04	1.76E+07	9.50E+03
No. 129		
7.25E-04	7.27E+06	2.77E+03
6.81E-04	7.66E+06	2.99E+03
6.59E-04	8.05E+06	3.17E+03
6.46E-04	8.44E+06	3.37E+03
6.13E-04	8.80E+06	3.54E+03
5.97E-04	9.19E+06	3.73E+03
6.14E-04	9.58E+06	3.93E+03
5.99E-04	9.93E+06	4.05E+03
5.69E-04	1.03E+07	4.20E+03
5.65E-04	1.06E+07	4.37E+03
5.67E-04	1.10E+07	4.50E+03
5.69E-04	1.14E+07	4.61E+03
5.54E-04	1.25E+07	5.13E+03

N_{St}	R_x	R_θ
No. 130		
6.31E-04	9.59E+06	3.53E+03
5.97E-04	1.05E+07	4.07E+03
5.76E-04	1.15E+07	4.49E+03
5.76E-04	1.24E+07	5.00E+03
5.47E-04	1.33E+07	5.44E+03
5.19E-04	1.44E+07	6.00E+03
5.05E-04	1.64E+07	6.90E+03
4.84E-04	1.75E+07	7.30E+03
4.92E-04	1.86E+07	7.85E+03
4.75E-04	1.93E+07	8.10E+03
4.63E-04	2.03E+07	8.50E+03
4.54E-04	2.13E+07	8.90E+03
4.29E-04	2.24E+07	9.30E+03
4.16E-04	2.33E+07	9.70E+03
4.29E-04	2.43E+07	1.00E+04
4.40E-04	2.54E+07	1.03E+04
4.19E-04	2.63E+07	1.07E+04
4.42E-04	2.73E+07	1.11E+04
4.21E-04	2.82E+07	1.14E+04
4.25E-04	2.91E+07	1.17E+04
4.12E-04	3.02E+07	1.22E+04
3.98E-04	3.31E+07	1.31E+04
No. 131		
7.15E-04	6.88E+06	3.50E+03
6.70E-04	8.07E+06	4.20E+03
5.42E-04	9.20E+06	4.84E+03
6.03E-04	1.03E+07	5.49E+03
5.95E-04	1.16E+07	6.10E+03
5.48E-04	1.27E+07	6.70E+03
5.46E-04	1.39E+07	7.25E+03
5.53E-04	1.50E+07	7.90E+03
5.51E-04	1.61E+07	8.35E+03
5.26E-04	1.74E+07	9.00E+03
5.16E-04	1.99E+07	1.02E+04
5.10E-04	2.11E+07	1.07E+04
4.95E-04	2.25E+07	1.12E+04
4.88E-04	2.33E+07	1.16E+04
4.83E-04	2.45E+07	1.22E+04
4.68E-04	2.58E+07	1.26E+04
4.40E-04	2.70E+07	1.32E+04
4.40E-04	2.82E+07	1.36E+04
4.55E-04	2.94E+07	1.41E+04
4.40E-04	3.07E+07	1.46E+04
4.57E-04	3.18E+07	1.50E+04
4.45E-04	3.29E+07	1.54E+04
4.30E-04	3.41E+07	1.58E+04
4.38E-04	3.52E+07	1.63E+04
4.25E-04	3.65E+07	1.68E+04
4.03E-04	4.00E+07	1.82E+04

N_{St}	R_x	R_θ
No. 132		
8.04E-04	6.38E+06	3.57E+03
7.65E-04	7.30E+06	4.18E+03
7.31E-04	7.76E+06	4.49E+03
7.26E-04	8.26E+06	4.80E+03
7.00E-04	8.55E+06	4.95E+03
6.74E-04	9.01E+06	5.22E+03
6.57E-04	9.46E+06	5.48E+03
6.18E-04	9.92E+06	5.76E+03
5.92E-04	1.03E+07	6.00E+03
6.14E-04	1.08E+07	6.20E+03
6.14E-04	1.13E+07	6.50E+03
5.79E-04	1.17E+07	6.70E+03
5.75E-04	1.21E+07	6.90E+03
5.71E-04	1.25E+07	7.10E+03
5.84E-04	1.29E+07	7.30E+03
5.92E-04	1.47E+07	8.10E+03
No. 133		
7.22E-04	6.61E+06	3.27E+03
6.81E-04	7.02E+06	3.50E+03
6.81E-04	7.47E+06	3.80E+03
6.52E-04	7.74E+06	3.92E+03
6.34E-04	8.16E+06	4.17E+03
6.05E-04	9.57E+06	4.37E+03
5.73E-04	8.99E+06	4.60E+03
5.47E-04	9.37E+06	4.80E+03
5.73E-04	9.78E+06	5.00E+03
5.65E-04	1.02E+07	5.18E+03
5.44E-04	1.06E+07	5.37E+03
5.47E-04	1.09E+07	5.53E+03
5.30E-04	1.13E+07	5.72E+03
5.47E-04	1.17E+07	5.89E+03
5.27E-04	1.21E+07	6.10E+03
4.60E-04	1.33E+07	6.50E+03
No 134		
7.87E-04	6.82E+06	3.06E+03
7.10E-04	7.49E+06	3.56E+03
7.05E-04	8.16E+06	3.96E+03
7.18E-04	8.83E+06	4.37E+03
6.83E-04	9.50E+06	4.75E+03
6.57E-04	1.02E+07	5.20E+03
6.17E-04	1.17E+07	6.00E+03
5.56E-04	1.24E+07	6.40E+03
5.93E-04	1.32E+07	6.80E+03
5.74E-04	1.37E+07	7.00E+03
5.58E-04	1.44E+07	7.35E+03
5.43E-04	1.52E+07	7.70E+03
5.05E-04	1.59E+07	7.90E+03
4.92E-04	1.66E+07	8.35E+03

N_{St}	R_x	R_θ
No. 134 Continued		
5.16E-04	1.73E+07	8.70E+03
5.16E-04	1.81E+07	9.00E+03
4.95E-04	1.87E+07	9.30E+03
4.81E-04	1.94E+07	9.60E+03
4.79E-04	2.01E+07	9.90E+03
4.89E-04	2.07E+07	1.02E+04
4.79E-04	2.15E+07	1.05E+04
4.60E-04	2.35E+07	1.13E+04
No. 135		
7.42E-04	7.97E+06	3.24E+03
6.44E-04	9.23E+06	4.02E+03
6.29E-04	1.06E+07	4.73E+03
5.89E-04	1.12E+07	5.09E+03
5.93E-04	1.19E+07	5.46E+03
5.67E-04	1.24E+07	5.60E+03
5.45E-04	1.30E+07	5.96E+03
5.35E-04	1.37E+07	6.20E+03
4.98E-04	1.44E+07	6.55E+03
4.84E-04	1.50E+07	6.85E+03
5.02E-04	1.56E+07	7.10E+03
5.05E-04	1.63E+07	7.45E+03
4.84E-04	1.69E+07	7.70E+03
4.84E-04	1.75E+07	7.95E+03
4.69E-04	1.81E+07	8.20E+03
4.84E-04	1.87E+07	8.45E+03
4.69E-04	1.94E+07	8.70E+03
4.55E-04	2.12E+07	9.40E+03
No. 136		
6.33E-04	6.56E+06	2.77E+03
6.18E-04	6.83E+06	2.93E+03
6.27E-04	7.14E+06	3.10E+03
6.25E-04	7.44E+06	3.27E+03
6.02E-04	7.71E+06	3.40E+03
6.02E-04	7.99E+06	3.55E+03
5.81E-04	8.27E+06	3.68E+03
5.85E-04	8.54E+06	3.83E+03
5.67E-04	8.84E+06	3.97E+03
5.30E-04	9.70E+06	4.36E+03

R_θ determined assuming S = 1.16

The symbol E and the following plus or minus sign and two digits represent the exponent of 10 by which to multiply the number to place the decimal correctly.

TABLE IV.- HEAT-TRANSFER DATA - FLAT PLATE- Continued

N_{St}	R_x	R_θ
Identity No. 137		
8.44E-04	5.95E+06	3.10E+03
7.88E-04	6.33E+06	3.43E+03
7.88E-04	6.73E+06	3.73E+03
7.47E-04	6.97E+06	3.85E+03
7.30E-04	7.35E+06	4.12E+03
6.95E-04	7.72E+06	4.34E+03
6.60E-04	8.10E+06	4.60E+03
6.30E-04	8.44E+06	4.83E+03
6.30E-04	8.81E+06	5.01E+03
6.62E-04	9.18E+06	5.25E+03
6.30E-04	9.52E+06	5.45E+03
6.39E-04	9.86E+06	5.64E+03
6.22E-04	1.02E+07	5.83E+03
6.34E-04	1.05E+07	6.00E+03
6.22E-04	1.09E+07	6.15E+03
5.81E-04	1.20E+07	6.70E+03
No. 138		
6.90E-04	7.50E+06	3.18E+03
6.86E-04	7.82E+06	3.36E+03
6.61E-04	8.11E+06	3.50E+03
6.65E-04	8.40E+06	3.69E+03
6.44E-04	8.69E+06	3.86E+03
6.52E-04	8.98E+06	4.00E+03
6.25E-04	9.29E+06	4.17E+03
5.70E-04	1.02E+07	4.58E+03
No. 139		
7.88E-04	6.74E+06	3.25E+03
7.47E-04	6.97E+06	3.38E+03
7.30E-04	7.35E+06	3.63E+03
6.95E-04	7.72E+06	3.84E+03
6.60E-04	8.10E+06	4.10E+03
6.30E-04	8.44E+06	4.28E+03
6.30E-04	8.81E+06	4.50E+03
6.62E-04	9.18E+06	4.74E+03
6.30E-04	9.53E+06	4.90E+03
6.39E-04	9.87E+06	5.08E+03
6.22E-04	1.02E+07	5.27E+03
6.34E-04	1.05E+07	5.43E+03
6.22E-04	1.09E+07	5.64E+03
5.81E-04	1.20E+07	6.15E+03
No. 140		
8.00E-04	6.10E+06	2.88E+03
7.47E-04	6.31E+06	3.00E+03
7.39E-04	6.52E+06	3.13E+03
6.92E-04	6.75E+06	3.28E+03
6.82E-04	7.17E+06	3.54E+03
6.69E-04	7.40E+06	3.67E+03
No. 141		
5.52E-04	1.09E+07	4.03E+03
5.35E-04	1.13E+07	4.18E+03
No. 142		
5.73E-04	1.12E+07	3.81E+03
5.44E-04	1.16E+07	4.00E+03
5.49E-04	1.20E+07	4.20E+03
5.40E-04	1.24E+07	4.39E+03
5.10E-04	1.32E+07	4.75E+03
5.25E-04	1.33E+07	4.81E+03
5.40E-04	1.37E+07	5.00E+03
No. 143		
5.53E-04	1.13E+07	4.32E+03
5.68E-04	1.17E+07	4.54E+03
5.44E-04	1.22E+07	4.77E+03
5.45E-04	1.26E+07	5.00E+03
5.25E-04	1.31E+07	5.24E+03
5.37E-04	1.35E+07	5.46E+03
5.25E-04	1.40E+07	5.69E+03
4.95E-04	1.49E+07	6.14E+03
4.97E-04	1.50E+07	6.19E+03
5.12E-04	1.55E+07	6.42E+03
No. 144		
5.49E-04	1.06E+07	3.64E+03
5.31E-04	1.13E+07	3.98E+03
5.31E-04	1.20E+07	4.30E+03
5.10E-04	1.24E+07	4.45E+03
5.03E-04	1.31E+07	4.74E+03
4.85E-04	1.38E+07	5.00E+03
4.54E-04	1.44E+07	5.30E+03
4.46E-04	1.50E+07	5.55E+03
4.54E-04	1.57E+07	5.80E+03
4.68E-04	1.64E+07	6.10E+03
4.50E-04	1.70E+07	6.30E+03
4.50E-04	1.76E+07	6.55E+03
4.39E-04	1.82E+07	6.80E+03
4.50E-04	1.88E+07	7.00E+03
4.43E-04	1.79E+07	7.30E+03
4.14E-04	2.13E+07	7.90E+03
No. 145		
5.77E-04	8.92E+06	3.58E+03
5.91E-04	9.31E+06	3.79E+03
6.08E-04	9.71E+06	4.00E+03
5.84E-04	1.01E+07	4.17E+03
5.85E-04	1.04E+07	4.35E+03
5.73E-04	1.11E+07	4.68E+03
5.73E-04	1.15E+07	4.87E+03
5.42E-04	1.19E+07	5.02E+03
5.24E-04	1.27E+07	5.37E+03
No. 146		
5.68E-04	7.21E+06	2.73E+03
5.83E-04	7.53E+06	2.88E+03
5.91E-04	7.85E+06	3.04E+03
5.81E-04	8.14E+06	3.16E+03
5.72E-04	8.43E+06	3.32E+03
5.61E-04	8.72E+06	3.46E+03
5.61E-04	9.01E+06	3.58E+03
5.66E-04	9.33E+06	3.73E+03
5.08E-04	1.02E+07	4.14E+03
No. 147		
5.12E-04	1.12E+07	3.20E+03
5.16E-04	1.28E+07	3.88E+03
4.89E-04	1.36E+07	4.23E+03
4.85E-04	1.45E+07	4.57E+03
4.59E-04	1.50E+07	4.74E+03
4.47E-04	1.58E+07	5.07E+03
4.28E-04	1.66E+07	5.37E+03
4.51E-04	1.74E+07	5.70E+03
4.13E-04	1.82E+07	5.99E+03
4.17E-04	1.90E+07	6.30E+03
4.32E-04	1.98E+07	6.55E+03
4.28E-04	2.05E+07	6.75E+03
4.32E-04	2.13E+07	7.10E+03
4.17E-04	2.20E+07	7.40E+03
4.28E-04	2.27E+07	7.60E+03
4.17E-04	2.35E+07	7.90E+03
3.97E-04	2.58E+07	8.60E+03
No. 148		
4.86E-04	1.29E+07	3.40E+03
4.72E-04	1.48E+07	4.16E+03
4.61E-04	1.57E+07	4.20E+03
4.64E-04	1.67E+07	4.43E+03
4.44E-04	1.73E+07	5.16E+03
4.47E-04	1.83E+07	5.53E+03
4.30E-04	1.92E+07	5.84E+03
4.10E-04	2.01E+07	6.20E+03
3.96E-04	2.10E+07	6.50E+03
4.05E-04	2.19E+07	6.85E+03
4.21E-04	2.28E+07	7.15E+03
4.13E-04	2.37E+07	7.50E+03
4.19E-04	2.45E+07	7.80E+03
4.05E-04	2.54E+07	8.10E+03
4.13E-04	2.62E+07	8.35E+03
4.05E-04	2.71E+07	8.70E+03
3.96E-04	2.98E+07	9.60E+03
No. 149		
5.64E-04	1.10E+07	3.53E+03
5.64E-04	1.14E+07	3.71E+03
5.34E-04	1.17E+07	3.93E+03
5.38E-04	1.21E+07	4.08E+03
5.29E-04	1.26E+07	4.29E+03
5.17E-04	1.38E+07	4.83E+03
No. 150		
5.49E-04	1.18E+07	4.05E+03
5.63E-04	1.23E+07	4.24E+03
5.44E-04	1.27E+07	4.47E+03
5.50E-04	1.32E+07	4.66E+03
5.35E-04	1.36E+07	4.83E+03
5.20E-04	1.41E+07	5.07E+03
4.89E-04	1.54E+07	5.63E+03
No. 151		
6.71E-04	7.09E+06	3.37E+03
6.35E-04	7.44E+06	3.57E+03
6.06E-04	7.75E+06	3.75E+03
6.35E-04	8.09E+06	3.95E+03
6.35E-04	8.43E+06	4.15E+03
6.14E-04	8.75E+06	4.27E+03
6.14E-04	9.06E+06	4.45E+03
5.90E-04	9.37E+06	4.62E+03
5.98E-04	9.68E+06	4.77E+03
5.74E-04	1.00E+07	4.95E+03
5.42E-04	1.10E+07	5.40E+03
No. 152		
6.20E-04	8.54E+06	3.34E+03
5.86E-04	9.08E+06	3.67E+03
6.01E-04	9.66E+06	3.98E+03
5.61E-04	1.00E+07	4.12E+03
5.47E-04	1.05E+07	4.38E+03
5.27E-04	1.11E+07	4.60E+03
5.08E-04	1.16E+07	4.87E+03
4.88E-04	1.21E+07	5.10E+03
4.93E-04	1.26E+07	5.30E+03
5.08E-04	1.32E+07	5.54E+03
4.88E-04	1.37E+07	5.74E+03
4.88E-04	1.41E+07	5.97E+03
4.74E-04	1.46E+07	6.15E+03
4.81E-04	1.51E+07	6.30E+03
4.76E-04	1.57E+07	6.55E+03
4.49E-04	1.72E+07	7.10E+03
No. 153		
3.82E-04	2.37E+07	6.08E+03
3.64E-04	2.62E+07	6.96E+03
3.43E-04	2.88E+07	7.78E+03
3.25E-04	3.13E+07	8.46E+03
2.98E-04	3.39E+07	9.22E+03
3.09E-04	3.75E+07	1.03E+04
2.94E-04	4.10E+07	1.12E+04
2.75E-04	4.46E+07	1.22E+04
2.54E-04	4.82E+07	1.32E+04
No. 154		
4.60E-04	1.42E+07	5.50E+03
5.14E-04	1.61E+07	6.40E+03
4.36E-04	1.80E+07	7.26E+03
4.48E-04	1.99E+07	8.03E+03
4.19E-04	2.18E+07	8.82E+03
3.88E-04	2.37E+07	9.57E+03
3.73E-04	2.64E+07	1.06E+04
3.64E-04	2.90E+07	1.15E+04
3.49E-04	3.17E+07	1.24E+04
3.48E-04	3.43E+07	1.34E+04
No. 155		
6.36E-04	9.46E+06	4.07E+03
5.37E-04	1.22E+07	5.76E+03
5.39E-04	1.48E+07	7.37E+03
5.02E-04	2.29E+07	1.07E+04
4.71E-04	2.50E+07	1.32E+04
4.45E-04	2.83E+07	1.43E+04
4.38E-04	3.10E+07	1.56E+04
4.07E-04	3.37E+07	1.68E+04
4.30E-04	3.75E+07	1.86E+04
4.08E-04	4.13E+07	2.03E+04
3.85E-04	4.51E+07	2.19E+04

R_θ determined assuming S = 1.16

The symbol E and the following plus or minus sign and two digits represent the exponent of 10 by which to multiply the number to place the decimal correctly.

TABLE IV. - HEAT-TRANSFER DATA - FLAT PLATE - Continued

N_{St}	R_x	R_θ
Identity No. 156		
5.18E-04	9.00E+06	4.56E+03
6.29E-04	1.06E+07	5.62E+03
5.42E-04	1.22E+07	6.63E+03
5.86E-04	1.39E+07	7.67E+03
5.31E-04	1.55E+07	8.60E+03
5.73E-04	1.71E+07	9.47E+03
4.90E-04	1.88E+07	1.04E+04
4.73E-04	2.04E+07	1.12E+04
4.86E-04	2.27E+07	1.24E+04
4.60E-04	2.49E+07	1.35E+04
4.54E-04	2.72E+07	1.47E+04
4.46E-04	2.95E+07	1.57E+04
No. 157		
5.64E-04	1.51E+07	6.49E+03
5.81E-04	1.79E+07	8.22E+03
5.12E-04	2.06E+07	9.78E+03
5.64E-04	2.34E+07	1.13E+04
4.99E-04	2.62E+07	1.28E+04
5.33E-04	2.89E+07	1.42E+04
4.65E-04	3.15E+07	1.55E+04
4.59E-04	3.44E+07	1.70E+04
4.96E-04	3.82E+07	1.90E+04
5.03E-04	4.21E+07	2.08E+04
4.59E-04	4.60E+07	2.26E+04
4.42E-04	4.98E+07	2.42E+04
No. 158		
5.96E-04	1.34E+07	6.47E+03
5.00E-04	1.54E+07	7.61E+03
5.73E-04	1.75E+07	8.67E+03
5.34E-04	1.96E+07	9.84E+03
5.31E-04	2.16E+07	1.09E+04
5.00E-04	2.37E+07	1.19E+04
4.78E-04	2.57E+07	1.29E+04
4.72E-04	2.86E+07	1.42E+04
4.62E-04	3.15E+07	1.55E+04
4.45E-04	3.44E+07	1.68E+04
4.38E-04	3.72E+07	1.82E+04
No. 159		
6.84E-04	6.43E+06	4.44E+03
6.72E-04	7.14E+06	5.01E+03
6.62E-04	7.86E+06	5.60E+03
6.16E-04	8.58E+06	6.16E+03
5.11E-04	9.30E+06	6.69E+03
5.77E-04	1.00E+07	7.20E+03

N_{St}	R_x	R_θ
No. 160		
4.80E-04	8.60E+06	2.62E+03
4.75E-04	8.84E+06	2.72E+03
4.68E-04	9.09E+06	2.80E+03
4.56E-04	9.34E+06	2.70E+03
4.48E-04	9.60E+06	3.00E+03
4.40E-04	9.86E+06	3.09E+03
4.20E-04	1.01E+07	3.18E+03
4.36E-04	1.05E+07	3.31E+03
4.23E-04	1.06E+07	3.35E+03
4.24E-04	1.09E+07	3.47E+03
4.34E-04	1.11E+07	3.53E+03
4.40E-04	1.14E+07	3.62E+03
4.35E-04	1.16E+07	3.70E+03
4.15E-04	1.20E+07	3.87E+03
4.06E-04	1.21E+07	3.90E+03
No. 161		
4.77E-04	6.75E+06	2.07E+03
4.80E-04	6.99E+06	2.16E+03
4.80E-04	7.08E+06	2.20E+03
4.76E-04	7.16E+06	2.23E+03
4.77E-04	7.41E+06	2.33E+03
4.73E-04	7.59E+06	2.39E+03
4.60E-04	7.76E+06	2.47E+03
4.55E-04	8.00E+06	2.57E+03
4.37E-04	8.09E+06	2.60E+03
No 162		
4.18E-04	1.33E+07	3.89E+03
4.14E-04	1.36E+07	4.01E+03
4.14E-04	1.39E+07	4.14E+03
3.97E-04	1.42E+07	4.25E+03
4.00E-04	1.58E+07	4.60E+03
4.00E-04	1.55E+07	4.71E+03
3.95E-04	1.58E+07	4.82E+03
4.03E-04	1.61E+07	4.90E+03
No. 163		
8.57E-04	7.42E+06	4.18E+03
8.30E-04	7.86E+06	4.47E+03
7.27E-04	9.58E+06	5.57E+03
7.07E-04	1.04E+07	6.07E+03
7.10E-04	1.13E+07	6.61E+03
6.48E-04	1.22E+07	7.02E+03
6.32E-04	1.30E+07	7.58E+03
No. 164		
8.66E-04	6.07E+06	3.66E+03
8.49E-04	6.61E+06	4.04E+03
8.39E-04	7.16E+06	4.40E+03
7.56E-04	7.71E+06	4.80E+03
7.39E-04	8.25E+06	5.16E+03

N_{St}	R_x	R_θ
No. 165		
9.90E-04	5.04E+06	2.96E+03
9.05E-04	6.02E+06	3.78E+03
8.47E-04	7.01E+06	4.50E+03
8.12E-04	8.00E+06	5.21E+03
8.41E-04	8.99E+06	5.89E+03
7.22E-04	1.19E+07	7.76E+03
6.72E-04	1.39E+07	8.90E+03
6.72E-04	1.49E+07	9.44E+03
No. 166		
9.69E-04	5.38E+06	3.11E+03
9.00E-04	7.15E+06	4.40E+03
8.50E-04	8.18E+06	5.17E+03
7.53E-04	9.43E+06	6.00E+03
No. 167		
9.82E-04	7.35E+06	4.02E+03
9.38E-04	7.84E+06	4.43E+03
9.25E-04	8.32E+06	4.82E+03
9.46E-04	8.80E+06	5.22E+03
8.72E-04	1.07E+07	6.73E+03
8.26E-04	1.17E+07	7.37E+03
8.16E-04	1.27E+07	8.10E+03
7.61E-04	1.36E+07	8.73E+03
7.66E-04	1.46E+07	9.39E+03
No. 168		
1.15E-03	4.40E+06	3.01E+03
1.03E-03	4.71E+06	3.30E+03
1.00E-03	5.02E+06	3.57E+03
9.79E-04	5.34E+06	3.86E+03
1.02E-03	5.64E+06	4.10E+03
9.39E-04	6.88E+06	5.08E+03
8.90E-04	7.49E+06	5.57E+03
8.86E-04	8.12E+06	6.09E+03
8.48E-04	8.74E+06	6.43E+03
8.18E-04	9.36E+06	6.84E+03
No. 169		
7.54E-04	8.06E+06	4.02E+03
7.02E-04	9.76E+06	5.07E+03
6.94E-04	1.08E+07	5.74E+03
6.46E-04	1.15E+07	6.06E+03
6.44E-04	1.21E+07	6.46E+03
6.23E-04	1.31E+07	7.00E+03
6.00E-04	1.40E+07	7.50E+03
5.80E-04	1.60E+07	8.60E+03
No. 170		
6.59E-04	1.26E+07	6.60E+03
6.39E-04	1.49E+07	7.20E+03
6.08E-04	1.71E+07	8.40E+03

N_{St}	R_x	R_θ
No. 171		
7.71E-04	6.79E+06	4.03E+03
7.12E-04	1.01E+07	4.90E+03
7.39E-04	1.14E+07	5.75E+03
7.09E-04	1.27E+07	6.36E+03
6.67E-04	1.42E+07	7.43E+03
6.78E-04	1.48E+07	7.85E+03
6.36E-04	1.64E+07	8.81E+03
6.46E-04	1.74E+07	9.41E+03
6.14E-04	2.02E+07	1.09E+04
No. 172		
8.83E-04	5.66E+06	3.09E+03
8.08E-04	6.30E+06	3.58E+03
8.36E-04	6.68E+06	3.84E+03
7.66E-04	7.70E+06	4.35E+03
No. 173		
7.69E-04	8.12E+06	4.55E+03
7.40E-04	9.44E+06	5.48E+03
6.82E-04	1.08E+07	6.32E+03
6.37E-04	1.34E+07	7.91E+03
6.41E-04	1.54E+07	9.08E+03
6.05E-04	1.88E+07	1.09E+04
No. 174		
7.84E-04	5.15E+06	3.56E+03
7.77E-04	5.89E+06	4.04E+03
7.04E-04	7.19E+06	4.87E+03
No. 175		
1.02E-03	3.83E+06	2.94E+03
9.46E-04	4.77E+06	3.67E+03
9.24E-04	5.45E+06	4.20E+03
8.63E-04	6.66E+06	5.06E+03
No. 176		
1.04E-03	5.24E+06	3.12E+03
9.98E-04	5.83E+06	3.60E+03
9.82E-04	6.18E+06	3.88E+03
9.20E-04	7.13E+06	4.60E+03

R_θ determined assuming S = 1.16

The symbol E and the following plus or minus sign and two digits represent the exponent of 10 by which to multiply the number to place the decimal correctly

N_{St}	R_x	R_θ
No. 177		
4.40E-04	1.81E+07	4.40E+03
4.58E-04	1.86E+07	4.61E+03
4.21E-04	1.92E+07	4.83E+03
4.26E-04	1.97E+07	5.03E+03
4.21E-04	2.03E+07	5.26E+03
4.01E-04	2.09E+07	5.46E+03
4.15E-04	2.14E+07	5.68E+03
3.79E-04	2.20E+07	5.88E+03
4.14E-04	2.26E+07	6.06E+03
3.99E-04	2.31E+07	6.16E+03
4.04E-04	2.38E+07	6.47E+03
3.82E-04	2.43E+07	6.64E+03
3.91E-04	2.49E+07	6.86E+03
3.84E-04	2.54E+07	7.03E+03
3.76E-04	2.60E+07	7.20E+03
3.56E-04	2.66E+07	7.39E+03
3.55E-04	2.71E+07	7.58E+03
3.33E-04	2.77E+07	7.75E+03
3.47E-04	2.83E+07	7.92E+03
3.42E-04	2.88E+07	8.06E+03
3.55E-04	2.94E+07	8.24E+03
3.30E-04	3.00E+07	8.42E+03
3.51E-04	3.05E+07	8.58E+03
3.30E-04	3.11E+07	8.77E+03
3.33E-04	3.16E+07	8.93E+03
3.40E-04	3.22E+07	9.03E+03
No. 178		
5.05E-04	1.01E+07	3.42E+03
4.69E-04	1.04E+07	3.53E+03
4.65E-04	1.06E+07	3.64E+03
4.88E-04	1.09E+07	3.77E+03
4.49E-04	1.12E+07	3.86E+03
4.65E-04	1.17E+07	4.10E+03
4.46E-04	1.20E+07	4.21E+03
4.61E-04	1.23E+07	4.31E+03
4.43E-04	1.26E+07	4.41E+03
4.45E-04	1.28E+07	4.51E+03
4.14E-04	1.31E+07	4.61E+03
4.34E-04	1.34E+07	4.71E+03
4.24E-04	1.34E+07	4.71E+03
4.12E-04	1.36E+07	4.80E+03
3.87E-04	1.39E+07	4.89E+03
4.03E-04	1.42E+07	4.98E+03
4.03E-04	1.45E+07	5.08E+03
4.03E-04	1.47E+07	5.19E+03
3.64E-04	1.50E+07	5.29E+03
3.95E-04	1.53E+07	5.36E+03
3.80E-04	1.55E+07	5.46E+03

TABLE IV. - HEAT-TRANSFER DATA - FLAT PLATE- Continued

N_{St}	R_x	R_θ
Identity No. 179		
5.33E-04	6.82E+06	2.59E+03
5.16E-04	6.93E+06	2.65E+03
5.30E-04	7.13E+06	2.71E+03
5.16E-04	7.28E+06	2.78E+03
5.02E-04	7.43E+06	2.84E+03
4.82E-04	7.43E+06	2.84E+03
5.02E-04	7.58E+06	2.89E+03
4.87E-04	7.73E+06	2.96E+03
4.87E-04	7.88E+06	3.03E+03
4.59E-04	7.88E+06	3.03E+03
4.59E-04	8.04E+06	3.09E+03
4.59E-04	8.18E+06	3.14E+03
4.44E-04	8.34E+06	3.19E+03
4.21E-04	8.49E+06	3.26E+03
4.41E-04	8.64E+06	3.32E+03
No. 180		
6.95E-04	5.36E+06	3.12E+03
6.54E-04	5.76E+06	3.37E+03
6.68E-04	6.16E+06	3.57E+03
6.46E-04	6.54E+06	3.80E+03
6.16E-04	6.94E+06	4.02E+03
6.61E-04	7.34E+06	4.25E+03
6.34E-04	7.74E+06	4.47E+03
6.55E-04	8.13E+06	4.69E+03
6.50E-04	8.53E+06	4.91E+03
6.57E-04	8.53E+06	4.91E+03
6.89E-04	9.32E+06	5.33E+03
6.10E-04	9.71E+06	5.55E+03
6.18E-04	1.01E+07	5.72E+03
6.38E-04	1.09E+07	6.17E+03
6.38E-04	1.17E+07	6.56E+03
No. 181		
6.17E-04	5.18E+06	2.17E+03
6.22E-04	5.40E+06	2.29E+03
5.70E-04	5.70E+06	2.46E+03
6.18E-04	5.93E+06	2.58E+03
5.70E-04	6.18E+06	2.69E+03
6.33E-04	6.40E+06	2.82E+03
5.37E-04	6.63E+06	2.94E+03
5.32E-04	6.86E+06	3.06E+03
5.64E-04	7.09E+06	3.17E+03
5.64E-04	7.32E+06	3.27E+03
5.43E-04	7.56E+06	3.38E+03
5.43E-04	7.79E+06	3.49E+03
5.69E-04	8.02E+06	3.60E+03
5.24E-04	8.26E+06	3.71E+03
5.26E-04	8.49E+06	3.82E+03
5.05E-04	8.72E+06	3.92E+03
5.26E-04	8.95E+06	4.02E+03
5.37E-04	9.18E+06	4.12E+03

N_{St}	R_x	R_θ
No. 182		
5.75E-04	9.40E+06	3.68E+03
5.51E-04	9.80E+06	3.87E+03
5.14E-04	1.03E+07	4.11E+03
5.35E-04	1.07E+07	4.30E+03
4.96E-04	1.11E+07	4.48E+03
5.43E-04	1.15E+07	4.70E+03
5.07E-04	1.20E+07	4.88E+03
5.28E-04	1.29E+07	5.29E+03
4.75E-04	1.33E+07	5.48E+03
4.75E-04	1.50E+07	6.20E+03
4.36E-04	1.68E+07	6.94E+03
4.36E-04	1.75E+07	7.24E+03
3.94E-04	1.85E+07	7.58E+03
3.94E-04	1.94E+07	7.94E+03
3.88E-04	2.02E+07	8.27E+03
3.99E-04	2.13E+07	8.68E+03
4.14E-04	2.22E+07	8.98E+03
4.10E-04	2.31E+07	9.28E+03
4.18E-04	2.39E+07	9.59E+03
4.12E-04	2.48E+07	9.89E+03
4.14E-04	2.57E+07	1.01E+04
4.10E-04	2.65E+07	1.05E+04
3.86E-04	2.74E+07	1.07E+04
3.91E-04	2.83E+07	1.11E+04
3.81E-04	2.91E+07	1.14E+04
3.86E-04	3.00E+07	1.17E+04
3.92E-04	3.09E+07	1.20E+04
3.76E-04	3.26E+07	1.25E+04
3.49E-04	3.35E+07	1.28E+04
3.76E-04	3.44E+07	1.31E+04
3.57E-04	3.52E+07	1.34E+04
No. 183		
4.49E-04	2.21E+07	7.05E+03
4.23E-04	2.51E+07	8.20E+03
4.21E-04	2.64E+07	8.65E+03
4.21E-04	2.77E+07	9.18E+03
4.27E-04	2.83E+07	9.45E+03
4.34E-04	2.96E+07	9.93E+03
4.05E-04	3.09E+07	1.03E+04
3.85E-04	3.14E+07	1.06E+04
3.91E-04	3.19E+07	1.07E+04
3.83E-04	3.27E+07	1.10E+04
3.75E-04	3.30E+07	1.12E+04
4.00E-04	3.35E+07	1.13E+04
3.85E-04	3.37E+07	1.14E+04
3.94E-04	3.43E+07	1.16E+04
4.05E-04	3.45E+07	1.17E+04
4.04E-04	3.59E+07	1.22E+04
3.77E-04	3.67E+07	1.23E+04
3.75E-04	3.74E+07	1.26E+04
3.75E-04	3.97E+07	1.34E+04

N_{St}	R_x	R_θ
No. 183 Continued		
3.82E-04	4.05E+07	1.36E+04
3.79E-04	4.13E+07	1.38E+04
3.61E-04	4.28E+07	1.46E+04
3.77E-04	4.43E+07	1.50E+04
3.80E-04	4.59E+07	1.54E+04
No. 184		
4.05E-04	2.53E+07	7.42E+03
3.88E-04	2.73E+07	8.15E+03
4.01E-04	2.86E+07	8.65E+03
3.90E-04	3.00E+07	9.10E+03
3.90E-04	3.07E+07	9.37E+03
3.99E-04	3.21E+07	9.90E+03
3.94E-04	3.28E+07	1.00E+04
3.66E-04	3.35E+07	1.03E+04
3.62E-04	3.41E+07	1.05E+04
3.55E-04	3.45E+07	1.06E+04
3.64E-04	3.46E+07	1.07E+04
3.77E-04	3.55E+07	1.10E+04
3.62E-04	3.57E+07	1.10E+04
3.72E-04	3.63E+07	1.12E+04
3.62E-04	3.66E+07	1.13E+04
3.51E-04	3.72E+07	1.15E+04
3.75E-04	3.74E+07	1.16E+04
3.46E-04	3.80E+07	1.18E+04
3.42E-04	3.83E+07	1.19E+04
3.88E-04	3.89E+07	1.22E+04
3.75E-04	3.98E+07	1.24E+04
3.75E-04	4.06E+07	1.26E+04
3.55E-04	4.31E+07	1.34E+04
3.60E-04	4.39E+07	1.38E+04
3.66E-04	4.47E+07	1.38E+04
3.49E-04	4.64E+07	1.46E+04
3.49E-04	4.81E+07	1.50E+04
3.66E-04	4.97E+07	1.55E+04
No. 185		
4.72E-04	2.60E+07	6.22E+03
4.99E-04	2.80E+07	7.15E+03
4.14E-04	3.50E+07	1.00E+04
4.21E-04	3.54E+07	1.02E+04
4.53E-04	3.56E+07	1.03E+04
4.26E-04	3.67E+07	1.07E+04
4.21E-04	3.85E+07	1.15E+04
4.25E-04	3.91E+07	1.17E+04
4.48E-04	4.00E+07	1.22E+04
4.49E-04	4.09E+07	1.24E+04
4.36E-04	4.43E+07	1.38E+04
4.50E-04	4.51E+07	1.41E+04
4.46E-04	4.60E+07	1.43E+04
4.33E-04	4.77E+07	1.50E+04
4.55E-04	4.94E+07	1.57E+04
4.53E-04	5.11E+07	1.63E+04

N_{St}	R_x	R_θ
No. 186		
4.23E-04	2.67E+07	7.75E+03
4.26E-04	2.88E+07	8.55E+03
4.03E-04	3.39E+07	1.05E+04
3.90E-04	3.54E+07	1.10E+04
3.97E-04	3.65E+07	1.13E+04
3.91E-04	3.84E+07	1.21E+04
4.04E-04	3.86E+07	1.22E+04
4.07E-04	3.93E+07	1.23E+04
4.18E-04	3.95E+07	1.25E+04
4.04E-04	4.01E+07	1.27E+04
3.94E-04	4.04E+07	1.28E+04
4.17E-04	4.20E+07	1.34E+04
4.13E-04	4.29E+07	1.36E+04
4.26E-04	4.55E+07	1.46E+04
4.26E-04	4.64E+07	1.48E+04
4.23E-04	4.73E+07	1.52E+04
4.11E-04	4.90E+07	1.57E+04
3.98E-04	5.08E+07	1.64E+04
4.05E-04	5.25E+07	1.66E+04
No. 187		
4.61E-04	3.02E+07	8.75E+03
3.99E-04	3.56E+07	1.07E+04
3.86E-04	3.84E+07	1.17E+04
3.81E-04	3.96E+07	1.22E+04
3.89E-04	4.03E+07	1.25E+04
4.04E-04	4.06E+07	1.25E+04
3.74E-04	4.12E+07	1.27E+04
4.04E-04	4.15E+07	1.29E+04
3.91E-04	4.21E+07	1.32E+04
3.91E-04	4.24E+07	1.33E+04
4.21E-04	4.32E+07	1.36E+04
4.09E-04	4.41E+07	1.38E+04
3.94E-04	4.50E+07	1.41E+04
3.91E-04	4.78E+07	1.51E+04
3.96E-04	4.87E+07	1.55E+04
3.77E-04	4.96E+07	1.58E+04
3.74E-04	5.15E+07	1.65E+04
3.81E-04	5.33E+07	1.72E+04
4.09E-04	5.52E+07	1.77E+04

R_θ determined assuming S = 1.16

The symbol E and the following plus or minus sign and two digits represent the exponent of 10 by which to multiply the number to place the decimal correctly.

N_{St}	R_x	R_θ
No. 188		
4.47E-04	6.33E+07	1.92E+04
4.28E-04	6.82E+07	2.10E+04
3.40E-04	1.21E+08	2.25E+04
3.32E-04	1.26E+08	3.87E+04
3.28E-04	1.28E+08	4.10E+04
3.19E-04	1.29E+08	4.12E+04
3.33E-04	1.30E+08	4.15E+04
3.30E-04	1.33E+08	4.25E+04
3.26E-04	1.34E+08	4.27E+04
3.28E-04	1.36E+08	4.33E+04
3.47E-04	1.37E+08	4.35E+04
3.32E-04	1.40E+08	4.41E+04
3.46E-04	1.40E+08	4.48E+04
3.25E-04	1.43E+08	4.51E+04
3.18E-04	1.44E+08	4.55E+04
3.53E-04	1.46E+08	4.62E+04
3.54E-04	1.49E+08	4.70E+04
3.32E-04	1.52E+08	4.80E+04
3.16E-04	1.62E+08	5.05E+04
3.19E-04	1.65E+08	5.15E+04
3.09E-04	1.68E+08	5.22E+04
3.04E-04	1.74E+08	5.40E+04
3.05E-04	1.80E+08	5.57E+04
3.18E-04	1.87E+08	5.71E+04
No. 189		
3.54E-04	4.75E+07	1.22E+04
3.32E-04	5.14E+07	1.35E+04
3.34E-04	5.54E+07	1.47E+04
3.42E-04	7.73E+07	2.14E+04
3.65E-04	8.32E+07	2.32E+04
3.64E-04	9.15E+07	2.56E+04
3.62E-04	9.38E+07	2.63E+04
3.60E-04	1.02E+08	2.90E+04
3.50E-04	1.04E+08	2.96E+04
3.36E-04	1.05E+08	3.00E+04
3.62E-04	1.08E+08	3.07E+04
3.40E-04	1.09E+08	3.10E+04
3.56E-04	1.11E+08	3.18E+04
3.62E-04	1.12E+08	3.19E+04
3.65E-04	1.13E+08	3.22E+04
3.50E-04	1.14E+08	3.27E+04
3.40E-04	1.16E+08	3.31E+04
3.34E-04	1.17E+08	3.32E+04
3.60E-04	1.21E+08	3.48E+04
3.67E-04	1.24E+08	3.55E+04
3.44E-04	1.31E+08	3.80E+04
3.46E-04	1.34E+08	3.87E+04
3.48E-04	1.37E+08	3.93E+04
3.46E-04	1.42E+08	4.10E+04
3.28E-04	1.47E+08	4.25E+04
3.44E-04	1.52E+08	4.40E+04

TABLE IV. – HEAT-TRANSFER DATA – FLAT PLATE – Concluded

N_{St}	R_x	R_θ
Identity No. 190		
4.06E-04	1.25E+07	3.95E+03
3.81E-04	1.41E+07	4.50E+03
3.78E-04	1.45E+07	4.67E+03
3.73E-04	1.50E+07	4.81E+03
3.71E-04	1.56E+07	5.00E+03
3.62E-04	1.58E+07	5.07E+03
3.62E-04	1.61E+07	5.16E+03
3.41E-04	1.63E+07	5.23E+03
3.59E-04	1.68E+07	5.37E+03
3.64E-04	1.70E+07	5.45E+03
3.50E-04	1.83E+07	5.82E+03
3.36E-04	1.88E+07	5.97E+03
3.17E-04	1.92E+07	6.12E+03
3.37E-04	1.97E+07	6.25E+03
No. 191		
4.62E-04	1.22E+07	4.73E+03
4.20E-04	1.37E+07	5.38E+03
3.91E-04	1.41E+07	5.50E+03
3.83E-04	1.45E+07	5.68E+03
3.88E-04	1.46E+07	5.72E+03
3.89E-04	1.47E+07	5.73E+03
4.03E-04	1.48E+07	5.78E+03
3.84E-04	1.52E+07	5.91E+03
4.03E-04	1.54E+07	6.00E+03
4.04E-04	1.56E+07	6.13E+03
3.64E-04	1.59E+07	6.20E+03
4.04E-04	1.63E+07	6.35E+03
4.00E-04	1.66E+07	6.45E+03
3.72E-04	1.70E+07	6.60E+03
3.99E-04	1.78E+07	6.90E+03
3.55E-04	1.82E+07	7.00E+03
3.57E-04	1.87E+07	7.22E+03
3.72E-04	1.92E+07	7.35E+03

N_{St}	R_x	R_θ
No. 192		
4.27E-04	1.65E+07	4.58E+03
4.00E-04	1.91E+07	5.55E+03
3.70E-04	2.17E+07	6.42E+03
3.71E-04	2.26E+07	6.70E+03
3.80E-04	2.35E+07	6.98E+03
3.03E-04	2.83E+07	8.40E+03
3.31E-04	3.05E+07	9.00E+03
2.79E-04	3.19E+07	9.35E+03
2.79E-04	3.28E+07	9.60E+03
2.87E-04	3.33E+07	9.75E+03
2.74E-04	3.38E+07	9.85E+03
2.99E-04	3.40E+07	9.95E+03
2.92E-04	3.42E+07	1.00E+04
2.96E-04	3.44E+07	1.01E+04
2.85E-04	3.53E+07	1.02E+04
2.98E-04	3.58E+07	1.04E+04
3.07E-04	3.64E+07	1.05E+04
2.89E-04	3.70E+07	1.07E+04
3.03E-04	3.80E+07	1.09E+04
2.85E-04	3.85E+07	1.10E+04
2.74E-04	3.97E+07	1.13E+04
2.77E-04	4.13E+07	1.17E+04
2.70E-04	4.24E+07	1.20E+04
2.77E-04	4.36E+07	1.25E+04
2.82E-04	4.47E+07	1.26E+04
No. 193		
4.86E-04	1.11E+07	4.02E+03
4.44E-04	1.34E+07	4.93E+03
4.43E-04	1.44E+07	5.33E+03
3.98E-04	1.51E+07	5.60E+03
4.12E-04	1.55E+07	5.77E+03
4.12E-04	1.57E+07	5.82E+03
3.82E-04	1.60E+07	5.92E+03
3.92E-04	1.61E+07	5.97E+03
4.12E-04	1.61E+07	6.00E+03
3.98E-04	1.67E+07	6.17E+03
3.93E-04	1.69E+07	6.25E+03
3.80E-04	1.72E+07	6.35E+03
3.98E-04	1.75E+07	6.45E+03
4.09E-04	1.79E+07	6.62E+03
4.00E-04	1.82E+07	6.70E+03
4.00E-04	1.95E+07	7.15E+03
3.66E-04	2.00E+07	7.30E+03
3.77E-04	2.06E+07	7.50E+03
3.72E-04	2.11E+07	7.67E+03

N_{St}	R_x	R_θ
No. 194		
4.30E-04	2.04E+07	5.72E+03
3.55E-04	2.16E+07	6.10E+03
3.56E-04	2.27E+07	6.40E+03
3.24E-04	2.50E+07	7.20E+03
3.38E-04	2.84E+07	8.20E+03
3.31E-04	2.95E+07	8.50E+03
3.20E-04	3.06E+07	8.80E+03
2.84E-04	3.69E+07	1.03E+04
2.96E-04	3.98E+07	1.12E+04
2.57E-04	4.16E+07	1.16E+04
2.69E-04	4.29E+07	1.18E+04
2.58E-04	4.41E+07	1.22E+04
2.70E-04	4.44E+07	1.22E+04
2.66E-04	4.46E+07	1.23E+04
2.55E-04	4.49E+07	1.23E+04
2.65E-04	4.60E+07	1.26E+04
2.67E-04	4.68E+07	1.27E+04
2.60E-04	4.75E+07	1.28E+04
2.63E-04	4.82E+07	1.32E+04
2.71E-04	4.96E+07	1.34E+04
2.61E-04	5.03E+07	1.35E+04
2.62E-04	5.39E+07	1.44E+04
2.58E-04	5.54E+07	1.49E+04
2.45E-04	5.68E+07	1.51E+04
2.57E-04	5.83E+07	1.53E+04
No. 195		
4.25E-04	1.07E+07	4.68E+03
3.70E-04	1.93E+07	5.62E+03
3.49E-04	2.20E+07	6.43E+03
3.28E-04	2.28E+07	6.70E+03
3.40E-04	2.37E+07	6.95E+03
2.91E-04	2.86E+07	8.30E+03
2.68E-04	3.22E+07	9.20E+03
2.71E-04	3.41E+07	9.63E+03
2.76E-04	3.44E+07	9.75E+03
2.85E-04	3.45E+07	9.78E+03
2.78E-04	3.48E+07	9.82E+03
2.68E-04	3.56E+07	1.00E+04
2.76E-04	3.62E+07	1.02E+04
2.80E-04	3.68E+07	1.03E+04
2.64E-04	3.74E+07	1.04E+04
2.60E-04	3.84E+07	1.06E+04
2.59E-04	3.89E+07	1.07E+04
2.64E-04	4.17E+07	1.14E+04
2.51E-04	4.29E+07	1.17E+04
2.46E-04	4.40E+07	1.19E+04
2.56E-04	4.51E+07	1.22E+04

N_{ST}	R_x	R_θ
No. 196		
4.00E-04	2.04E+07	6.17E+03
4.00E-04	2.09E+07	6.35E+03
3.96E-04	2.15E+07	6.55E+03
3.88E-04	2.20E+07	6.75E+03

R_θ determined assuming S = 1.16

The symbol E and the following plus or minus sign and two digits represent the exponent of 10 by which to multiply the number to place the decimal correctly.

TABLE V.- CONDITIONS FOR HEAT-TRANSFER DATA – CONE

Symbol	Identity number	Reference	M_∞	M_e	ϕ, deg	r	T_w, K	$H_w/H_{t,\infty}$	R, cm^{-1}, $\times 10^{-5}$	$R_{x,i}$ $\times 10^{-6}$	$R_{x,p}$ $\times 10^{-6}$	$R_{\theta,i}$ $\times 10^{-3}$	$R_{\theta,p}$ $\times 10^{-3}$
○	301	26	10.10	8.80	5.0	0.89	252	0.21	0.67	3.80	7.40	0.70	1.53
	302	26	10.10	8.80			183	.15	.67	3.60	7.30	.75	1.44
	303	26	10.10	8.80			433	.37	.72	3.90	7.80	.66	1.54
	304	26	10.10	8.80			300	.26	.72	3.60	7.70	.66	1.58
	305	26	10.10	8.80			84.4	.08	.80	4.10	8.20	.75	1.92
□	306	Unpublished[a]	5.36	5.07			307	.54	1.37	3.60	6.70	.60	1.49
	307		5.25	4.93			311	.44	1.71	4.23	8.00	.65	1.90
	308		5.34	5.02			328	.40	1.81	3.70	7.50	.66	1.93
	309		5.36	5.07			122	.22	1.36	3.00	6.00	.63	1.86
	310		5.36	5.07			100	.18	2.26	2.90	5.70	.63	1.72
	311		7.22	4.91	15.0		383	.49	3.92	4.20	9.76	.58	2.18
	312						383	.37	2.67	4.00	8.02	.54	1.66
	313						328	.42	3.92	4.00	8.40	.57	1.85
	314						206	.23	3.44	4.00	8.56	.52	2.10
	315						175	.15	2.12	3.13	6.36	.60	1.78
	316						206	.17	2.12	3.13	6.36	.58	1.77
◇	317	26	7.67	6.65	6.33		309	.20	3.15	4.00	8.00	.74	1.64
	318	26	7.67	6.65	6.33		309	.20	3.15	2.90	5.80	.63	1.31
	319	26	7.92	6.84	6.33		308	.29	6.87	4.00	8.20	.77	1.80
	320	Unpublished[a]	7.23	6.63	5.0		194	.18	1.98	3.60	7.20	.59	1.50
	321						167	.16	2.00	1.85	3.50	.45	.92
	322						313	.41	3.12	3.70	7.30	.69	1.50
	323						320	.29	1.88	4.90	9.20	.70	1.76
	324						305	.39	1.66	3.60	7.30	.58	1.65
	325						192	.23	3.13	4.20	8.30	.76	1.98
	326						137	.12	2.00	3.50	7.00	.62	1.62
	327						106	.10	2.00	2.00	4.00	.44	1.04
△	328	26	6.44	5.70	6.33		323	.21	4.78	2.70	5.40	.61	1.57
	329	26	6.07	5.40	6.33		328	.11	1.82	2.80	5.40	.43	1.34
	330	26	6.07	5.40	6.33		328	.11	1.82	2.80	4.60	.43	.97
	331	26	6.07	5.40	6.33		328	.11	1.82	2.50	4.60	.38	1.03
◺	332	35	4.95	4.25	10.0		294	.62	13.42	7.00	11.50	.97	2.45
	333	35	4.95	4.25			294	.62	20.10	7.80	13.00	1.02	3.17
	334	35	4.95	4.25			294	.62	26.86	9.00	15.00	1.10	2.75
	335	35	4.95	4.25			294	.62	33.54	10.00	18.50	1.17	3.75
	336	36	5.00	4.29			306	.64	13.12	6.80	11.10	.97	2.32
	337	36	5.00	4.29			306	.64	19.68	7.50	12.50	1.02	2.91
	338	36	5.00	4.29			306	.64	26.25	9.00	15.50	1.11	3.23
	339	36	5.00	4.29			306	.64	32.80	9.00	17.00	1.13	3.05

[a]Source, G. C. Mateer, NASA.

TABLE VI. - HEAT-TRANSFER DATA - CONE

N_{St}	R_x	R_θ
Identity No. 301		
6.08E-04	9.25E+06	2.13E+03
5.38E-04	9.56E+06	2.22E+03
5.95E-04	9.87E+06	2.29E+03
6.24E-04	1.02E+07	2.37E+03
5.21E-04	1.08E+07	2.49E+03
No. 302		
4.77E-04	9.25E+06	1.94E+03
4.78E-04	9.56E+06	2.01E+03
No. 303		
5.29E-04	9.71E+06	2.20E+03
4.87E-04	1.07E+07	2.42E+03
No. 304		
5.84E-04	9.82E+06	2.30E+03
5.58E-04	1.01E+07	2.39E+03
6.08E-04	1.05E+07	2.50E+03
5.99E-04	1.09E+07	2.63E+03
6.08E-04	1.11E+07	2.70E+03
5.80E-04	1.15E+07	2.79E+03
No. 305		
5.63E-04	1.01E+07	2.47E+03
4.92E-04	1.05E+07	2.54E+03
5.16E-04	1.08E+07	2.61E+03
4.67E-04	1.12E+07	2.68E+03
5.14E-04	1.16E+07	2.75E+03
No. 306		
1.05E-03	8.25E+06	2.26E+03
1.01E-03	8.59E+06	2.41E+03
9.76E-04	9.29E+06	2.71E+03
9.91E-04	9.64E+06	2.84E+03
No. 307		
8.65E-04	1.03E+07	2.84E+03
8.49E-04	1.07E+07	3.01E+03
8.34E-04	1.16E+07	3.31E+03
8.32E-04	1.20E+07	3.46E+03
No. 308		
8.95E-04	1.00E+07	3.01E+03
8.98E-04	1.05E+07	3.19E+03
8.90E-04	1.09E+07	3.35E+03
8.79E-04	1.14E+07	3.53E+03
8.73E-04	1.23E+07	3.85E+03
8.70E-04	1.28E+07	4.02E+03

N_{St}	R_x	R_θ
No. 309		
9.86E-04	7.50E+06	2.59E+03
9.95E-04	7.85E+06	2.74E+03
9.77E-04	8.19E+06	2.88E+03
9.25E-04	8.53E+06	3.02E+03
9.08E-04	9.22E+06	3.27E+03
8.62E-04	9.57E+06	3.39E+03
No. 310		
9.15E-04	7.32E+06	2.48E+03
9.49E-04	7.89E+06	2.72E+03
8.48E-04	9.04E+06	3.13E+03
8.16E-04	1.02E+07	3.43E+03
8.13E-04	1.13E+07	3.76E+03
8.07E-04	1.31E+07	4.28E+03
7.79E-04	1.36E+07	4.45E+03
7.77E-04	1.42E+07	4.61E+03
8.04E-04	1.53E+07	4.95E+03
7.75E-04	1.59E+07	5.13E+03
No. 311		
7.55E-04	1.38E+07	3.48E+03
7.44E-04	1.57E+07	4.05E+03
7.11E-04	1.77E+07	4.56E+03
6.87E-04	1.97E+07	5.02E+03
6.65E-04	2.07E+07	5.22E+03
No. 312		
8.38E-04	1.07E+07	2.82E+03
7.72E-04	1.21E+07	3.25E+03
7.30E-04	1.34E+07	3.63E+03
7.24E-04	1.41E+07	3.76E+03
No. 313		
8.04E-04	1.38E+07	3.84E+03
7.83E-04	1.57E+07	4.46E+03
7.39E-04	1.77E+07	5.02E+03
7.10E-04	1.97E+07	5.53E+03
6.91E-04	2.07E+07	5.77E+03
No. 314		
8.38E-04	1.21E+07	3.56E+03
8.26E-04	1.38E+07	4.16E+03
8.14E-04	1.55E+07	4.68E+03
7.64E-04	1.73E+07	5.17E+03
7.71E-04	1.82E+07	5.43E+03

N_{St}	R_x	R_θ
No. 315		
1.02E-03	8.51E+06	2.87E+03
1.03E-03	9.59E+06	3.35E+03
9.48E-04	1.07E+07	3.76E+03
9.08E-04	1.12E+07	3.94E+03
No. 316		
1.01E-03	8.51E+06	2.81E+03
1.00E-03	9.59E+06	3.28E+03
9.25E-04	1.07E+07	3.66E+03
9.05E-04	1.12E+07	3.84E+03
No. 317		
6.44E-04	9.66E+06	2.21E+03
6.44E-04	1.13E+07	2.71E+03
No. 318		
6.29E-04	8.05E+06	2.08E+03
6.47E-04	8.05E+06	2.08E+03
6.25E-04	9.66E+06	2.56E+03
6.26E-04	9.66E+06	2.56E+03
5.80E-04	1.13E+07	2.97E+03
5.74E-04	1.13E+07	2.97E+03
No. 319		
6.89E-04	1.05E+07	2.55E+03
6.23E-04	1.05E+07	2.55E+03
6.40E-04	1.05E+07	2.55E+03
6.19E-04	1.41E+07	3.64E+03
6.13E-04	1.41E+07	3.64E+03
5.96E-04	1.41E+07	3.64E+03
5.57E-04	1.76E+07	4.57E+03
5.50E-04	1.76E+07	4.57E+03
5.79E-04	1.76E+07	4.57E+03
5.39E-04	2.11E+07	5.15E+03
5.61E-04	2.11E+07	5.15E+03
5.62E-04	2.11E+07	5.15E+03
5.54E-04	2.46E+07	6.22E+03
5.01E-04	2.46E+07	6.22E+03
5.12E-04	2.46E+07	6.22E+03
No. 320		
7.45E-04	8.91E+06	2.15E+03
7.02E-04	9.41E+06	2.31E+03
6.88E-04	9.91E+06	2.46E+03
6.90E-04	1.04E+07	2.60E+03
6.36E-04	1.14E+07	2.85E+03
5.95E-04	1.19E+07	2.97E+03
6.16E-04	1.24E+07	3.08E+03
5.70E-04	1.34E+07	3.30E+03

N_{St}	R_x	R_θ
No. 321		
9.05E-04	4.45E+06	1.35E+03
8.66E-04	4.96E+06	1.54E+03
8.36E-04	5.47E+06	1.72E+03
8.63E-04	5.97E+06	1.91E+03
7.94E-04	6.48E+06	2.07E+03
7.89E-04	6.99E+06	2.22E+03
7.10E-04	8.01E+06	2.50E+03
6.85E-04	9.02E+06	2.72E+03
6.65E-04	9.53E+06	2.84E+03
6.60E-04	1.00E+07	2.95E+03
6.27E-04	1.05E+07	3.05E+03
6.28E-04	1.16E+07	3.25E+03
6.01E-04	1.21E+07	3.35E+03
5.79E-04	1.26E+07	3.44E+03
5.72E-04	1.36E+07	3.63E+03
No. 322		
8.44E-04	9.31E+06	2.34E+03
7.45E-04	1.01E+07	2.60E+03
7.29E-04	1.09E+07	2.84E+03
6.67E-04	1.25E+07	3.25E+03
6.44E-04	1.33E+07	3.42E+03
6.48E-04	1.41E+07	3.61E+03
6.27E-04	1.49E+07	3.78E+03
6.25E-04	1.56E+07	3.94E+03
6.12E-04	1.64E+07	4.12E+03
5.84E-04	1.72E+07	4.28E+03
5.97E-04	1.80E+07	4.43E+03
5.89E-04	1.88E+07	4.59E+03
5.69E-04	1.96E+07	4.73E+03
5.73E-04	2.03E+07	4.87E+03
5.70E-04	2.12E+07	5.04E+03
No. 323		
6.79E-04	1.13E+07	2.50E+03
6.60E-04	1.18E+07	2.64E+03
6.65E-04	1.23E+07	2.77E+03
6.56E-04	1.28E+07	2.91E+03
No. 324		
7.43E-04	9.16E+06	2.34E+03
7.57E-04	9.58E+06	2.48E+03
7.16E-04	1.00E+07	2.61E+03
7.00E-04	1.04E+07	2.72E+03
6.96E-04	1.08E+07	2.83E+03
6.85E-04	1.13E+07	2.96E+03

N_{St}	R_x	R_θ
No. 325		
7.22E-04	1.09E+07	2.87E+03
6.71E-04	1.25E+07	3.31E+03
6.29E-04	1.33E+07	3.50E+03
6.25E-04	1.41E+07	3.68E+03
6.07E-04	1.49E+07	3.85E+03
5.82E-04	1.57E+07	4.01E+03
5.65E-04	1.65E+07	4.16E+03
5.66E-04	1.73E+07	4.28E+03
5.79E-04	1.81E+07	4.48E+03
5.65E-04	1.89E+07	4.60E+03
5.37E-04	1.97E+07	4.71E+03
5.06E-04	2.13E+07	4.97E+03
No. 326		
7.70E-04	9.04E+06	2.34E+03
6.95E-04	9.55E+06	2.50E+03
6.95E-04	1.01E+07	2.64E+03
7.11E-04	1.06E+07	2.83E+03
6.16E-04	1.11E+07	2.91E+03
6.50E-04	1.16E+07	3.03E+03
5.88E-04	1.21E+07	3.15E+03
5.70E-04	1.26E+07	3.24E+03
5.62E-04	1.36E+07	3.43E+03
No. 327		
8.00E-04	5.34E+06	1.53E+03
7.83E-04	5.97E+06	1.74E+03
7.47E-04	6.48E+06	1.91E+03
7.47E-04	6.99E+06	2.05E+03
6.86E-04	8.01E+06	2.34E+03
6.31E-04	8.52E+06	2.46E+03
6.89E-04	9.02E+06	2.57E+03
6.27E-04	9.53E+06	2.69E+03
6.16E-04	1.00E+07	2.79E+03
5.78E-04	1.05E+07	2.90E+03
5.49E-04	1.11E+07	2.97E+03
6.11E-04	1.16E+07	3.08E+03
5.84E-04	1.21E+07	3.18E+03
5.49E-04	1.26E+07	3.28E+03
5.82E-04	1.36E+07	3.47E+03

R_θ determined assuming S = 1.16

The symbol E and the following plus or minus sign and two digits represent the exponent of 10 by which to multiply the number to place the decimal correctly.

TABLE VI. - HEAT-TRANSFER DATA - CONE- Concluded

N_{St}	R_x	R_θ
No. 328		
7.27E-04	7.33E+06	2.09E+03
6.34E-04	7.33E+06	2.09E+03
7.68E-04	7.33E+06	2.09E+03
6.45E-04	9.79E+06	2.79E+03
5.85E-04	9.79E+06	2.78E+03
6.08E-04	9.79E+06	2.78E+03
5.81E-04	1.21E+07	3.38E+03
6.82E-04	1.21E+07	3.38E+03
6.18E-04	1.21E+07	3.38E+03
5.99E-04	1.47E+07	4.04E+03
6.10E-04	1.47E+07	4.04E+03
6.20E-04	1.47E+07	4.04E+03
5.77E-04	1.71E+07	4.61E+03
5.50E-04	1.71E+07	4.61E+03
5.73E-04	1.71E+07	4.61E+03
No. 329		
8.05E-04	5.51E+06	1.85E+03
No. 330		
8.58E-04	5.58E+06	1.45E+03
7.65E-04	5.51E+06	1.85E+03
No. 331		
7.53E-04	5.58E+06	1.49E+03
7.44E-04	6.51E+06	1.85E+03
No. 332		
8.50E-04	1.48E+07	4.15E+03
8.14E-04	1.53E+07	4.60E+03
7.51E-04	1.70E+07	5.21E+03
No. 333		
8.57E-04	1.66E+07	4.87E+03
8.20E-04	1.79E+07	5.36E+03
7.93E-04	1.92E+07	5.84E+03
7.50E-04	2.04E+07	6.26E+03
7.25E-04	2.17E+07	6.68E+03
7.21E-04	2.30E+07	7.14E+03
6.75E-04	2.55E+07	7.74E+03
No. 334		
7.88E-04	2.05E+07	5.39E+03
7.68E-04	2.22E+07	6.07E+03
7.50E-04	2.39E+07	6.71E+03
7.39E-04	2.56E+07	7.32E+03
6.86E-04	2.73E+07	7.88E+03
6.83E-04	2.90E+07	8.41E+03
6.62E-04	3.07E+07	9.01E+03
6.32E-04	3.41E+07	9.82E+03

N_{St}	R_x	R_θ
No. 335		
7.07E-04	2.56E+07	6.50E+03
7.08E-04	2.77E+07	7.24E+03
6.86E-04	2.98E+07	7.95E+03
6.75E-04	3.19E+07	8.64E+03
6.45E-04	3.41E+07	9.26E+03
6.32E-04	3.62E+07	9.89E+03
6.40E-04	3.83E+07	1.06E+04
6.00E-04	4.26E+07	1.15E+04
No. 336		
8.34E-04	1.33E+07	3.54E+03
7.90E-04	1.41E+07	3.92E+03
7.60E-04	1.50E+07	4.26E+03
No. 337		
8.01E-04	1.63E+07	4.72E+03
7.70E-04	1.75E+07	5.15E+03
7.40E-04	1.88E+07	5.62E+03
6.95E-04	2.00E+07	6.00E+03
6.70E-04	2.13E+07	6.43E+03
6.70E-04	2.25E+07	6.75E+03
No. 338		
7.30E-04	2.00E+07	5.04E+03
7.20E-04	2.17E+07	5.66E+03
6.97E-04	2.33E+07	6.22E+03
6.90E-04	2.50E+07	6.76E+03
6.40E-04	2.67E+07	7.25E+03
6.35E-04	2.83E+07	7.74E+03
6.20E-04	3.00E+07	8.18E+03
No. 339		
6.55E-04	2.50E+07	6.13E+03
6.64E-04	2.71E+07	6.81E+03
6.40E-04	2.92E+07	7.42E+03
6.32E-04	3.13E+07	8.04E+03
6.00E-04	3.33E+07	8.60E+03
5.90E-04	3.54E+07	9.20E+03
5.96E-04	3.75E+07	9.66E+03

R_θ determined assuming S = 1.16

The symbol E and the following plus or minus sign and two digits represent the exponent of 10 by which to multiply the number to place the decimal correctly.

TABLE VII.- SUMMARY OF ERRORS

Method	Ref.	Mach no. range	No. of points	Figure no.	S	Correlating parameter	Virtual origin	N_{St}		C_f	
								Mean, %	rms, %	Mean, %	rms, %
Eckert	10	4 to 10	N_{Sf} = 185	6	1.0	R_θ	--------	17.21	25.74	4.94	16.61
			N_{Ht} = 1291	17(a)	1.0	R_θ	$0.722R_{\theta,p}$	7.98	18.20	-1.18	15.28
				17(b)	1.0	R_x	$0.825R_{x,p}$	10.44	17.76	0.70	14.60
				14(a)	Kármán	R_θ	$0.722R_{\theta,p}$	-4.80	13.99	-1.18	15.28
				14(b)		R_x	$0.825R_{x,p}$	-2.60	11.59	0.70	14.60
Spalding and Chi	3			4	1.0	R_θ	--------	18.58	23.49	11.48	18.10
				9(a)	Kármán	R_θ	$0.722R_{\theta,p}$	-1.98	10.16	5.79	14.55
				9(b)		R_x	$0.825R_{x,p}$	-0.58	8.68	6.07	14.29
				12		R_x	$R_{x,p}$	-3.51	9.03	3.53	13.17
				----		R_θ	$R_{\theta,p}$	-5.84	11.28	2.42	13.65
				----	$0.178T_w/T_e + 0.982$	R_θ	$0.722R_{\theta,p}$	5.10	12.76	5.79	14.55
				----		R_x	$0.825R_{x,p}$	6.55	12.18	6.07	14.29
Coles	13			5	1.0	R_θ	--------	2.40	11.61	-8.83	15.81
				18	1.0	R_θ	$0.722R_{\theta,p}$	-5.07	11.98	-14.04	19.23
				15	Kármán	R_θ	$0.722R_{\theta,p}$	-14.74	17.67	-14.04	19.23
Van Driest	12			3	1.0	R_θ	--------	-1.19	13.15	-10.87	16.35
				13(a)	Kármán	R_θ	$0.722R_{\theta,p}$	-18.31	20.53	-15.92	19.79
				13(b)		R_x	$0.825R_{x,p}$	-14.19	16.46	-12.23	16.96
				16(a)	1.0	R_θ	$0.722R_{\theta,p}$	-8.84	14.18	-15.92	19.79
				16(b)	1.0	R_x	$0.825R_{x,p}$	-4.07	11.04	-12.23	16.96
				19	Kármán	R_θ	--------	-11.85	15.88	-10.87	16.35
				20	$0.178T_w/T_t + 0.982$	R_θ	--------	-5.77	12.90	-10.87	16.35
White and Christoph	9			8	1.0	R_θ	--------	-1.41	17.56	-16.68	22.93
Moore	11			7	1.0	R_θ	--------	-3.61	18.23	-23.62	28.35
Spalding and Chi	3	4 to 13	N_{Sf} = 270	21(a)	Kármán	R_θ	$0.722R_{\theta,p}$	-0.05	11.81	13.58	23.50
			N_{Ht} = 1523	21(b)		R_x	$0.825R_{x,p}$	0.93	10.01	12.85	21.52
Coles	13			23	1.0	R_θ	--------	2.31	11.45	-6.54	13.96
Van Driest	12			22	1.0	R_θ	--------	-0.80	13.39	-6.15	16.06

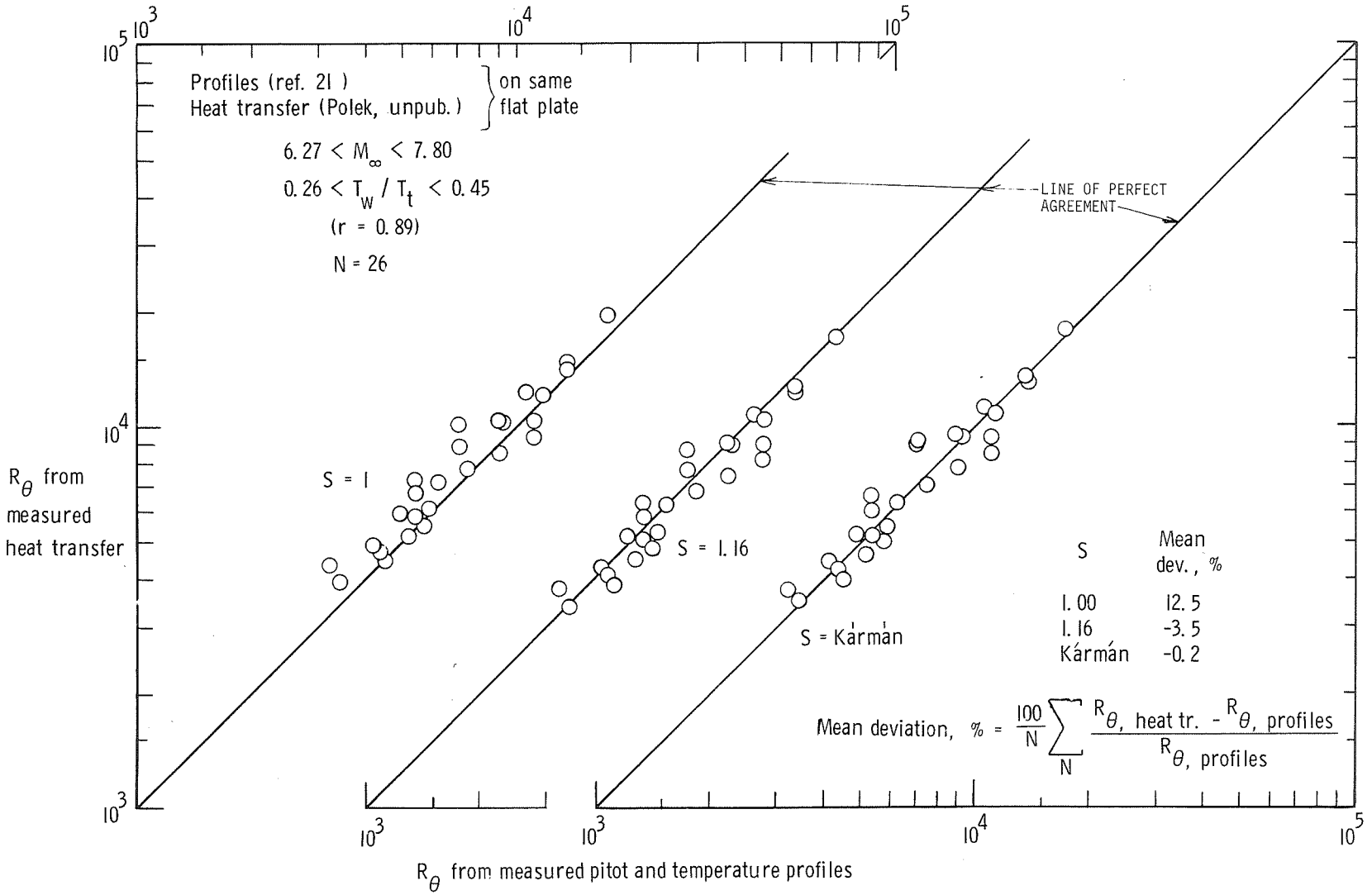

Figure 1.- Comparison of R_θ obtained from integrating heat-transfer distributions with R_θ obtained from profile measurements.

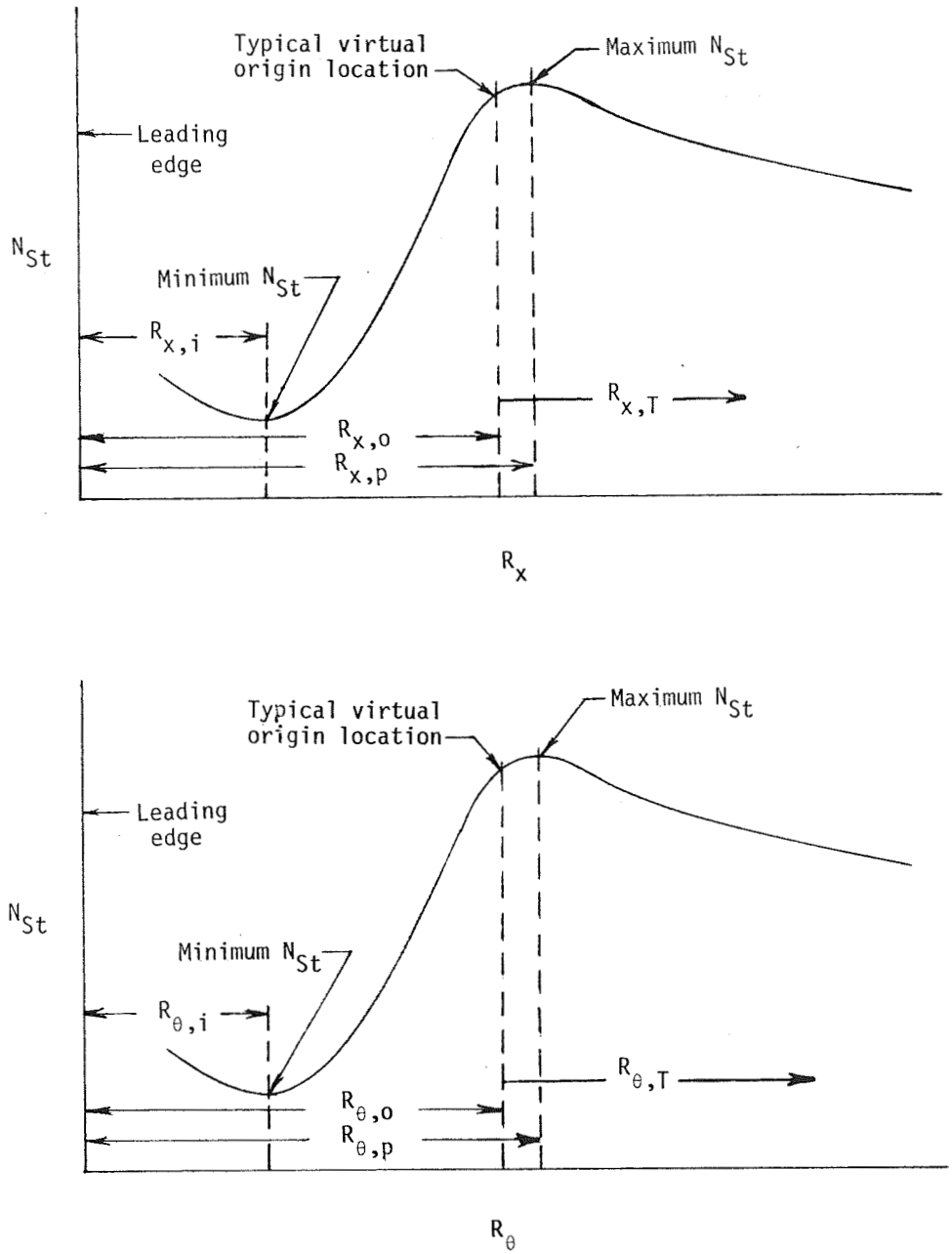

Figure 2.- Illustration of typical heating distribution defining Reynolds numbers.

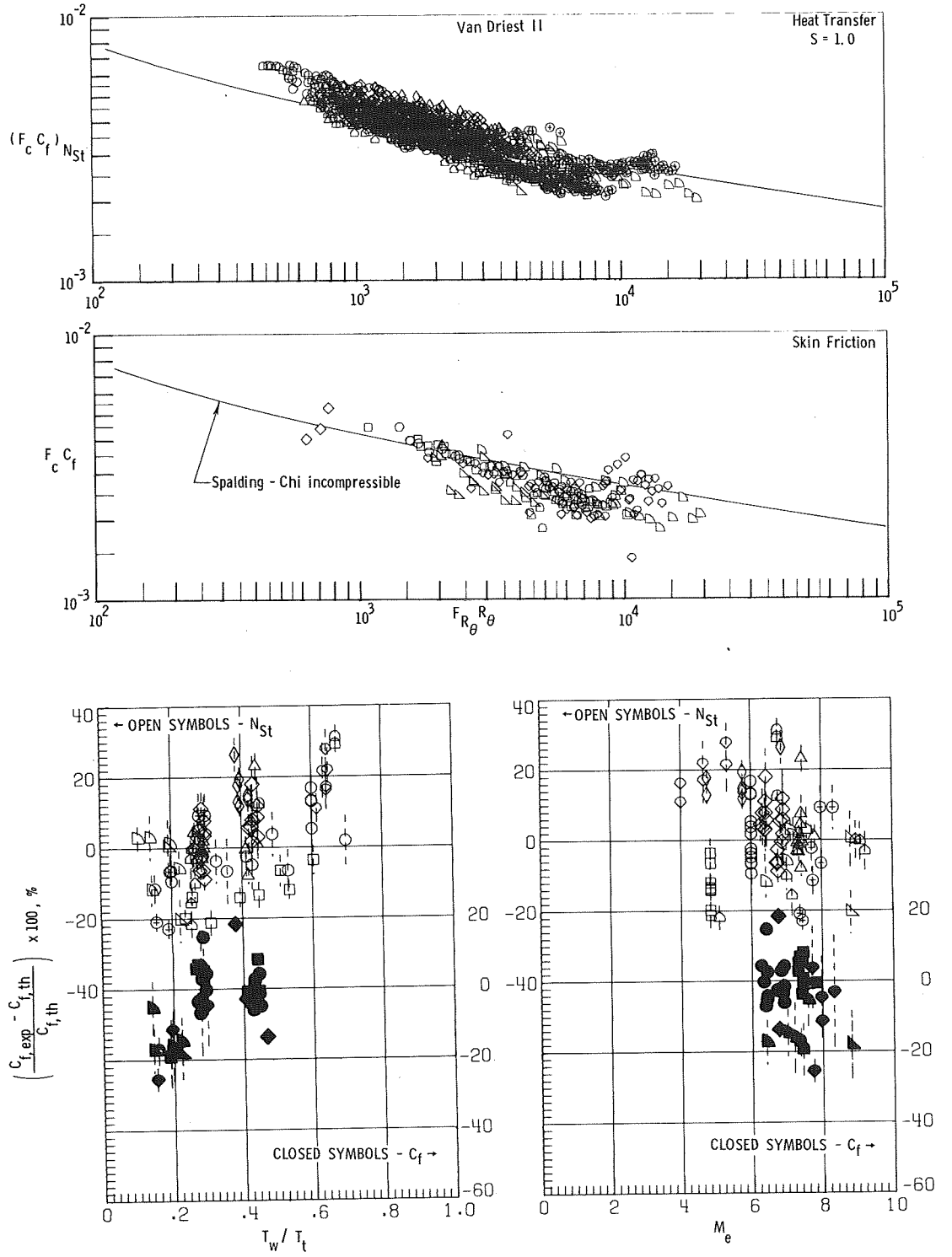

Figure 3.- Results from the Van Driest II method where C_f is assumed to be a unique function of R_θ and S = 1.0.

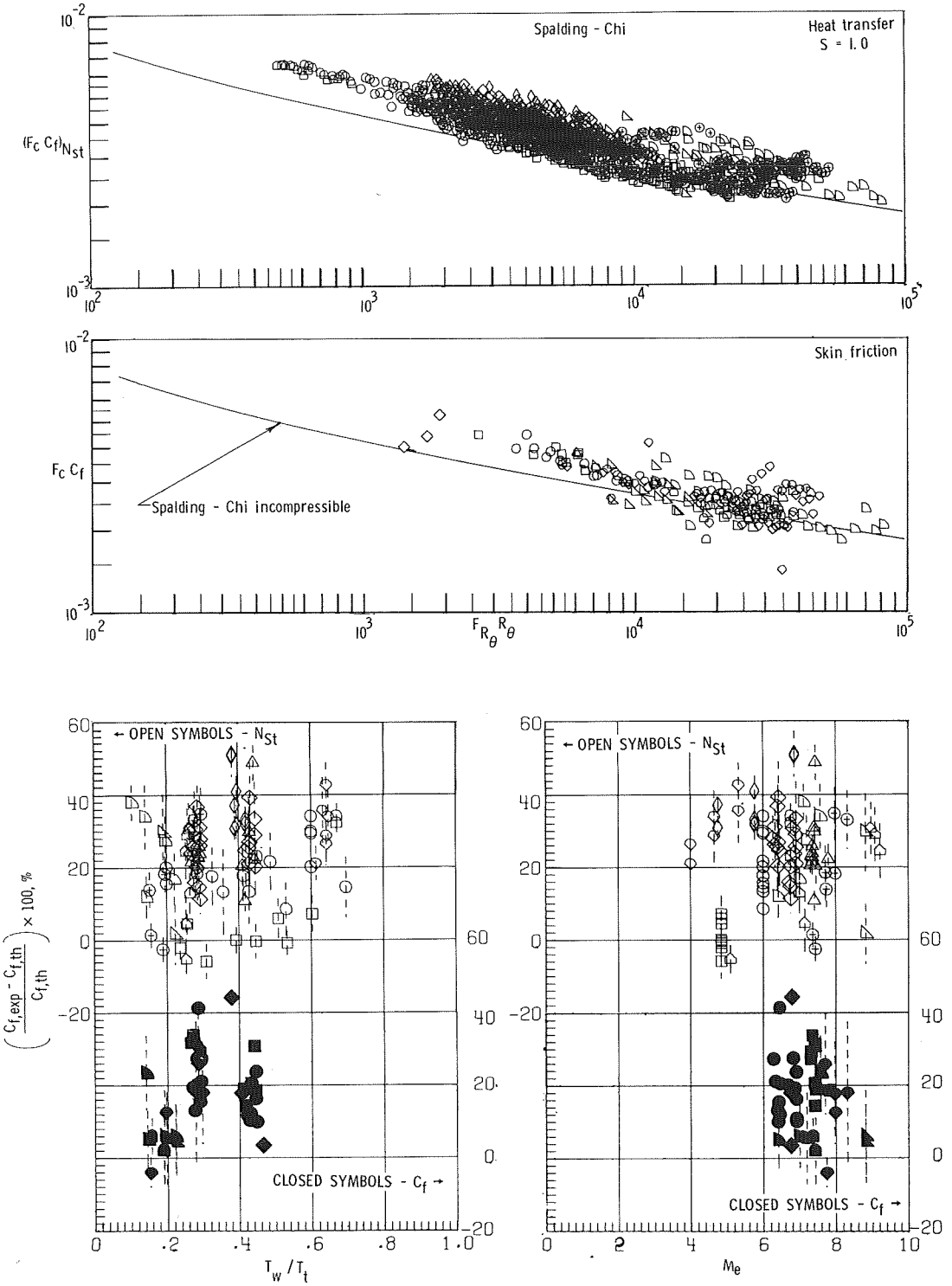

Figure 4.- Results from the Spalding and Chi method where C_f is assumed to be a unique function of R_θ and S = 1.0.

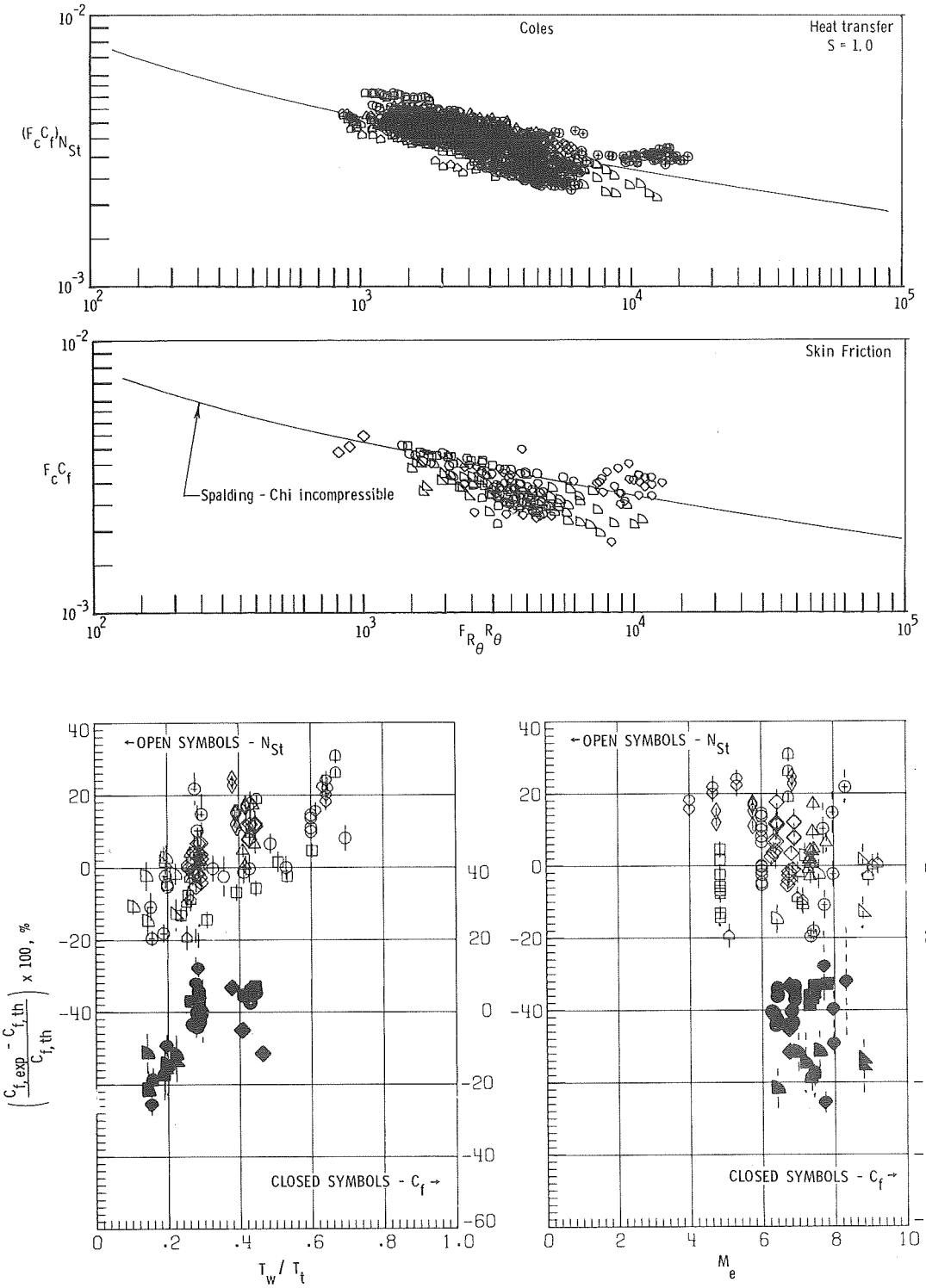

Figure 5.- Results from the Coles method where C_f is assumed to be a unique function of R_θ and S = 1.0.

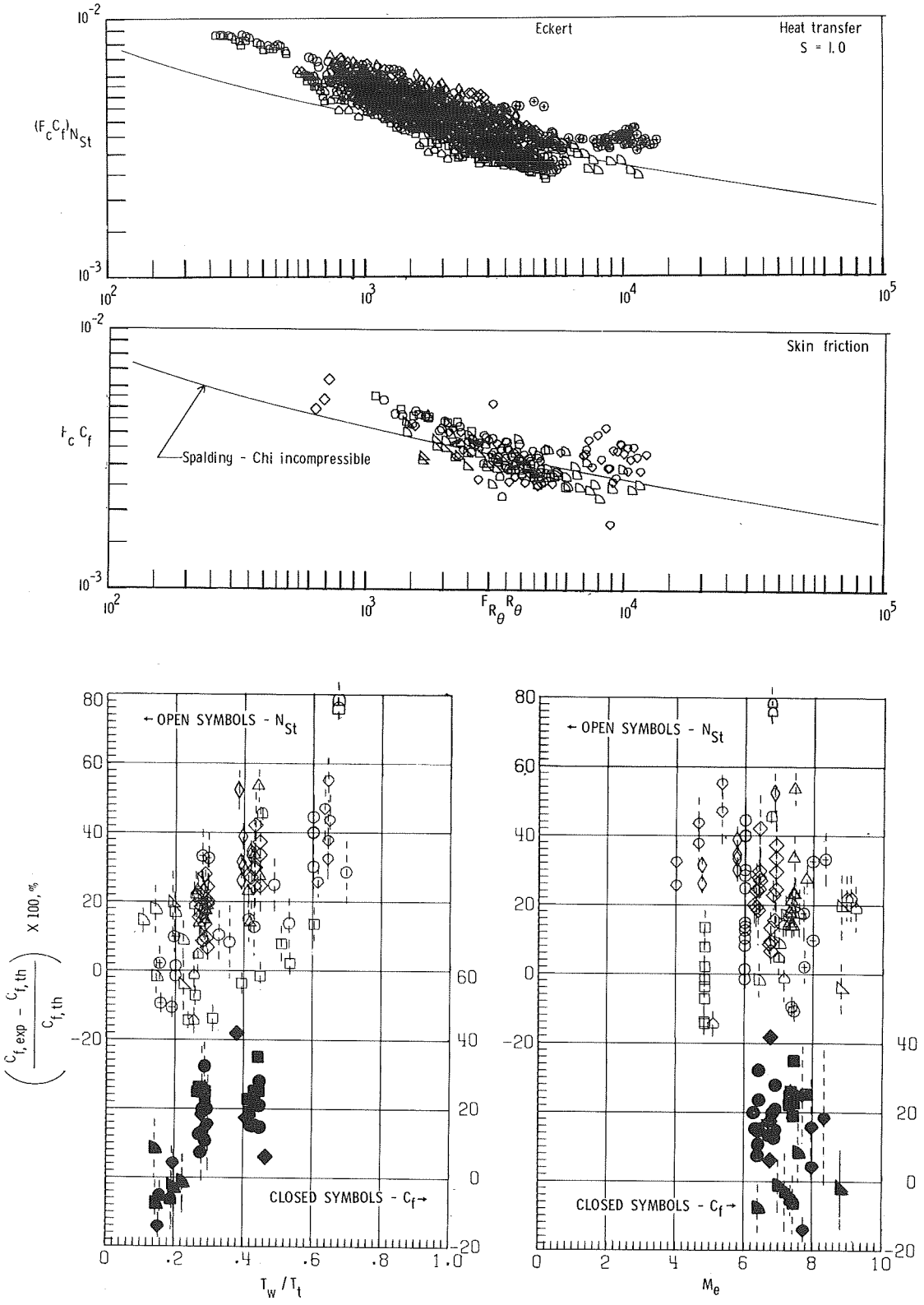

Figure 6.- Results from the Eckert method where C_f is assumed to be a unique function of R_θ and S = 1.0.

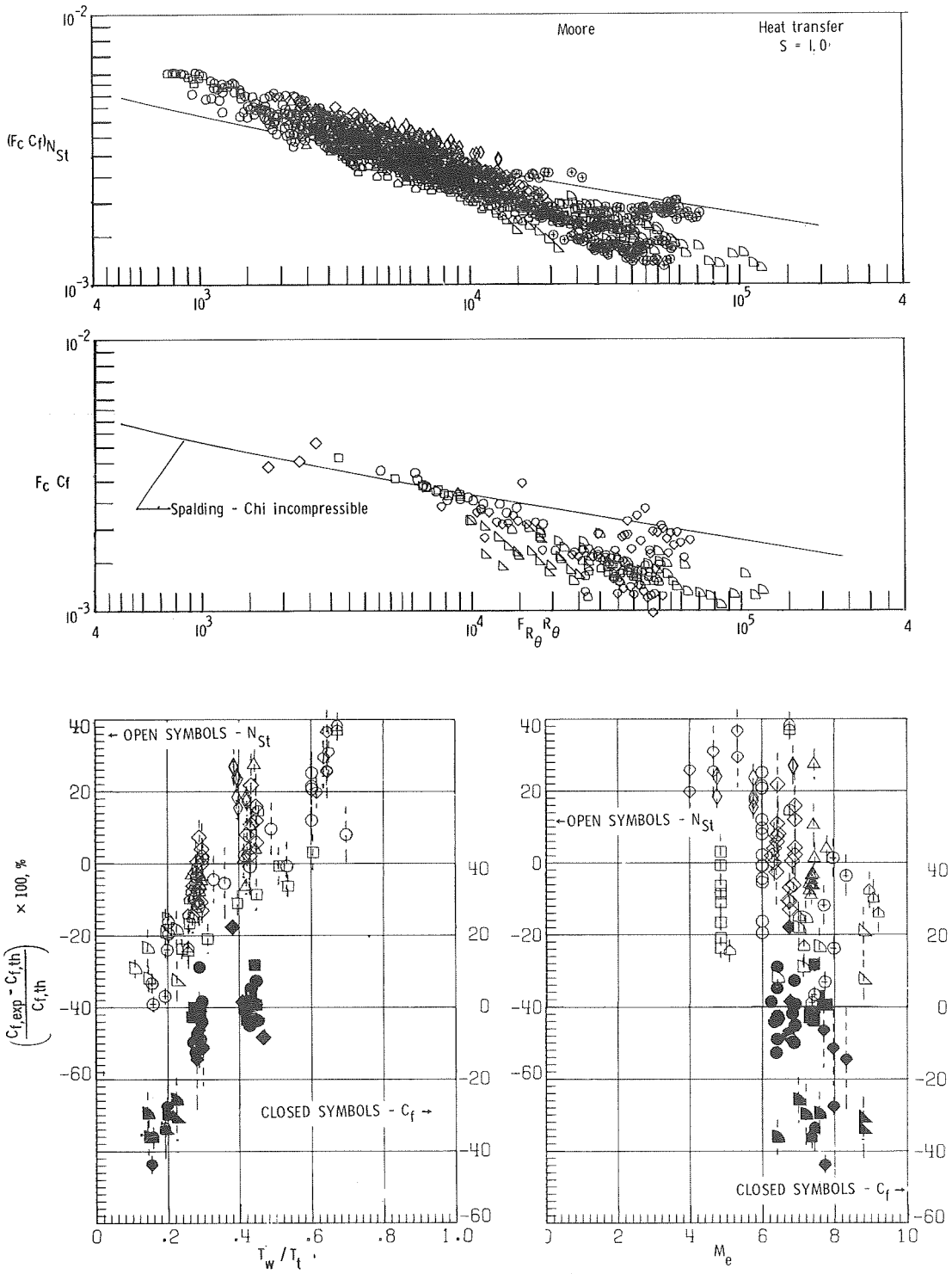

Figure 7.- Results from the Moore method where C_f is assumed to be a unique function of R_θ and S = 1.0.

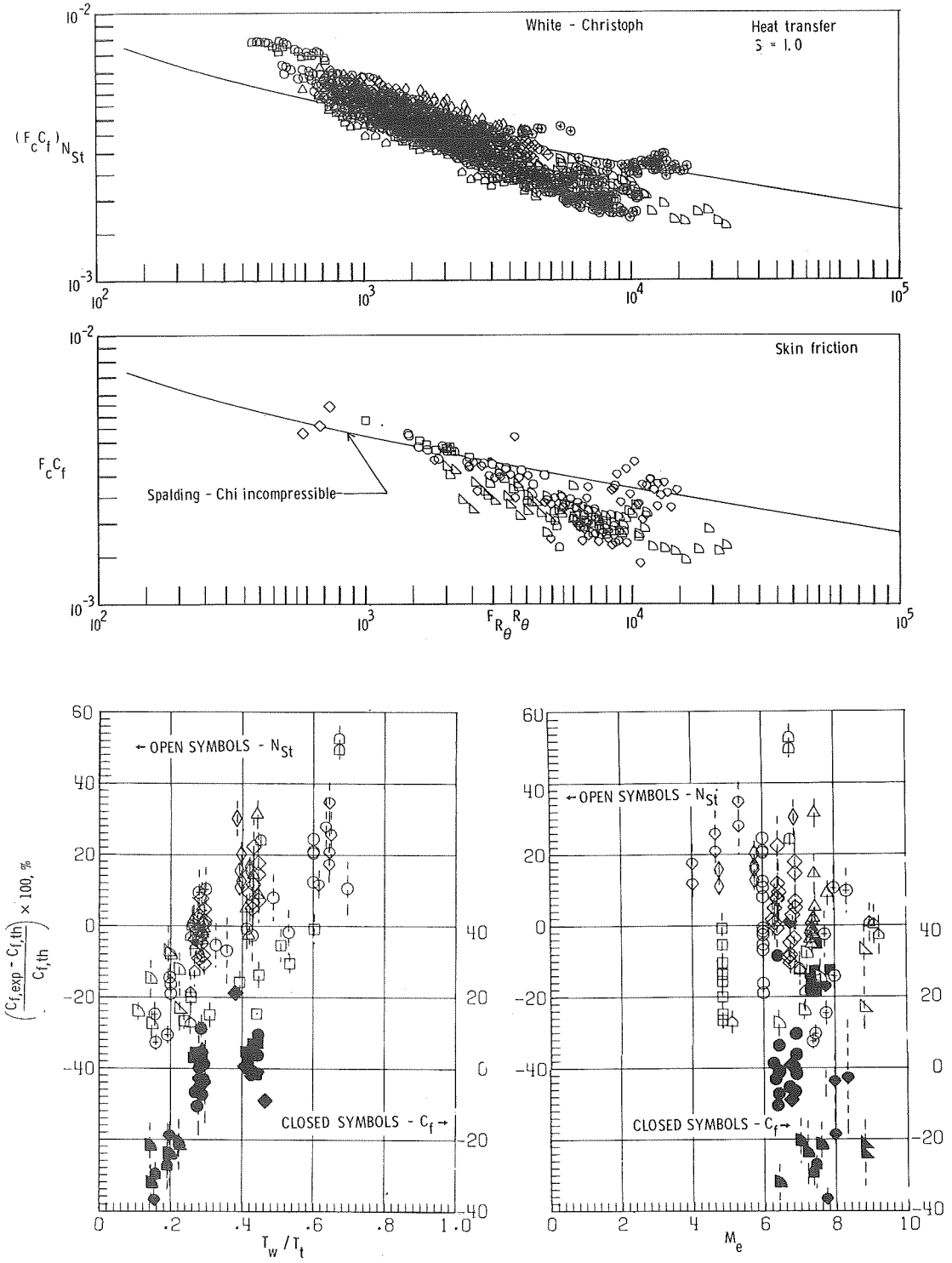

Figure 8.- Results from the White and Christoph method where C_f is assumed to be a unique function of R_θ and $S = 1.0$.

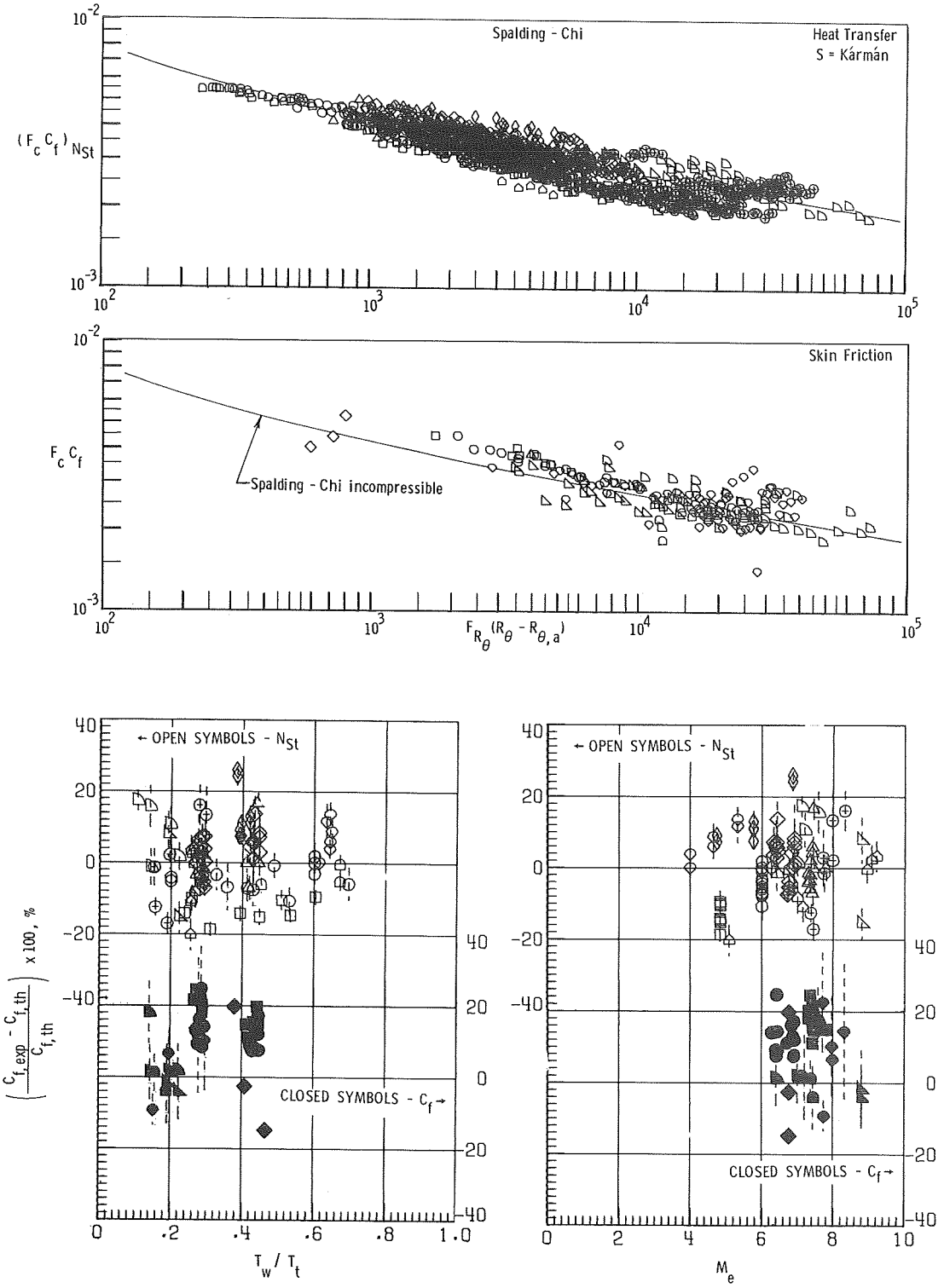

(a) Momentum-thickness Reynolds number correlation.

Figure 9.- Results from the Spalding and Chi method by using best virtual-origin location.

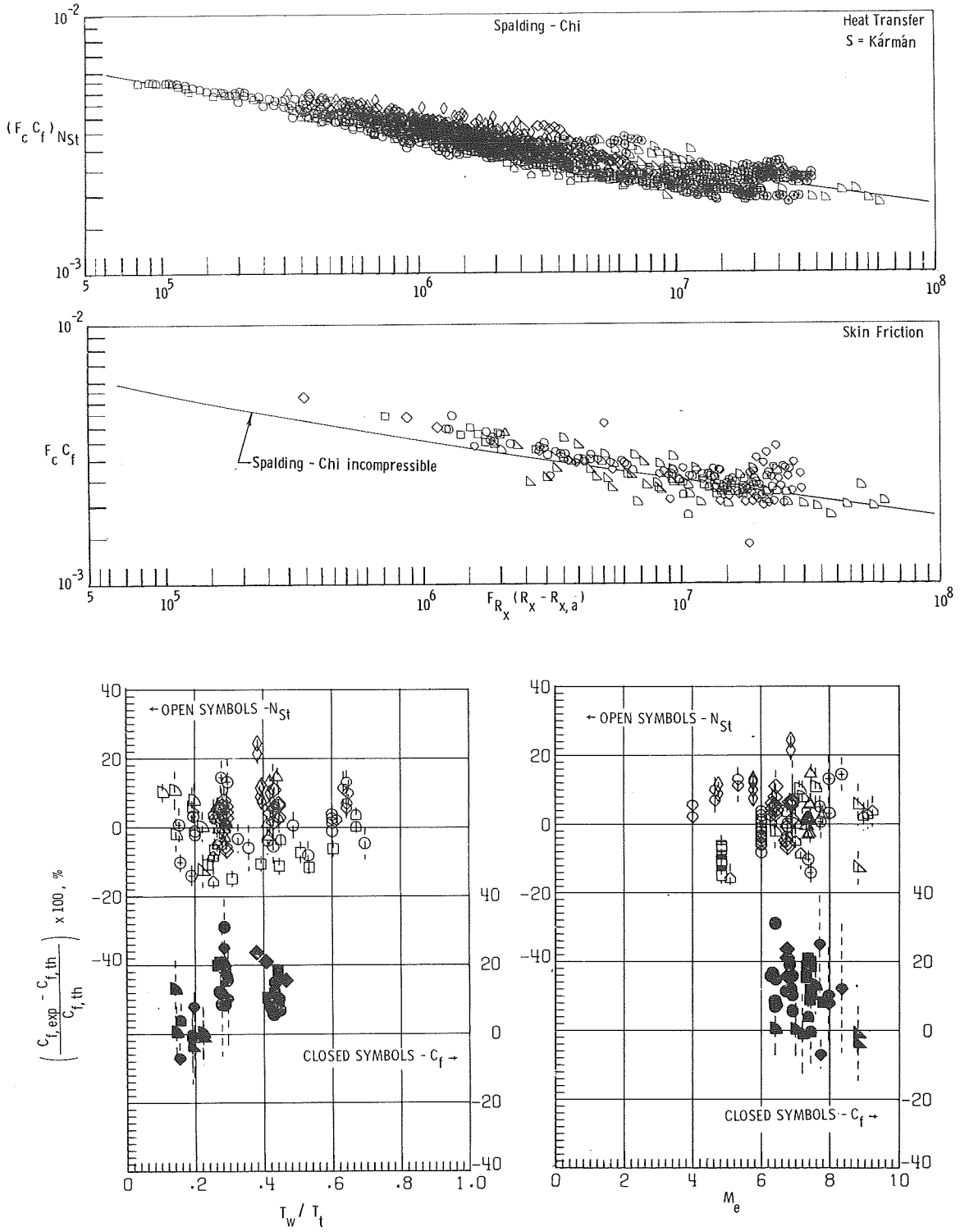

(b) Length Reynolds number correlation.

Figure 9.- Concluded.

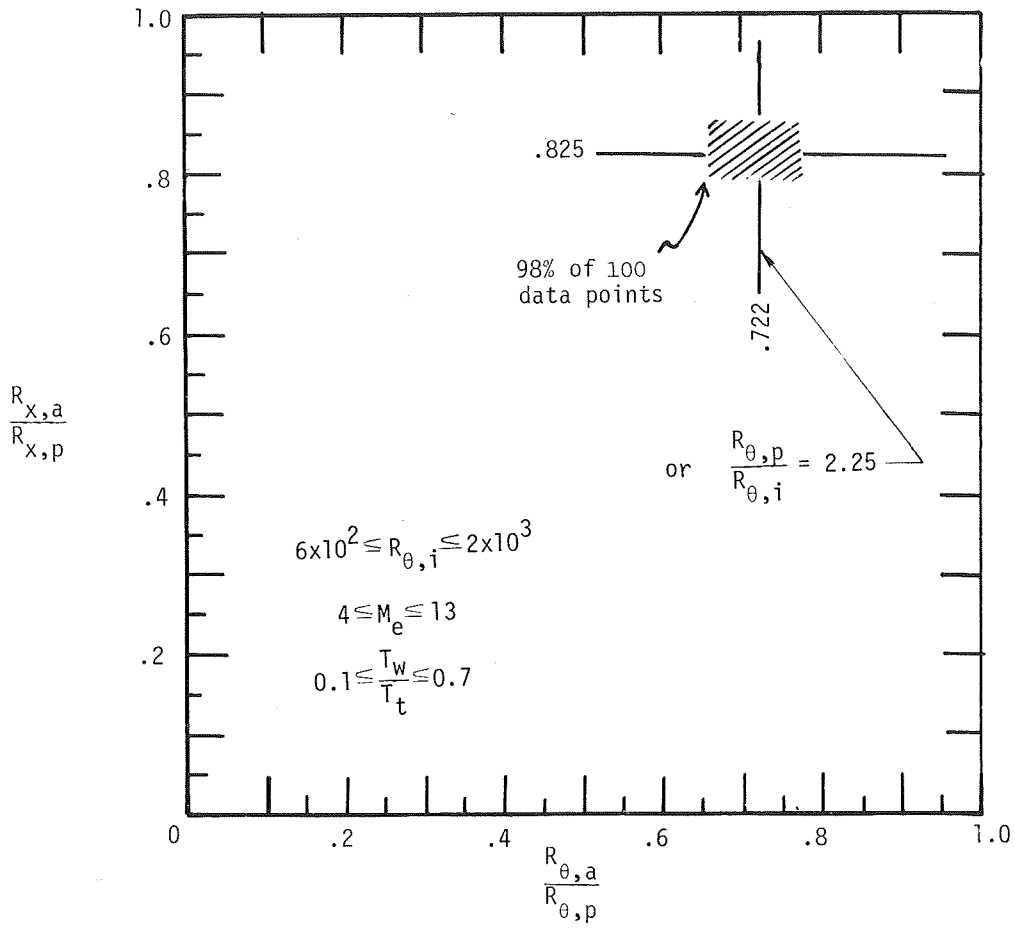

Figure 10.- Location of best virtual origin for the Spalding and Chi correlation.

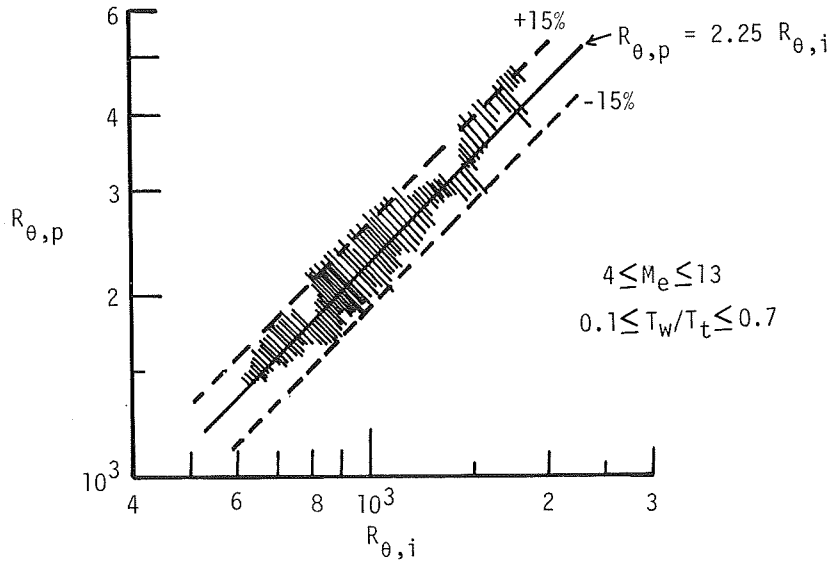

Figure 11.- Correlation of momentum-thickness Reynolds numbers at beginning and end of transition.

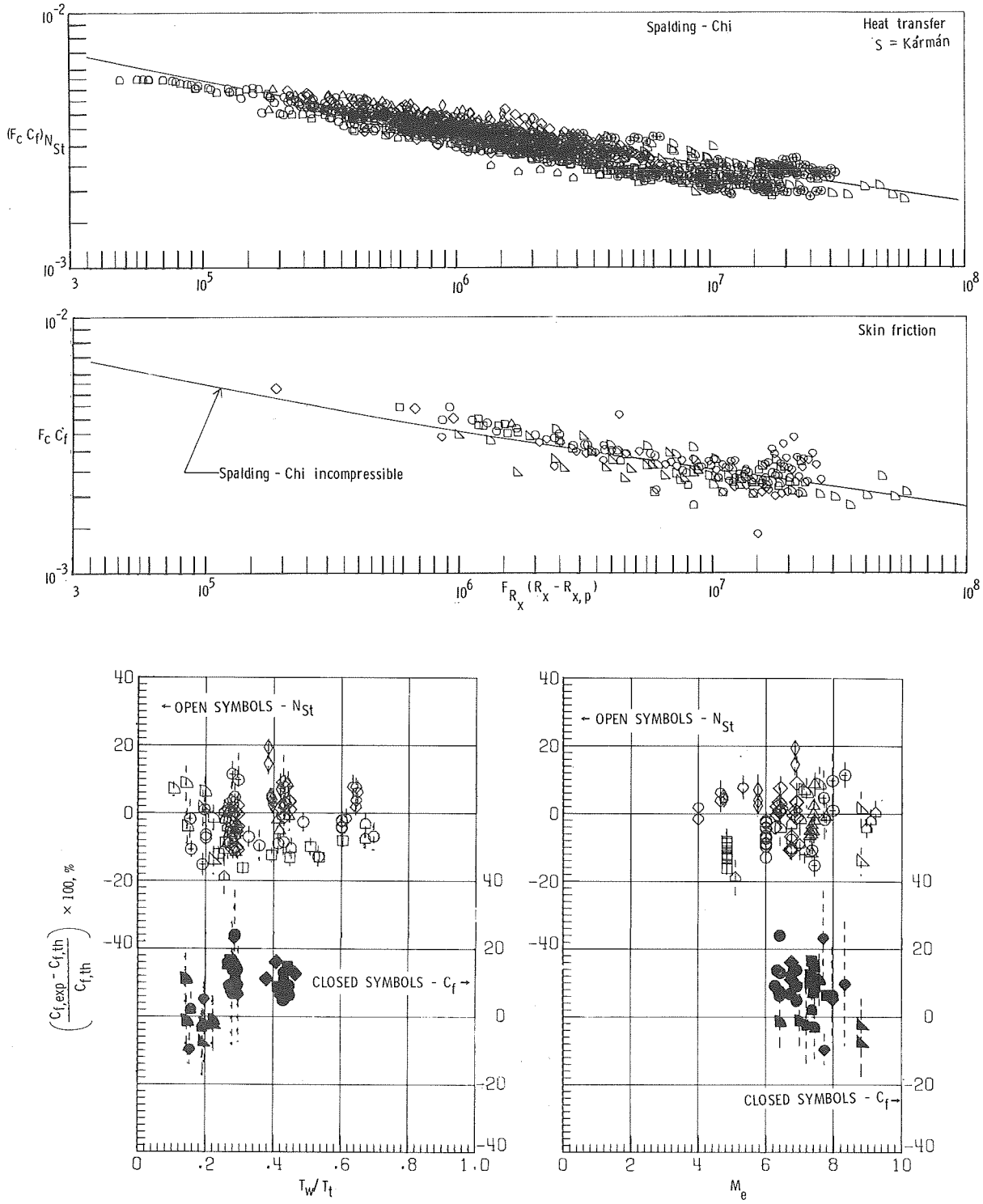

Figure 12.- Results from the Spalding and Chi method with virtual origin at peak heating near end of transition.

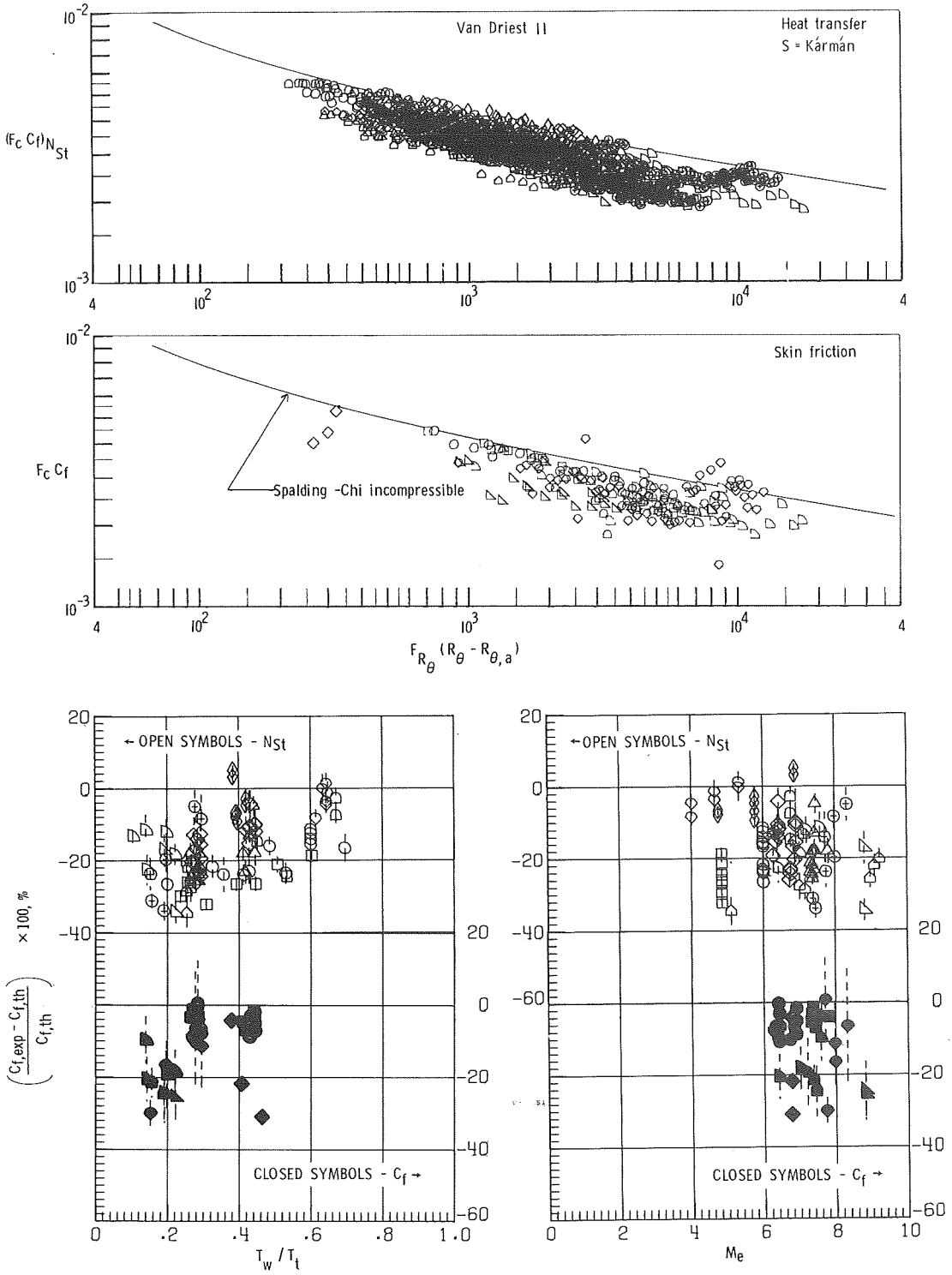

(a) Momentum-thickness Reynolds number correlation.

Figure 13.- Results from the Van Driest II method by using best virtual-origin location.

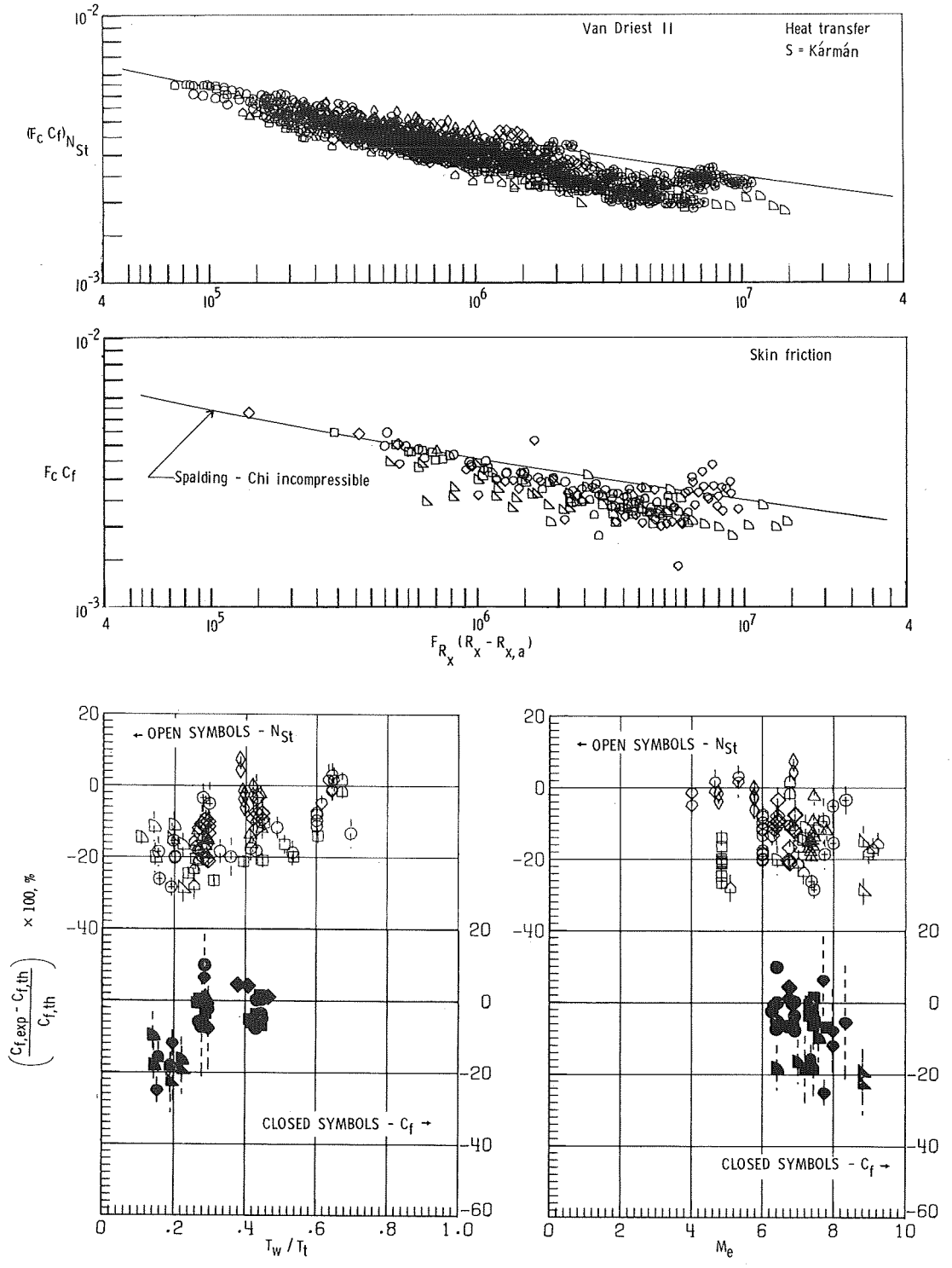

(b) Length Reynolds number correlation.

Figure 13.- Concluded.

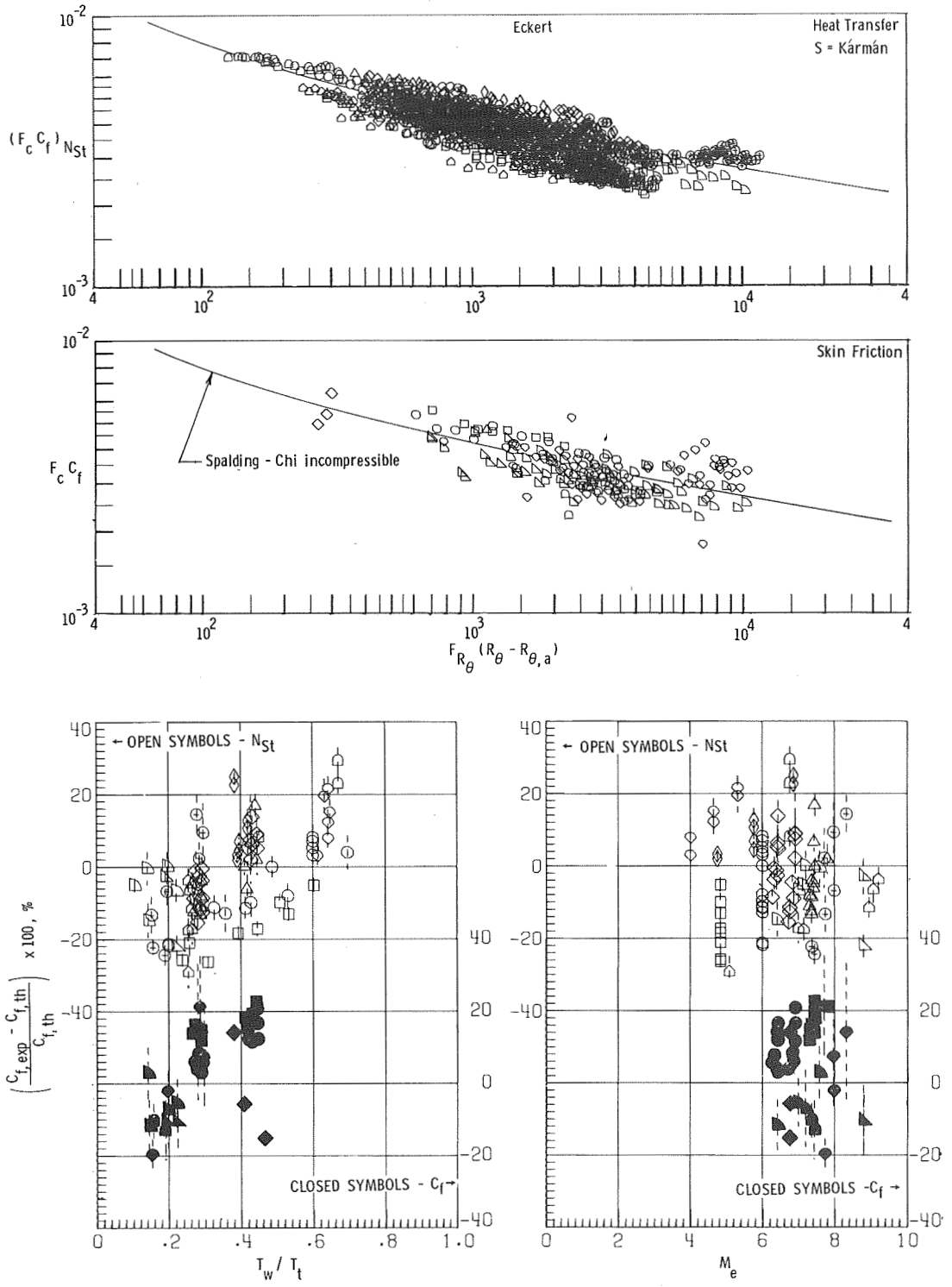

(a) Momentum-thickness Reynolds number correlation.

Figure 14.- Results from the Eckert method by using best virtual-origin location.

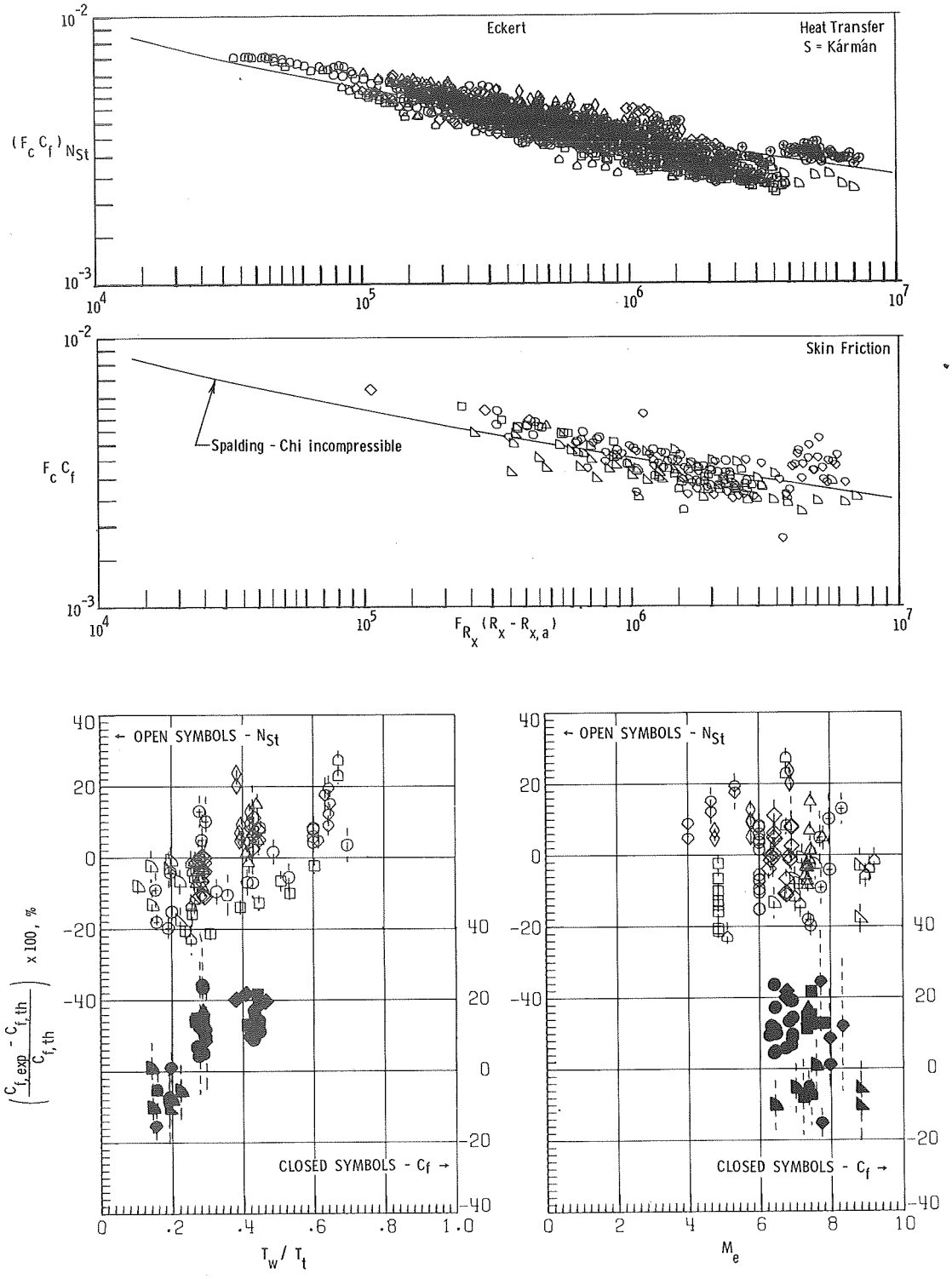

(b) Length Reynolds number correlation.

Figure 14.- Concluded.

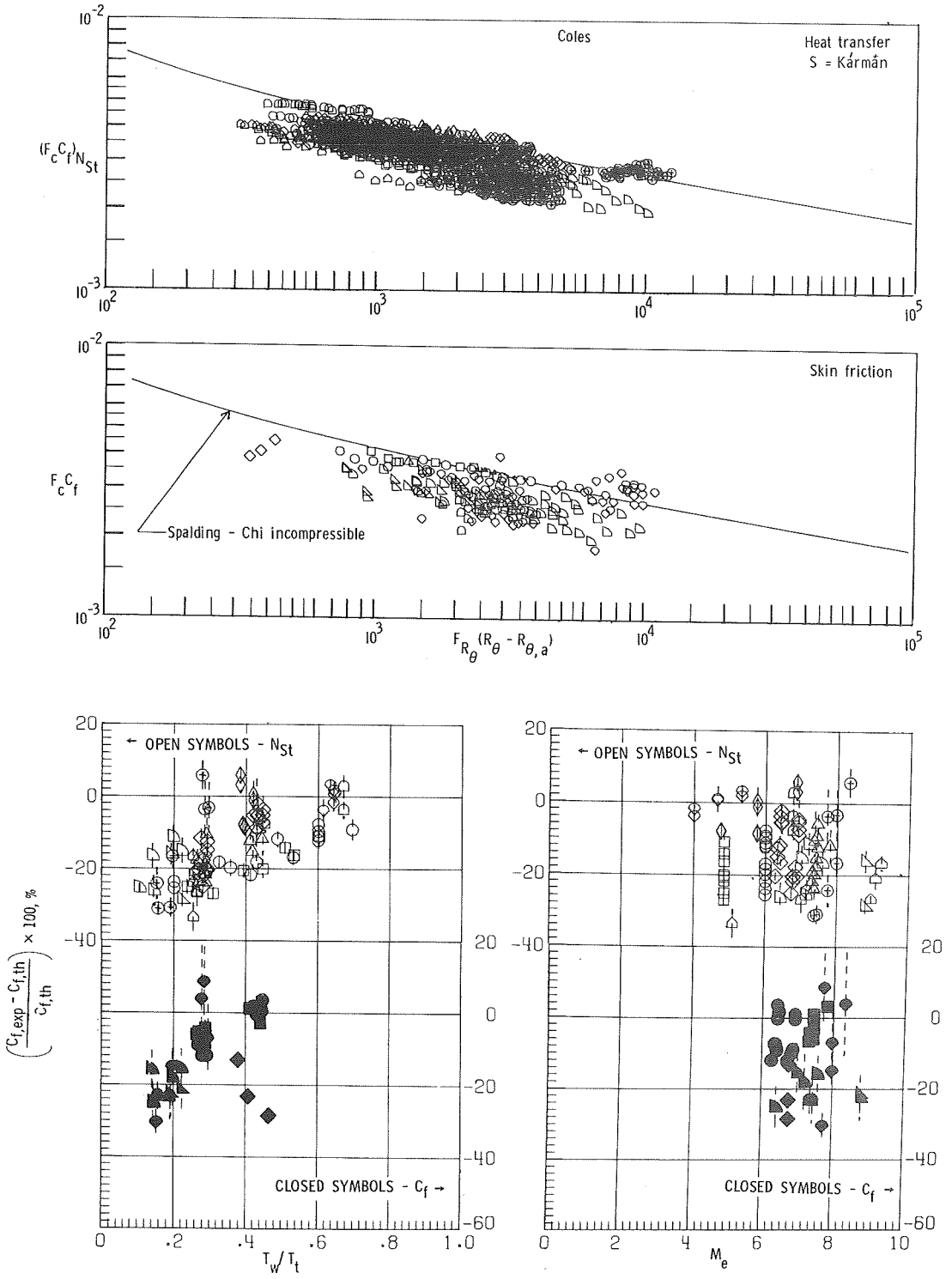

Figure 15.- Results from the Coles method by using best virtual-origin location.

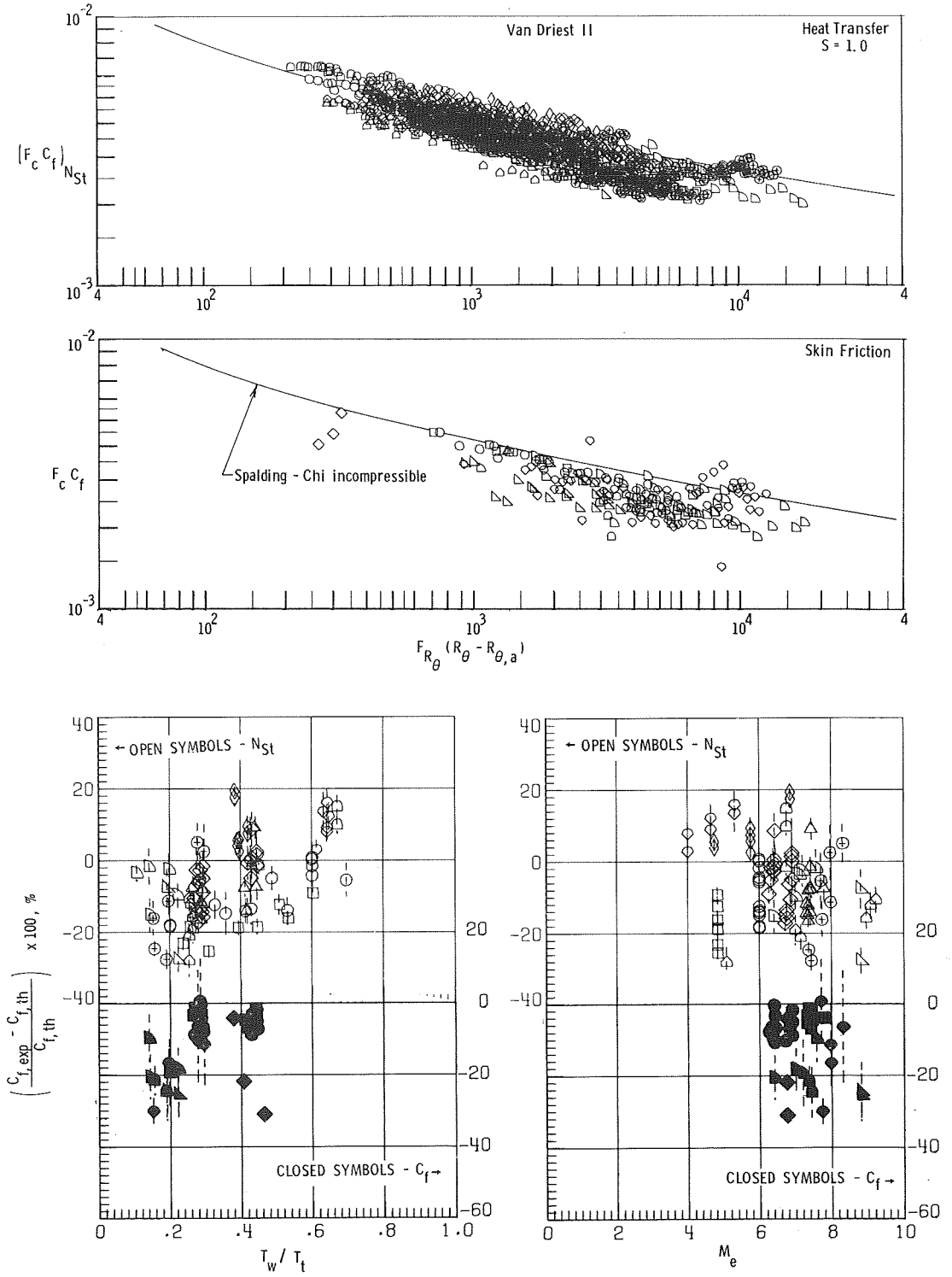

(a) Momentum-thickness Reynolds number correlation.

Figure 16.- Results from the Van Driest II method by using best virtual-origin location and S = 1.0.

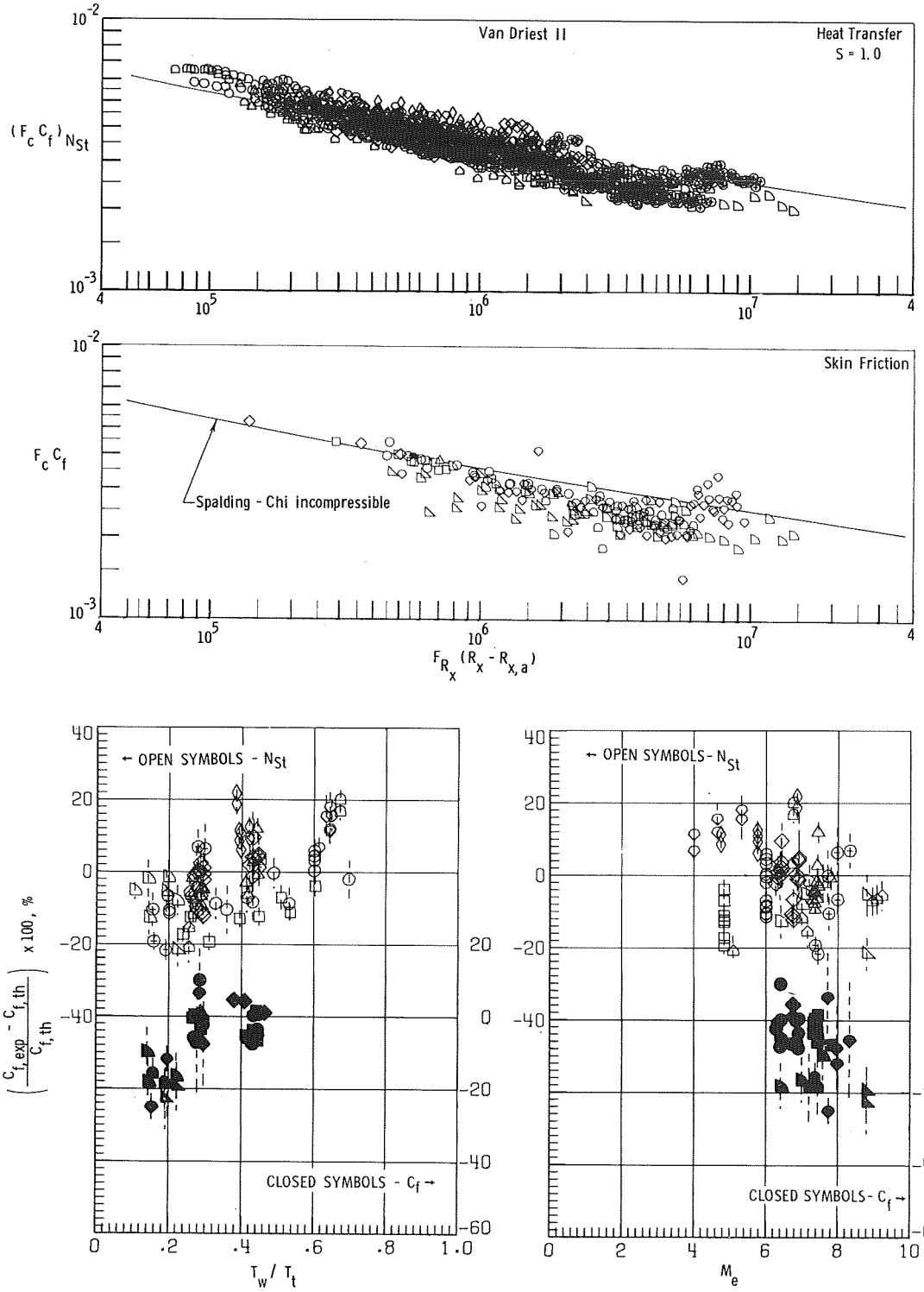

(b) Length Reynolds number correlation.

Figure 16.- Concluded.

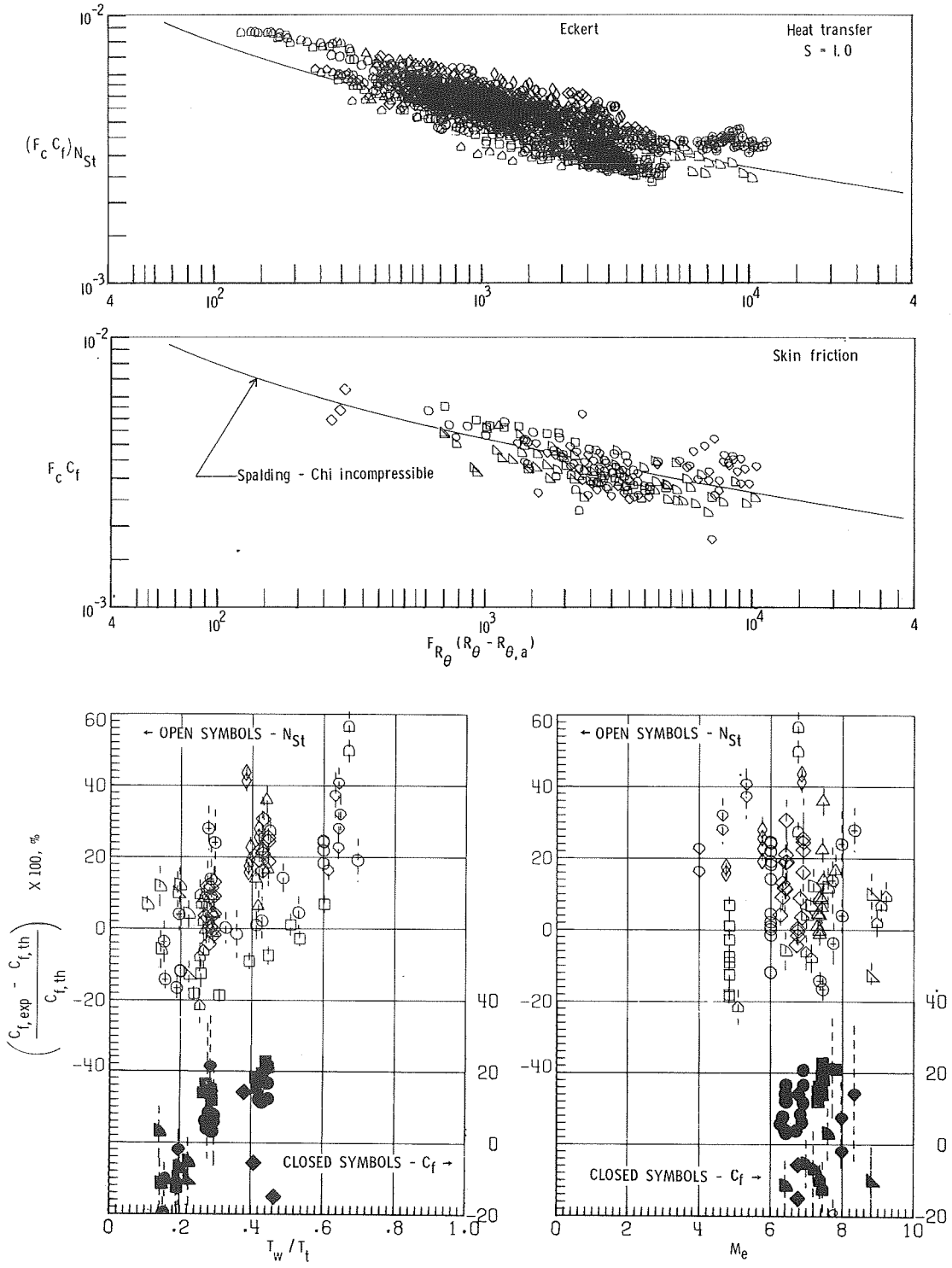

(a) Momentum-thickness Reynolds number correlation.

Figure 17.- Results from the Eckert method by using best virtual-origin location and S = 1.0.

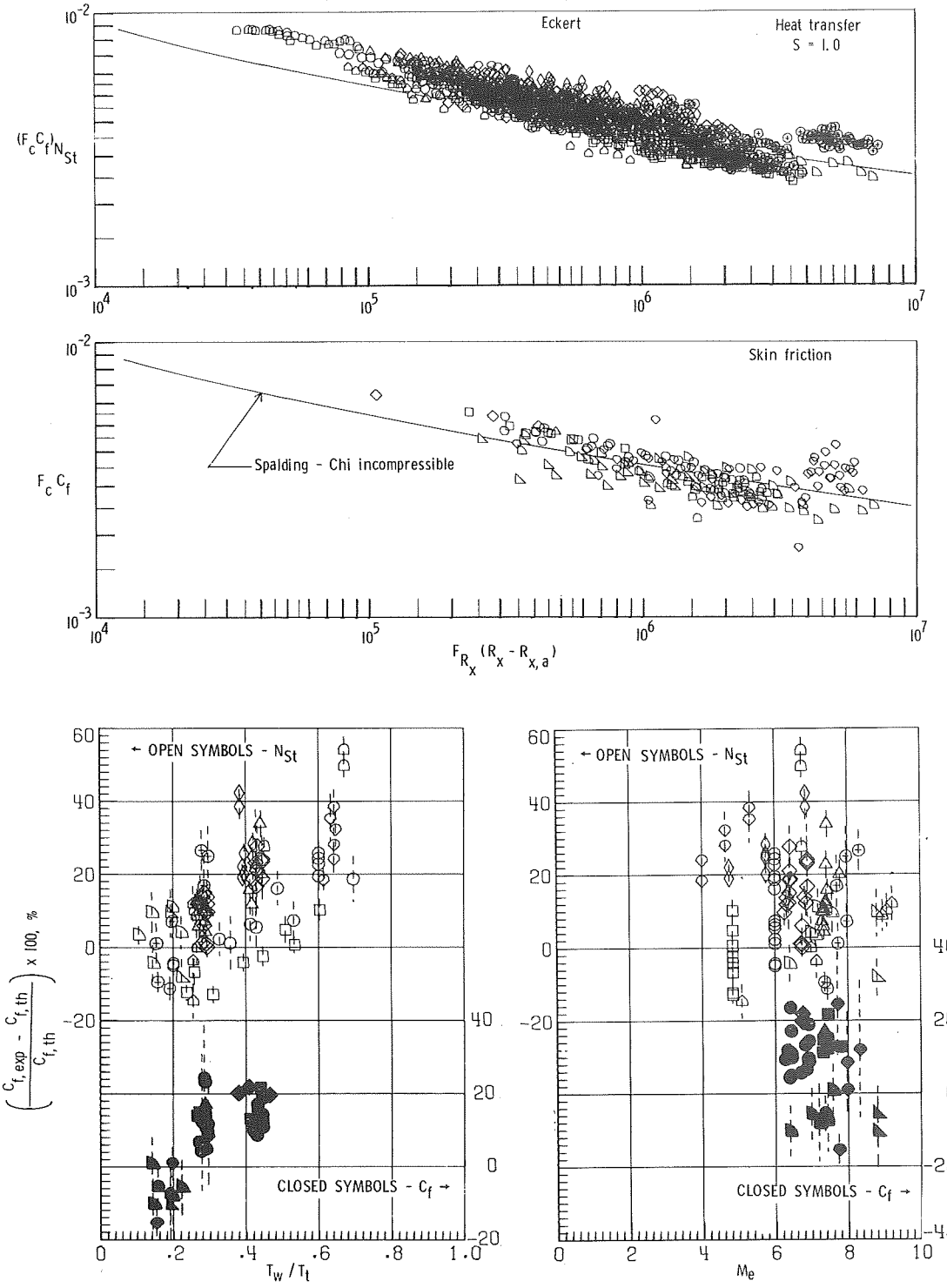

(b) Length Reynolds number correlation.

Figure 17.- Concluded.

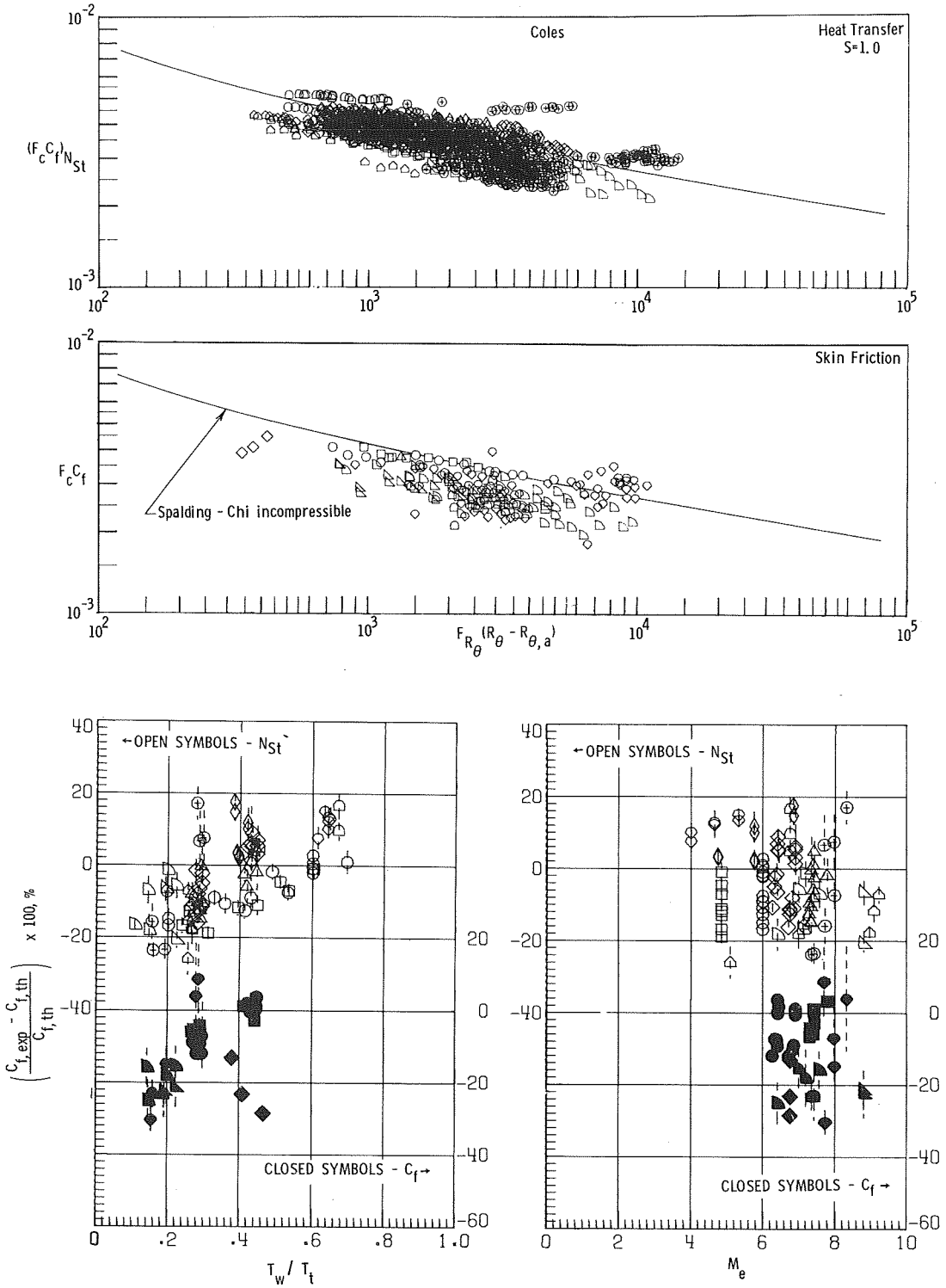

Figure 18.- Results from the Coles method by using best virtual-origin location and S = 1.0.

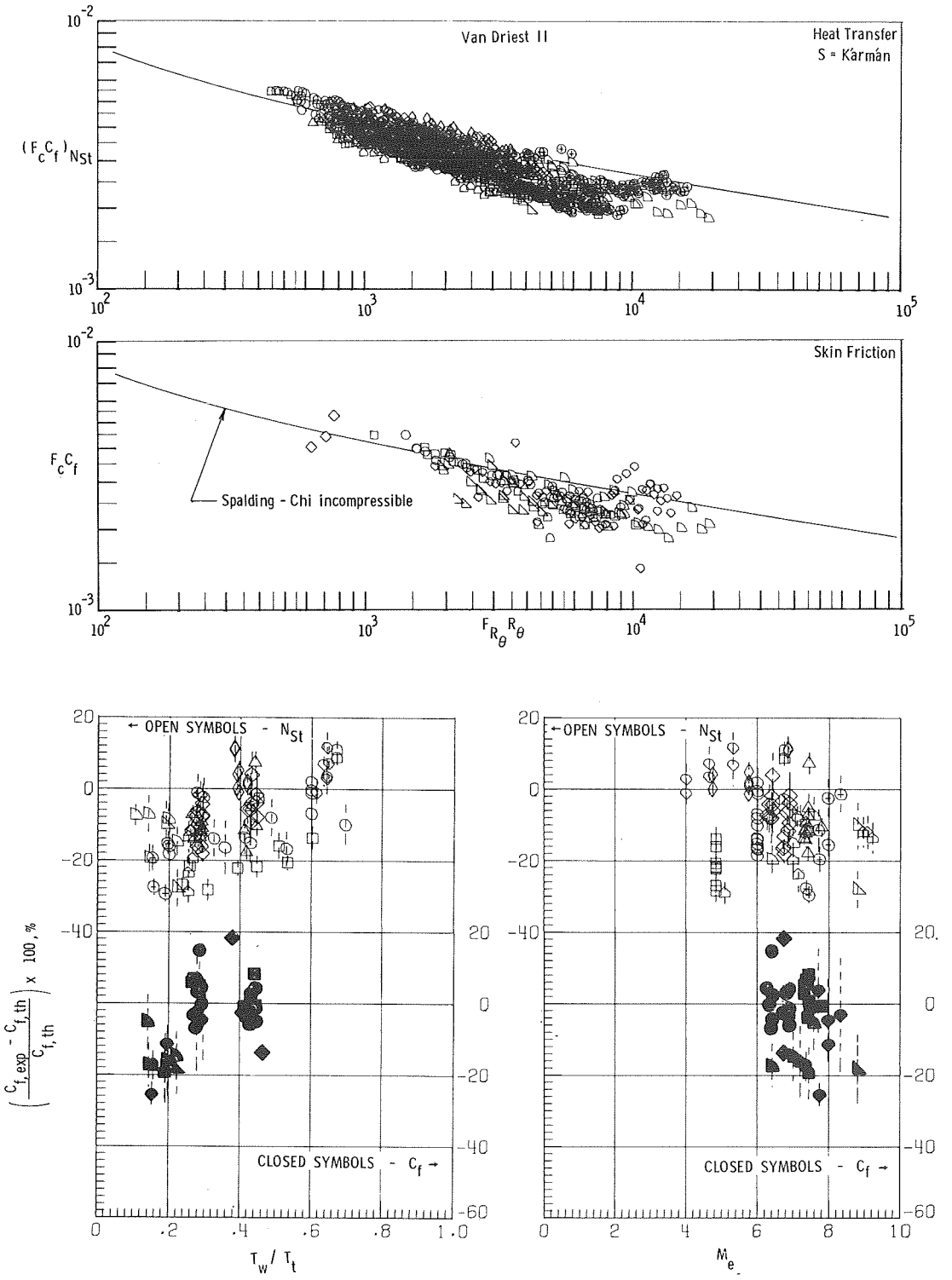

Figure 19.- Results from the Van Driest II method where C_f is assumed to be a unique function of R_θ and with Kármán's Reynolds analogy.

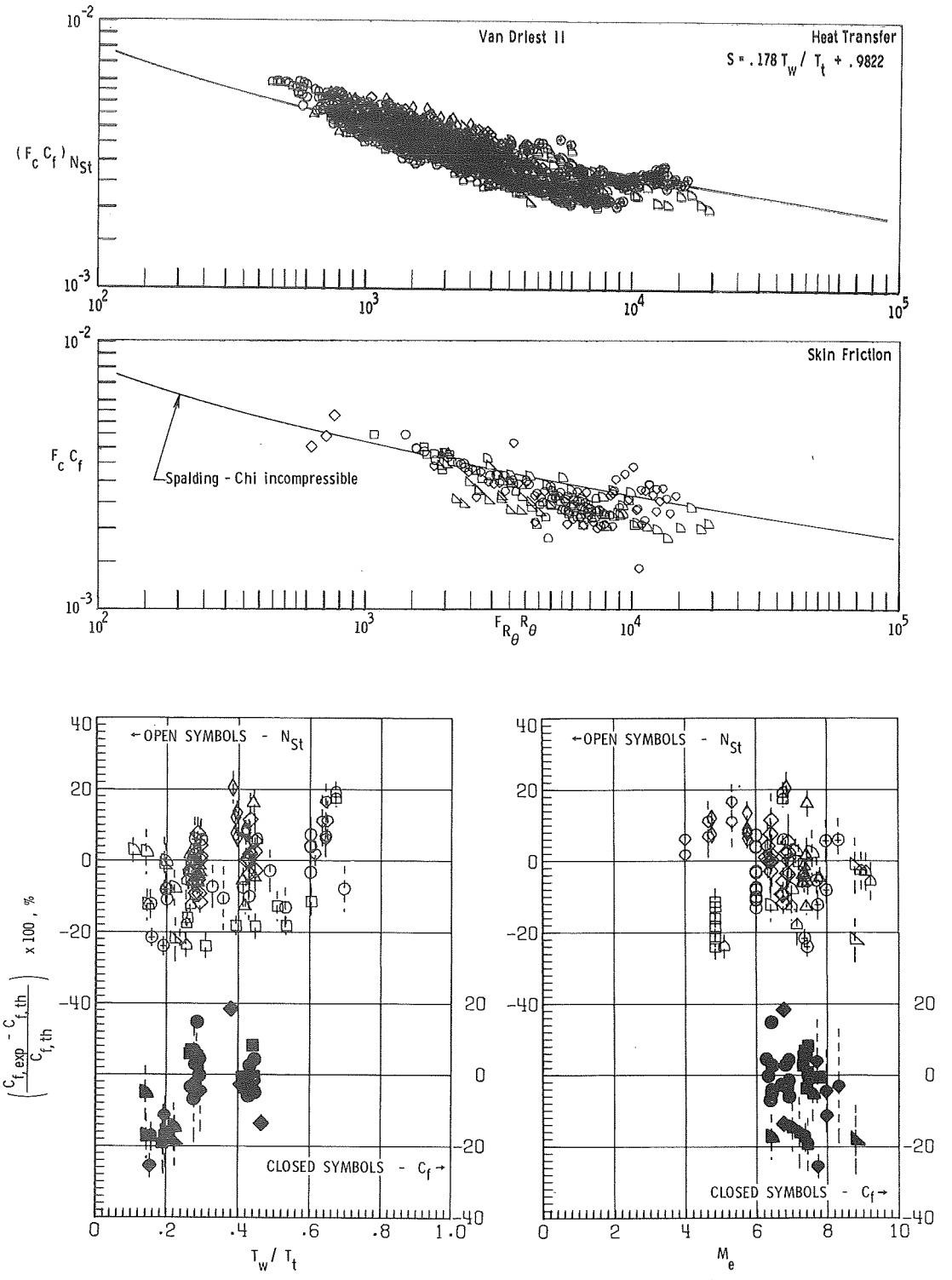

Figure 20.- Results from the Van Driest II method where C_f is assumed to be a unique function of R_θ and with S equal to an empirical function of ratio of wall to total temperature.

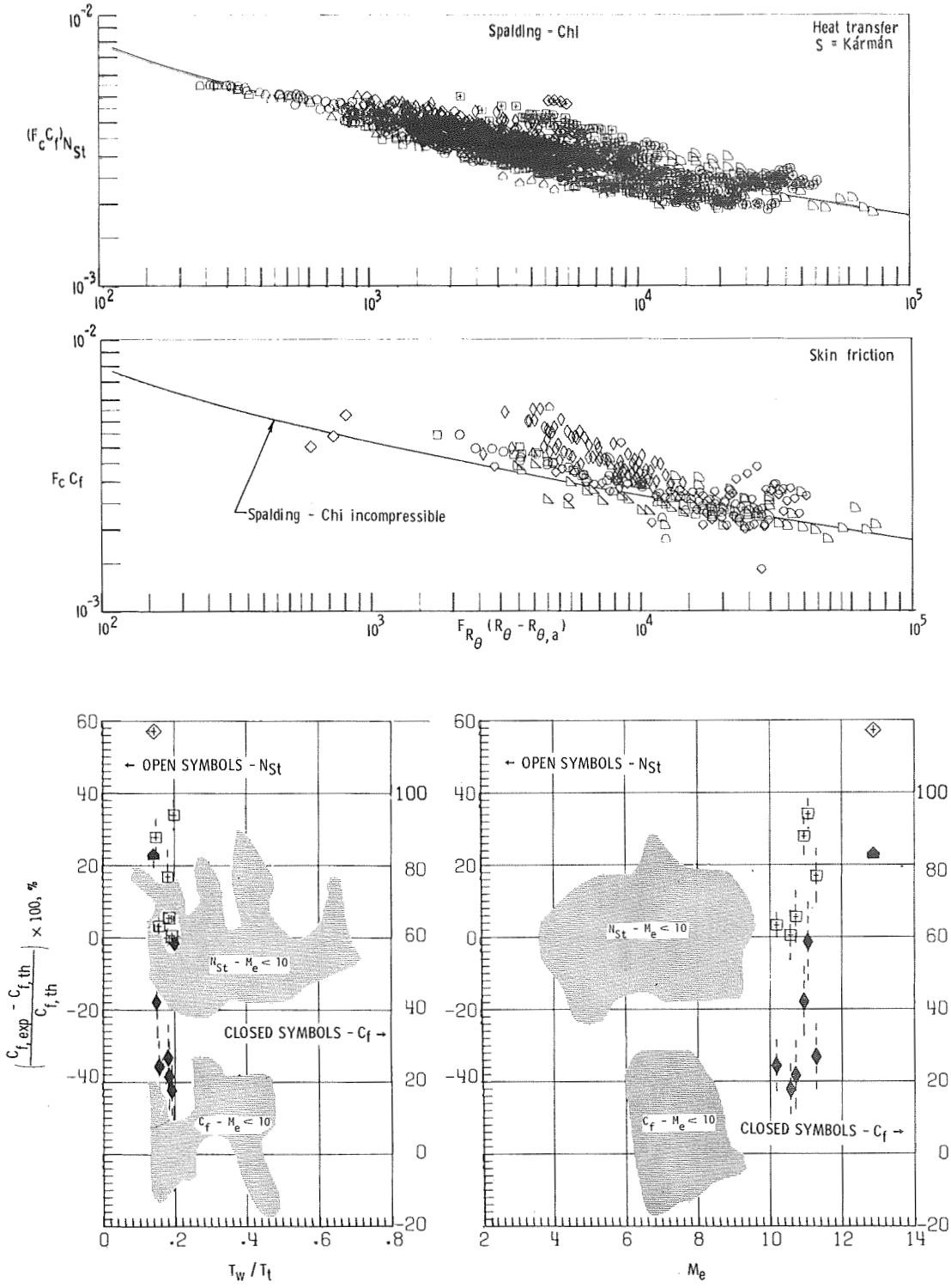

(a) Momentum-thickness Reynolds number correlation.

Figure 21.- Results from the Spalding and Chi method by using best virtual-origin location with $4 \leq M_e \leq 13$.

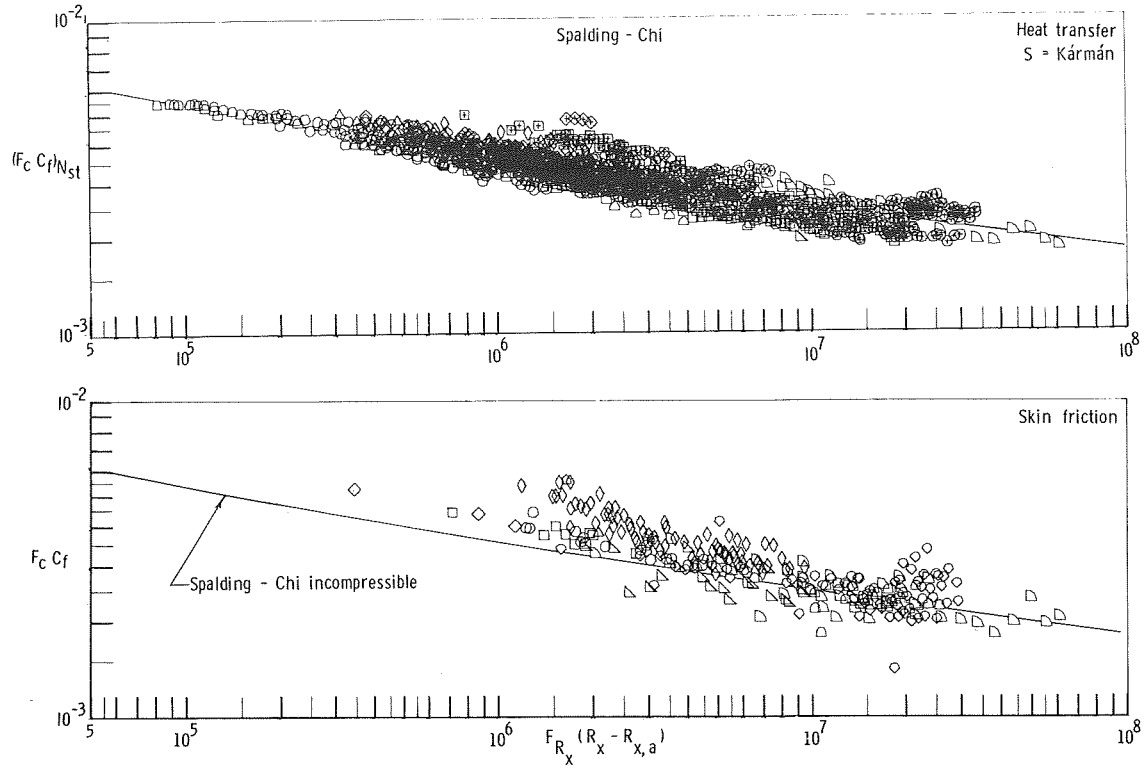

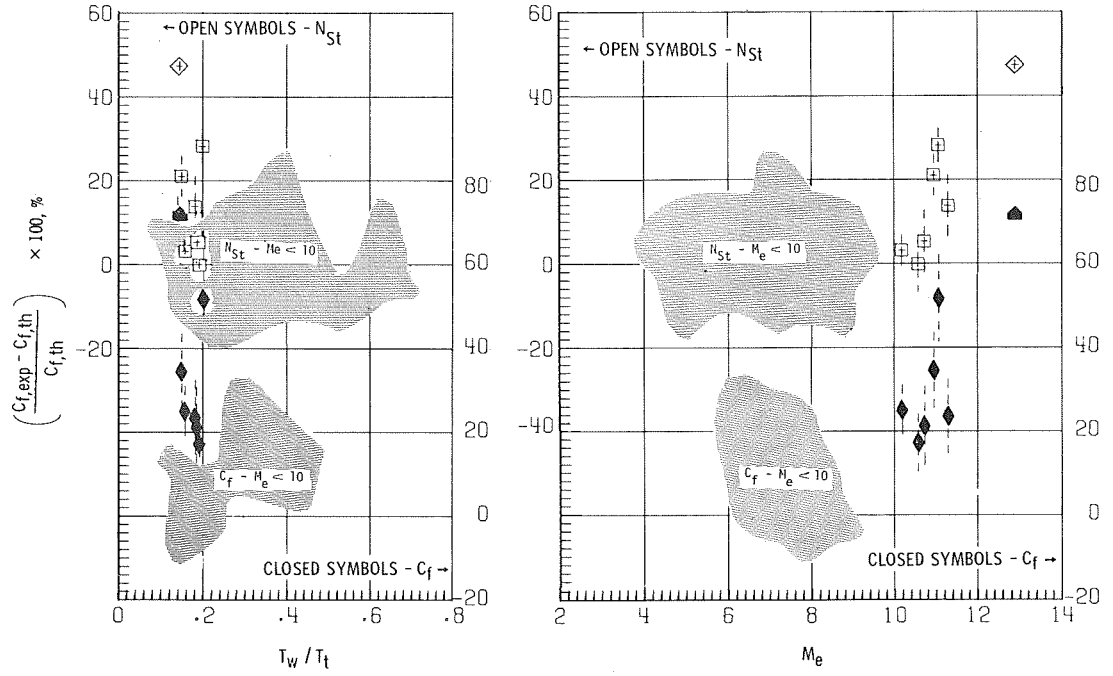

(b) Length Reynolds number correlation.

Figure 21.- Concluded.

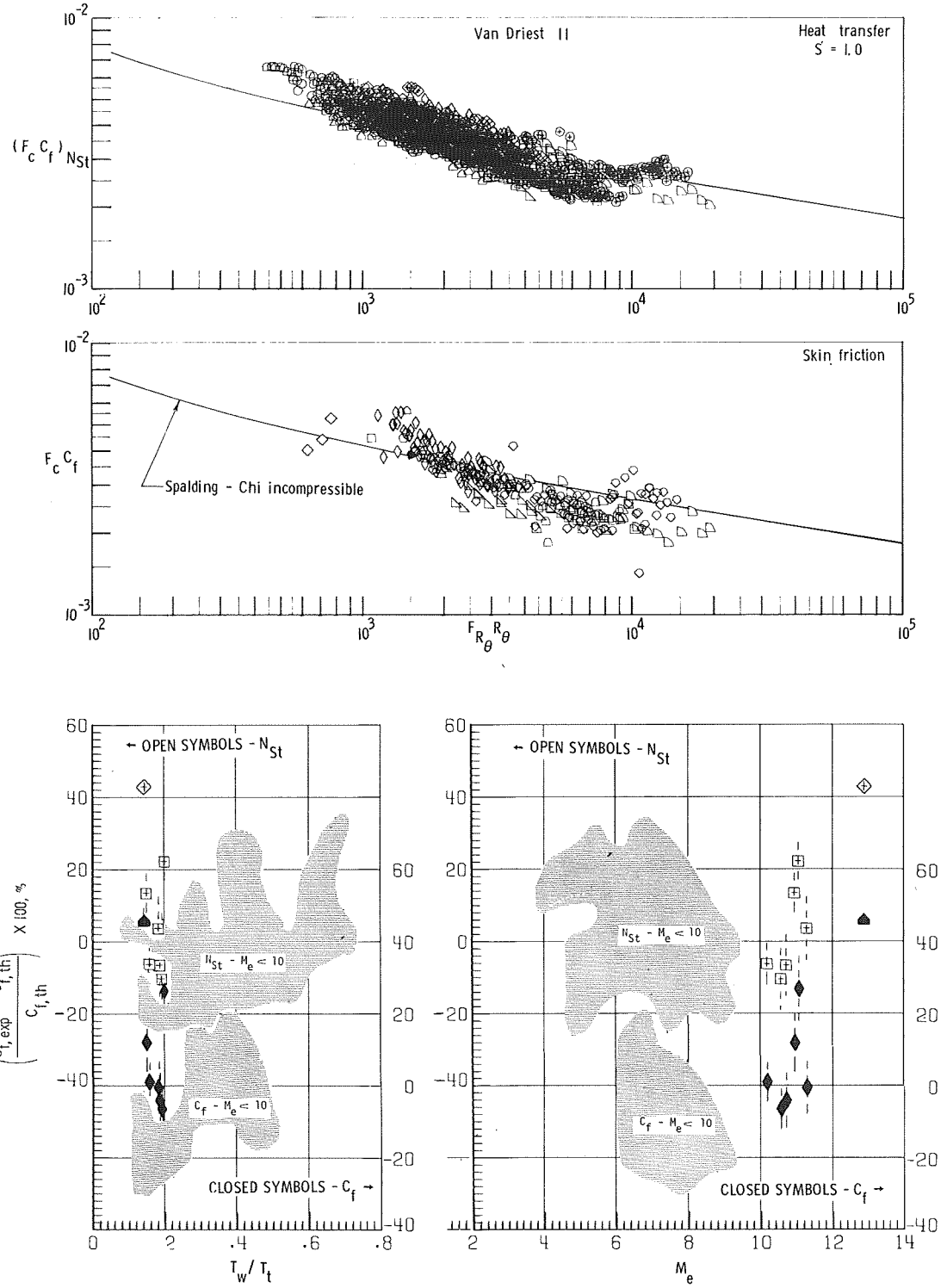

Figure 22.- Results from the Van Driest II method where C_f is assumed to be a unique function of R_θ and $S = 1.0$ with $4 \leqq M_e \leqq 13$.

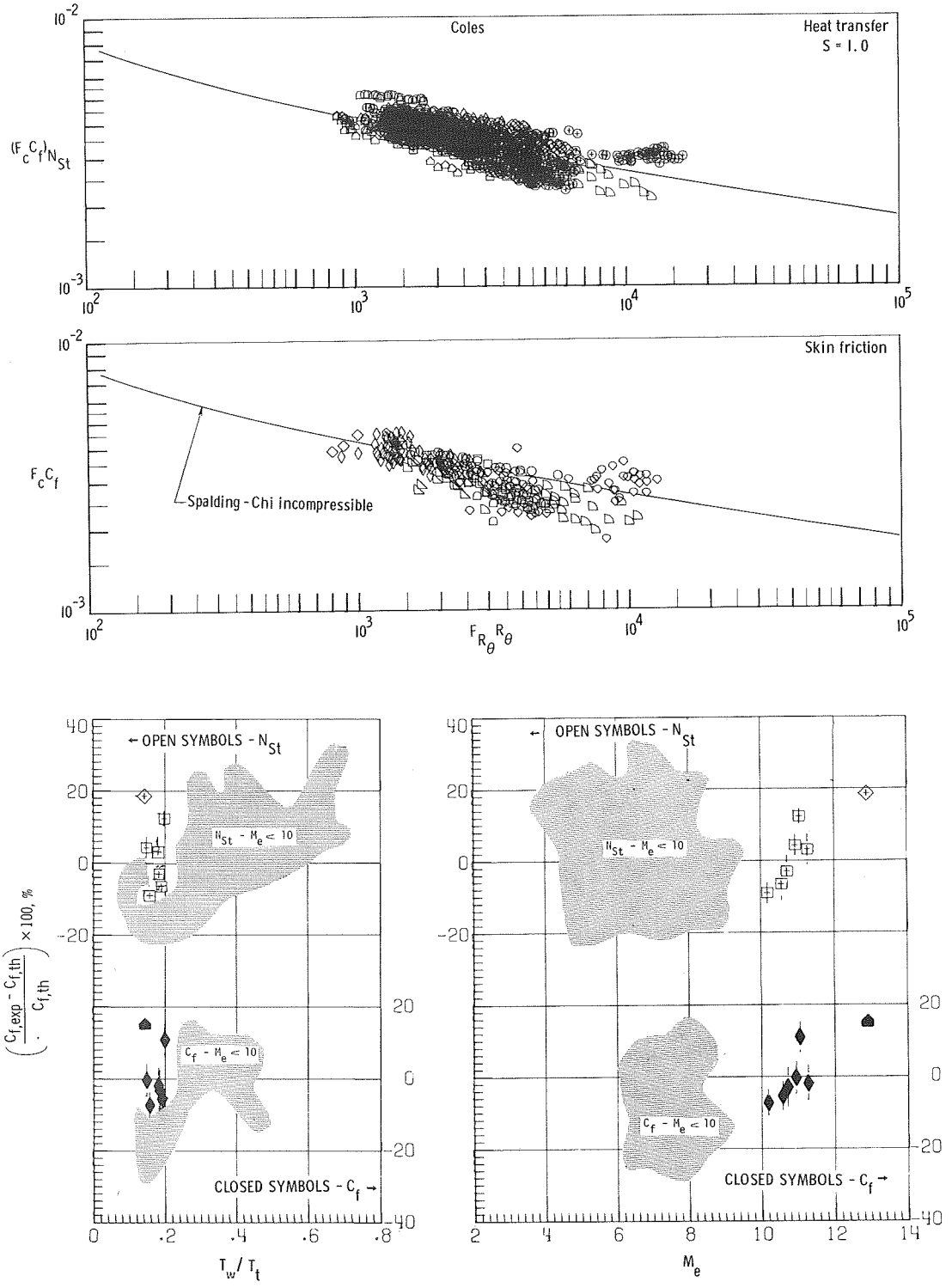

Figure 23.- Results from the Coles method where C_f is assumed to be a unique function of R_θ and $S = 1.0$ with $4 \leq M_e \leq 13$.

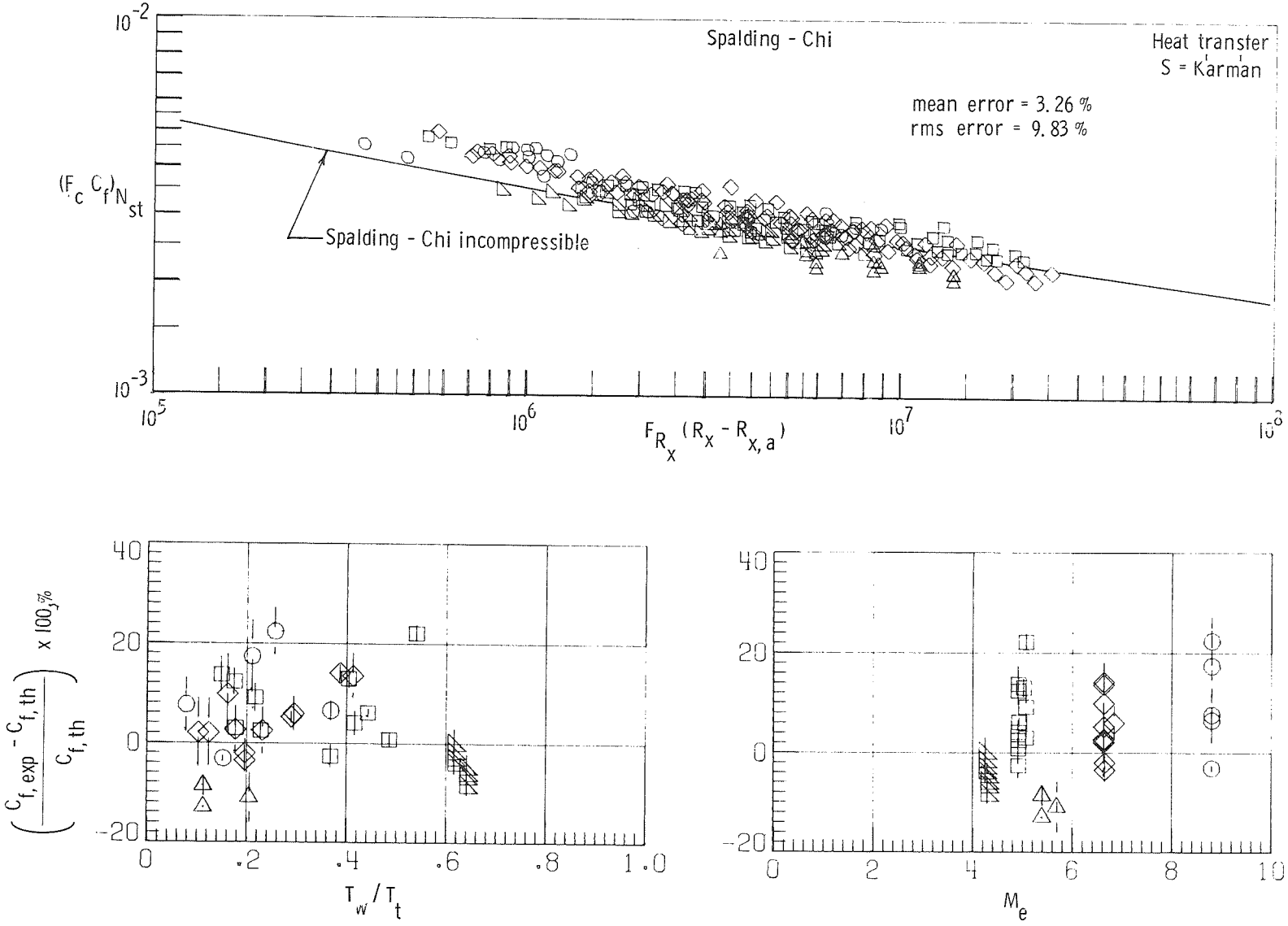

(a) Length Reynolds number correlation.

Figure 24.- Results from the Spalding and Chi method for cone flow and by using best virtual-origin location.

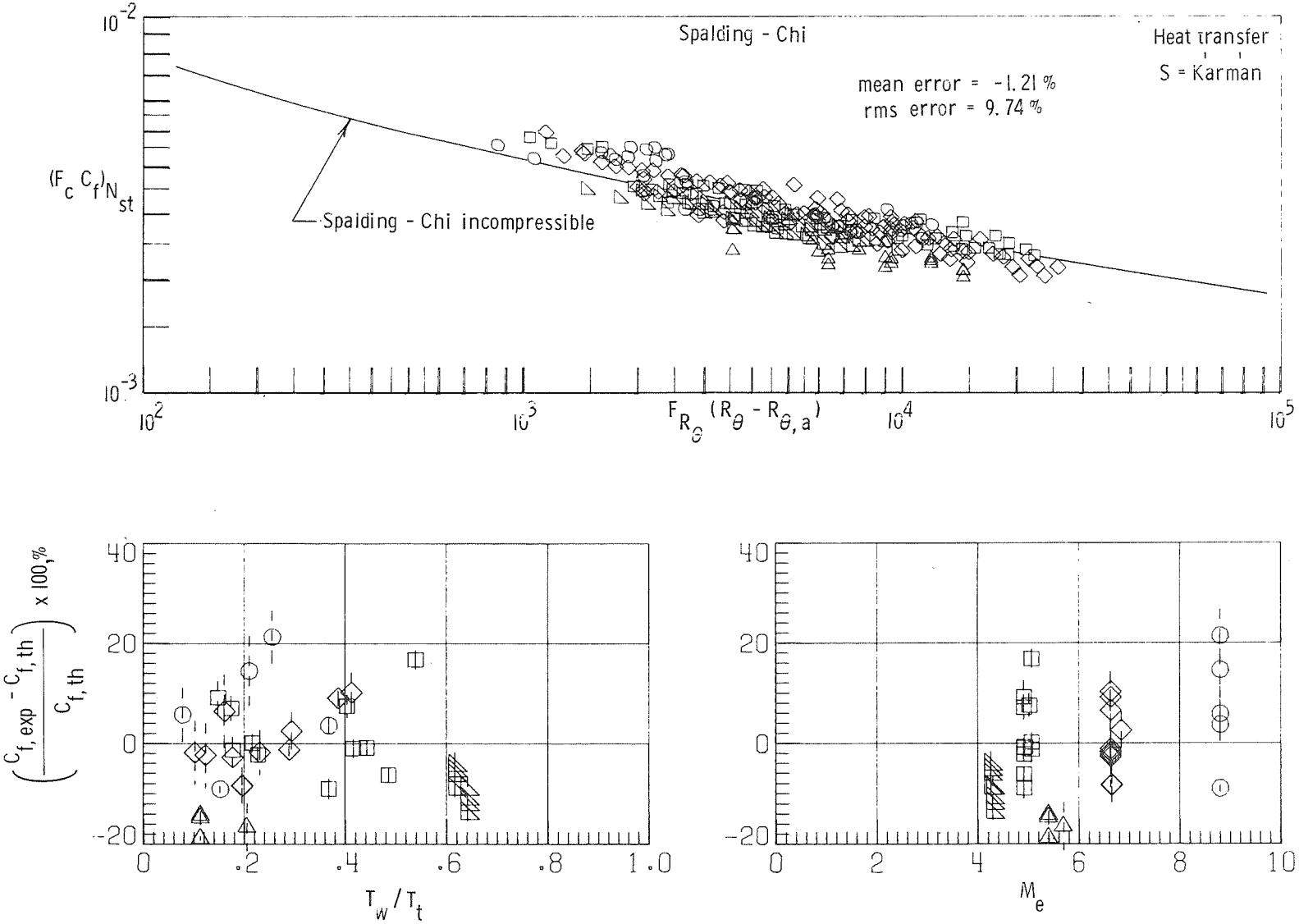

(b) Momentum-thickness Reynolds number correlation.

Figure 24.- Concluded.

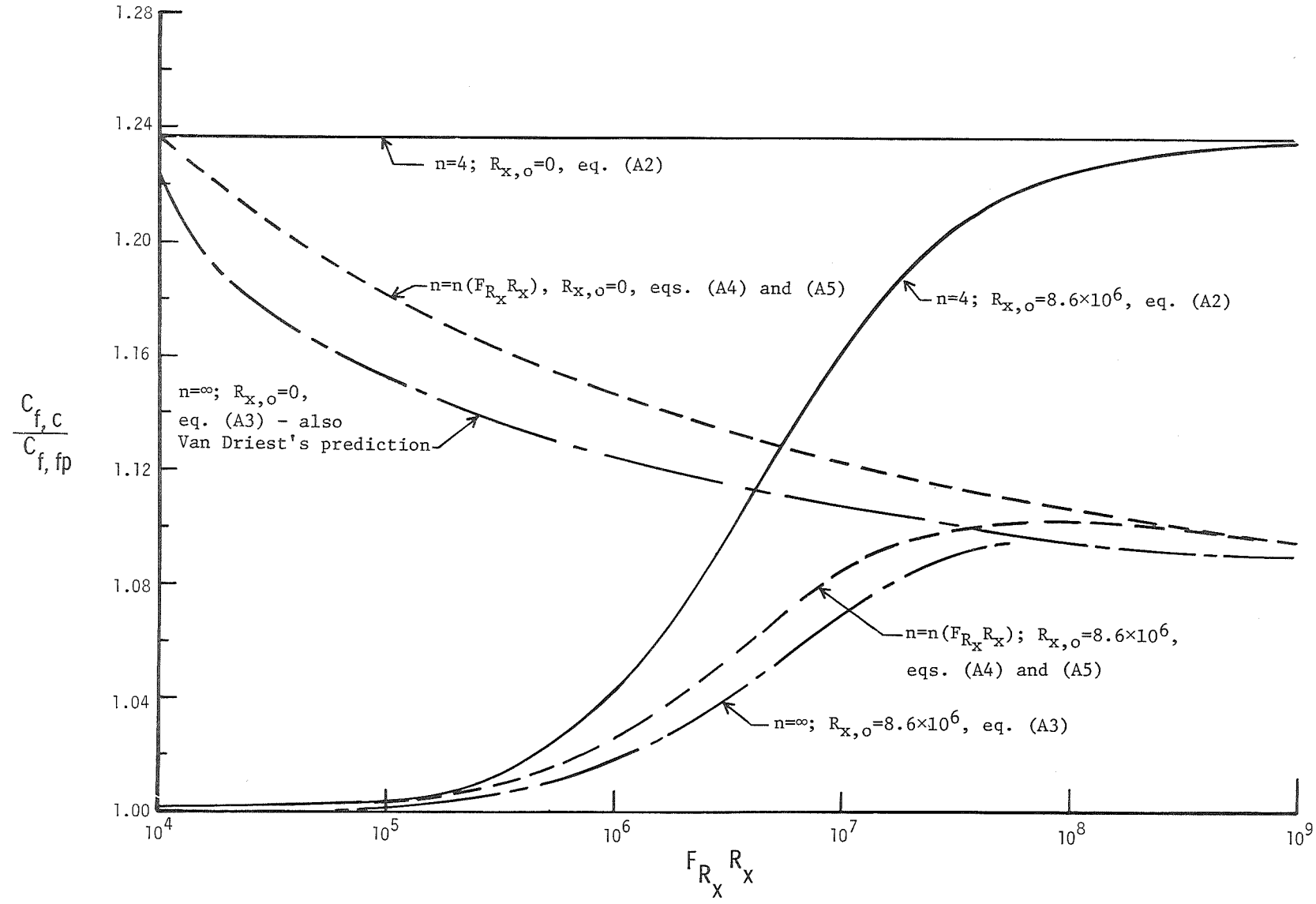

Figure 25.- Cone-to-flat-plate transformation.

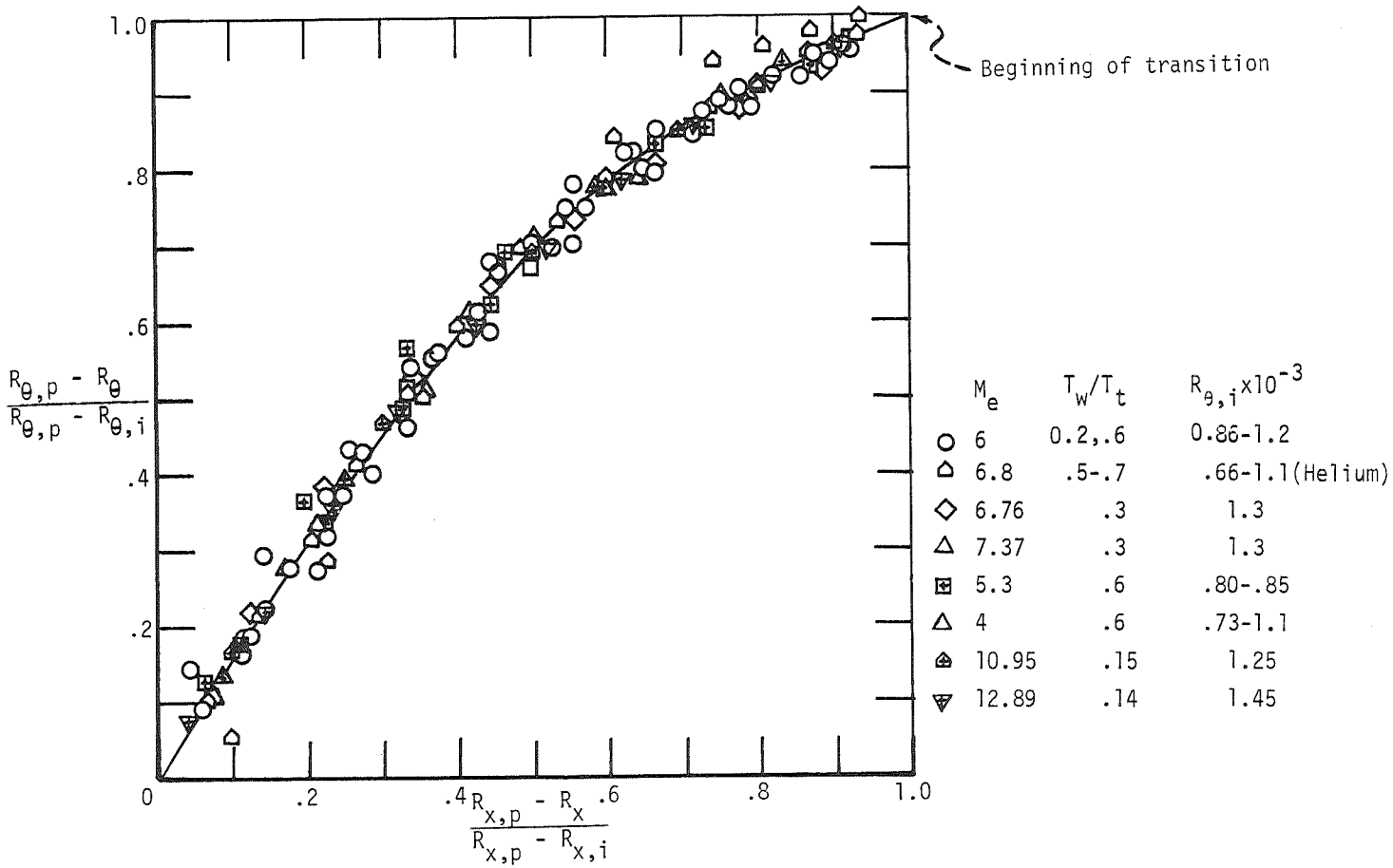

Figure 26.- Correlation of momentum-thickness distribution through transition.

NATIONAL AERONAUTICS AND SPACE ADMINISTRATION
WASHINGTON, D.C. 20546

OFFICIAL BUSINESS
PENALTY FOR PRIVATE USE $300

SPECIAL FOURTH-CLASS RATE BOOK

POSTAGE AND FEES PAID
NATIONAL AERONAUTICS AND SPACE ADMINISTRATION
451

U.S.MAIL

POSTMASTER : If Undeliverable (Section 158 Postal Manual) Do Not Return

"The aeronautical and space activities of the United States shall be conducted so as to contribute . . . to the expansion of human knowledge of phenomena in the atmosphere and space. The Administration shall provide for the widest practicable and appropriate dissemination of information concerning its activities and the results thereof."

—NATIONAL AERONAUTICS AND SPACE ACT OF 1958

NASA SCIENTIFIC AND TECHNICAL PUBLICATIONS

TECHNICAL REPORTS: Scientific and technical information considered important, complete, and a lasting contribution to existing knowledge.

TECHNICAL NOTES: Information less broad in scope but nevertheless of importance as a contribution to existing knowledge.

TECHNICAL MEMORANDUMS: Information receiving limited distribution because of preliminary data, security classification, or other reasons. Also includes conference proceedings with either limited or unlimited distribution.

CONTRACTOR REPORTS: Scientific and technical information generated under a NASA contract or grant and considered an important contribution to existing knowledge.

TECHNICAL TRANSLATIONS: Information published in a foreign language considered to merit NASA distribution in English.

SPECIAL PUBLICATIONS: Information derived from or of value to NASA activities. Publications include final reports of major projects, monographs, data compilations, handbooks, sourcebooks, and special bibliographies.

TECHNOLOGY UTILIZATION PUBLICATIONS: Information on technology used by NASA that may be of particular interest in commercial and other non-aerospace applications. Publications include Tech Briefs, Technology Utilization Reports and Technology Surveys.

Details on the availability of these publications may be obtained from:

SCIENTIFIC AND TECHNICAL INFORMATION OFFICE

NATIONAL AERONAUTICS AND SPACE ADMINISTRATION

Washington, D.C. 20546